Oscillatory cAMP Signaling in the Development of *Dictyostelium discoideum*

1 Introduction

One of the most essential characteristics of living organisms, from the unicellular level to the largest plants and animals, is their active interaction with their environment. From the unicellular level upward, organisms have developed sensitive signal detection systems that extract information from their environment and enable them to find food and mates, initiate developmental changes, avoid harmful environments or execute any of the multitude of actions and behaviors in their repertoire. Given that organisms are embedded in a 'sea of data', the extraction step is usually the first and perhaps most critical step. We view this process as essentially one of gathering the information and responding to it, and thus some basic information-theoretic definitions are in order. We use the definitions given in Parker[1].

Data Any representation of characters or analog quantities to which meaning, if not information, may be assigned.

Information Data which has been recorded, classified, organized, related or interpreted within a framework so that meaning emerges.

Noise Meaningless or erroneous bits that must be removed or ignored from a data stream.

Comments Theor. Biol
1998, Vol. 5, pp. 175–282
Reprints available directly from the publisher
Photocopying permitted by license only

Clearly there is some ambiguity in the definition of data, and perhaps a more useful definition in the biological realm is that data is simply the entire state of the environment of an organism. This includes all the usual physicochemical quantities such as temperature, concentrations, and so forth, but also includes other organisms. To extract information from this data requires a signal transduction system, the purpose of which is to detect, transduce, and possibly act upon available data. Our purpose here is to first discuss the processes of detection, transduction and response in abstract terms, and then to describe a particular unicellular organism, *Dictyostelium discoideum* (Dd) for which much is known about these processes.

1.1 An overview of signal transduction

Since most organisms maintain a clear distinction between inside and outside, many primary environmental signals do not penetrate very far into the organism. Instead there are mechanisms for transducing an external signal into an internal signal, and where appropriate, an internal response. For example, at the cellular level extracellular hydrophilic *first messenger* signals elicit a response through a transduction system in the cell membrane that translates the signal into an intracellular *second messenger* signal. Similarly, in the sensory systems of higher organisms light or mechanical stimuli are transduced by a multi-step cascade into an electrical signal that is processed at a higher level. The problem of how external information detected at the periphery of higher organisms is transmitted to the brain has fascinated scientists for hundreds of years. An early description due to Descartes of how this might occur is as follows.

> To understand, next, how external objects that strike the sense organs can incite [the machine] to move its members in a thousand different ways: think that
>
> (a) the filaments (I have already often told you that these come from the innermost part of the brain and compose the marrow of the nerves) are so arranged that they can very easily be moved by the objects of that sense and that
>
> (b) when they are moved, with however little force, they simultaneously pull the parts of the brain from which they come, and by this means open the entrances to certain pores in the internal surface of the brain ..
>
> Thus if fire A is near foot B, the particles of this fire have force enough to displace the area of skin they touch; and thus pulling the little thread (cc) which you see attached there, they simultaneously open the entrance to the pore (de) where

this thread terminates; just as, pulling on one end of a cord, one simultaneously rings a bell which hangs on the opposite end.

R. Descartes - *De Homine*

Not only do transduction or processing systems amplify the signal, but they often filter it as well, since not all features of a signal are equally important. For instance, the important information in a signal is often the short-term change in amplitude, rather than the absolute amplitude itself. Thus sensory systems frequently have evolved to ignore constant background signals, yet remain responsive to changes in the signal. Said otherwise, a step change in an external signal from one constant level to another often elicits a transient change in one or more components of the internal state or in some behavior of the organism, followed by a return to a basal level of that component or behavior. The process by which the sensory transduction system terminates the response in the face of a constant stimulus is usually called desensitization, habituation, or adaptation, depending on the context, but in this paper we distinguish between them. We use adaptation when the stimulus does not provoke any gross rearrangements or alterations in the signal-processing machinery, whereas desensitization may involve structural changes such as the degradation of receptors. The visual system and mechanoreceptors in the dermis of mammals provide several easily-observed examples of adaptation, but this capability is very common in sensory systems. Adaptation involves more than simply saturating the sensory system, for it is also important

to maintain sensitivity to further changes in the signal. Thus by an adapting sensory system we mean one that responds transiently to a transient change in the signal, returns to a basal activity level in the presence of a prolonged constant stimulus, and retains sensitivity to further changes in the stimulus. These characteristics are shown schematically in Figure 1. Clearly adaptation represents a form of learning, since having it in a

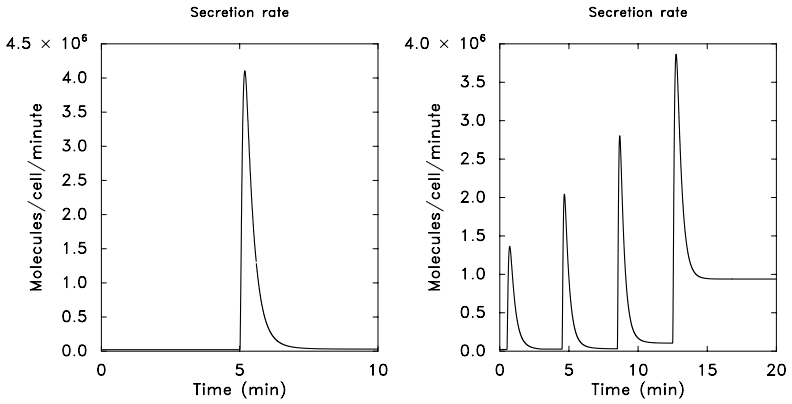

Figure 1. A schematic of the response of an adapting system to different stimuli. Shown here is the cyclic AMP (cAMP) relay response, as measured by the secreted cAMP, to extracellular cAMP stimuli in the cellular slime mold *Dictyostelium discoideum*. In (a) a step change in extracellular cAMP from 0 to $10^{-8}M$ elicits a single pulse of secreted cAMP. In (b) the system responds and adapts to a sequence of step increases ranging from $10^{-9}M$ to $10^{-6}M$, but at the highest stimulus the transduction system saturates. (Details are given in a later section.)

signal transduction system enables the organism to avoid responding to a constant signal when such a response is not advantageous. In addition, by adapting to background levels of a signal (or equivalently, changing the sensitivity to the amplitude of signals) the sensory system can process a far greater range of amplitudes. In fact the range of signal amplitudes that can be tolerated is enormous. For example, the visual system in certain amphibians can detect and respond to light stimuli whose amplitude ranges over five or more orders of magnitude[2].

1.2 Models of transduction and adaptation

The basic steps that characterize most signal transduction systems are shown in Figure 2. The sensory systems of interest here can be described

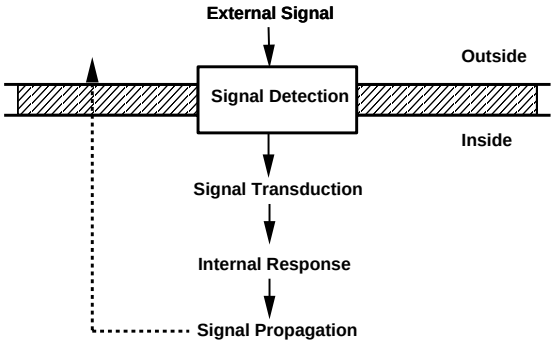

Figure 2. A schematic of the major steps in signal detection, transduction and processing to produce an inter- and possibly extracellular response. Adaptation may be involved at any of the steps shown.

by a finite number of state variables and an evolution equation that determines how the state changes under prescribed inputs or stimuli. We denote the state vector by $\mathbf{u}(\cdot) \in \mathbf{R}^n$ and write the evolution equation in the form

$$\frac{d\mathbf{u}}{d\tau} = \mathbf{F}(\mathbf{u}, S), \tag{1}$$

where $S \in \mathbf{R}$ represents the stimulus or input to the system. Typical state variables are a transmembrane voltage, gating variables, the concentration of a chemical transducer substance, etc. Frequently the dynamics described by (1) are 'excitable', in that the steady state at fixed S is stable and small changes in that state do not produce a significant response. For such dynamics the stimulus must exceed a threshold, and this provides a means of filtering out small amplitude noise in the environment. In general a change in S leads to a change in the transient and steady-state values of $\mathbf{u}$, but in systems that adapt some functional of $\mathbf{u}$ should be independent of S when S is time-independent. In this section we discuss the constraints imposed on $\mathbf{F}$ by this requirement. The reader can consult[3–6] for a review of models that involve adaptation, including some

for bacterial chemotaxis and adenylyl cyclase. Models for adaptation in *Dictyostelium discoideum* will be discussed later.

Suppose that the response $\mathcal{R}$ of the system is a functional $\mathcal{G}$ of the state $\mathbf{u}$ given as follows:

$$\mathcal{R}(\tau) = \mathcal{G}(\mathbf{u}(\tau)). \tag{2}$$

For example, in the neurobiological context $\mathcal{G}$ could represent the firing rate of a neuron, in bacteria it is the change in the relative probabilities of counterclockwise and clockwise flagellar rotation, and in *Dictyostelium* it is the rate of secretion of cyclic AMP. More generally, $\mathcal{G}$ could depend on the derivatives of the state variables, their past history, or directly on the stimulus and its derivatives. The first case is easily treated under the third case, for $\dot{\mathbf{u}}$ is given in terms of $\mathbf{u}$ and S by (1). Some of these generalizations will be treated elsewhere; for now we restrict ourselves to responses of the form (2). Furthermore, we shall only consider systems whose 'basal dynamics' are time independent, which means that the system has an asymptotically stable steady state in the presence of any constant stimulus. In that case we can define perfect adaptation to constant stimuli as follows.

Definition 1 The response $\mathcal{R}$ of a system whose dynamics are governed by (1) is said to adapt to constant stimuli if the steady state response is independent of the magnitude of the stimulus S.

Evidently this definition allows for the trivial case when $\mathbf{F}$ is independent of S, in which case there is no change in response to any changes in S. Furthermore this definition of adaptation does not imply that the steady state values of all variables must be independent of S, and in fact some of the state variables generally do change when the stimulus changes, as will be seen in a later example.

Now suppose that S is fixed. At a steady state $\mathbf{F}(\mathbf{u}, S) = 0$, and we shall assume that $\det(\mathbf{F}_{\mathbf{u}}) \neq 0$, where $\det(\cdot)$ denotes the determinant and the subscript denotes the partial derivative. This implies that locally there is a unique function $\mathbf{g} : \mathbf{R} \longrightarrow \mathbf{R^n}$ such that $\mathbf{F}(\mathbf{g}(S), S) = 0$. The steady state response is $\mathcal{R} = \mathcal{G}(\mathbf{g}(S))$, and this adapts to S if and only if

$d\mathcal{R}/dS \equiv 0$. We have that

$$\frac{d\mathcal{R}}{dS} = \left\langle \nabla \mathcal{G}, \frac{d\mathbf{u}}{dS} \right\rangle, \tag{3}$$

and

$$\mathbf{F}_{\mathbf{u}} \frac{d\mathbf{u}}{dS} + F_S = 0, \tag{4}$$

where $< ., . >$ denotes the Euclidean inner product. Therefore adaptation of the steady state response requires that the sensitivity of the steady state to changes in stimulus, as measured by $d\mathbf{u}/dS$, must be tangent to a level surface of the response. In other words, the following condition must be satisfied.

$$\left\langle \nabla \mathcal{G}, \frac{d\mathbf{u}}{dS} \right\rangle = - \left\langle \nabla \mathcal{G}(\mathbf{g}(S)), \mathbf{F}_{\mathbf{u}}^{-1}(\mathbf{g}(S), S) \mathbf{F}_S(\mathbf{g}(S), S) \right\rangle = 0 \tag{5}$$

for every S. Not all models can satisfy this condition, and even for those that can, this condition imposes constraints on the admissible choices of the parameters. A simple check of this condition alone suffices to show that a number of models that are purported to adapt cannot in fact show the desired adaptive behavior[4].

However, adaptation of the steady state response is only one aspect of adapting sensory systems. Another necessary property of such a system is that it retain the ability to respond to changes in the stimulus level over some range of stimuli, even though it has adapted to a certain level (cf. Figure 1). An *a priori* estimate of the magnitude of a response to a given stimulus would be useful, but in general it is difficult to characterize the entire response to a time-varying stimulus. Of course more can be said in special cases. For instance, it frequently happens that the rise of the transient response is very rapid compared to the return to the basal level, and in this case singular perturbation or quasi-steady-state arguments can be used to predict the magnitude of the response. An example is given later.

Some insight into the stimulus-response coupling can be gotten by examining changes in the response immediately following a step change in the input. This type of stimulus is particularly appropriate in the context of Dd in view of the experiments done by Devreotes, *et al.*[7–9], which

were designed to characterize the relay and adaptation response in this system. Suppose that the system is at steady state with input S, and that at time $\tau = \tau_0$ the input is instantaneously changed to $S + \Delta S$. Immediately after imposing the stimulus

$$\left.\frac{d\mathcal{R}}{d\tau}\right|_{\tau_0^+} = \left\langle \nabla\mathcal{G}(\mathbf{g}(S)), \frac{d\mathbf{u}}{d\tau}(\tau_0^+) \right\rangle = \langle \nabla\mathcal{G}(\mathbf{g}(S)), \mathbf{F}(\mathbf{g}(S), S + \Delta S)\rangle$$

and therefore the response will change provided that $\nabla\mathcal{G}$ is not orthogonal to $\mathbf{F}$, *i. e.* , provided that the vectorfield is not tangent to the level surface of $\mathcal{G}$ at $(\mathbf{g}(S), S + \triangle S)$. Since $\mathbf{F}$ vanishes at $(\mathbf{g}(S)), S)$, this will be true if $\mathcal{G}$ depends on at least one component of $\mathbf{u}$ (say u_i) that is directly influenced by the stimulus S in the sense that $\partial F_i/\partial S \neq 0$.

A model system that illustrates some of the essential features of an adaptive system is given as follows. Suppose that there are two internal state variables u_1 and u_2, and that these variables evolve according to the following equations.

$$\begin{aligned} \frac{du_1}{d\tau} &= \frac{f(S(\tau)) - (u_1 + u_2)}{\tau_e} \\ \frac{du_2}{d\tau} &= \frac{f(S(\tau)) - u_2}{\tau_a}. \end{aligned} \tag{6}$$

In these equations the function $f(\cdot)$ encodes the signal transduction steps, and it should have the property that $f(0) = 0$. For concreteness we suppose that the response is proportional to u_1, *i. e.* $\mathcal{G}(\mathbf{u}(\tau)) = au_1(\tau)$ where a is a constant. Then this simple scheme can be viewed as having two input pathways, an excitatory one in which the stimulus increases the production of u_1 and hence increases the response, and an inhibitory one that increases the production of u_2, which in turn shuts off the response.

Since this system is linear the solution can be obtained by quadrature once the stimulus is specified. For the special case in which $u_1(0) = u_2(0) = 0$ and $S(\tau)$ is a step function of amplitude S_0 that turns on at $\tau = 0$, the solution is as follows.

$$\begin{aligned} u_1 &= \frac{f(S_0)\tau_a}{\tau_a + \tau_e}(e^{-\tau/\tau_a} - e^{-\tau/\tau_e}) \\ u_2 &= f(S_0)(1 - e^{-\tau/\tau_a}) \end{aligned} \tag{7}$$

Thus the response occurs on two time scales, the scale of excitation, which is characterized by τ_e, and the scale of adaptation, which is characterized by τ_a. From this one sees that if $\tau_e << \tau_a$, then whenever $\tau >> \tau_e$, u_1 relaxes to

$$u_1 \sim f(S_0)e^{-\tau/\tau_a} \equiv f(S_0) - u_2(\tau).$$

This is just the pseudo-steady-state value of u_1 which is gotten by setting $du_1/d\tau = 0$. On the other hand, if $\tau_a << \tau_e$ then adaptation is rapid compared to excitation, u_1 never rises significantly above zero, and there is no significant response. The typical response for a single step in the stimulus when $\tau_e < \tau_a$ is shown in Figure 3(a), where one can see that when the system begins at $(u_1, u_2) = (0, 0)$ neither u_1 nor u_2 exceed S_1. The response to two step changes that are well separated compared to the adaptation time are shown in Figure 3(b).

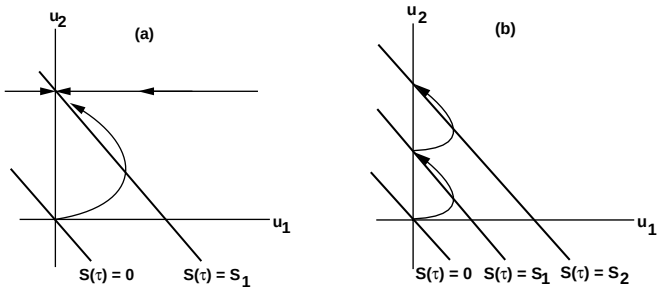

Figure 3. The phase plane for the model adapting system described by (6) when f is a linear function.

We note from (6) that when the stimulus $S(\tau)$ is constant the steady state level of u_1 is zero, *i. e.* , the response adapts perfectly to any constant stimulus, but the level of u_2 does not adapt. Moreover, when $\tau_e << \tau_a$ the system is excitable in the following sense. The rest state in the absence of a stimulus ($(u_1, u_2) = (0, 0)$) is asymptotically stable, but a brief stimulus of the proper type can produce a significant response, followed by a return to the steady state. Thus if f is linear, if the system is initially at $(0, 0)$, and if $S(\tau) = S_1$ for $\tau \in (0, \tau_e)$ and zero thereafter, then u_1 will rise to approximately $2S_1/3$ and then return to zero. Usually an excitable system is considered as one that has a threshold and shows an *all-or-nothing* response, such as the firing of a neuron, depending on

the magnitude of the stimulus. In contrast to this, the response of the present system is *graded* in that there is a response to any stimulus level. As we shall see later, this simple example contains some of the essential features needed in a model for signal transduction and relay in Dd. Other excitable systems that show a graded rather than an all-or-none response occur in models of intracellular calcium dynamics[10–12].

This simple model illustrates some of the basic features necessary in an adapting system, but there is no biochemical basis for it. A more realistic model, which is sometimes called the 'adapting box' model, is shown in Figure 4. This model was first proposed and analyzed by Katz and Thesleff[13] in a study of adaptation produced by acetylcholine at the motor end-plate of frog muscle, and more general forms were subsequently used by others in a similar context (Gero[14] and references therein). More recently Knox *et al.* [15,16] used it as a model for receptor adaptation in Dd.

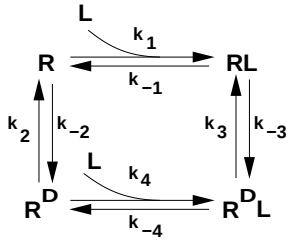

Figure 4. A schematic of the transitions in the adapting box model. R represents the active form of the receptor, R^D the inactive or refractory form of the receptor, and L represents the ligand.

Let $u_i, i = 1, \ldots 4$, denote the fractions in states R, RL, R^D and R^DL, respectively. Then in the symmetric form used by Katz and Thesleff, for

which $k_1 = k_4$ and $k_{-1} = k_{-4}$, the governing equations are

$$\begin{aligned}
\frac{du_1}{dt} &= -(k_1 L + k_{-2})u_1 + k_{-1}u_2 + k_2 u_3 \\
\frac{du_2}{dt} &= k_1 L u_1 - (k_{-1} + k_{-3})u_2 + k_3 u_4 \\
\frac{du_3}{dt} &= k_{-2}u_1 - (k_1 L + k_2)u_3 + k_{-1}u_4 \\
\frac{du_4}{dt} &= k_1 L u_3 + k_{-3}u_2 - (k_{-1} + k_3)u_4.
\end{aligned}$$

When these equations are used to describe ligand binding to a receptor on a channel[13], the response consists of opening the channel, and it is therefore proportional to the fraction in those receptor states that correspond to an open channel. In the Dd context Knox, *et al.* [15,16] assume that the downstream activity is a weighted sum of all states of the receptor.

If the ligand concentration is a specified function of time then the dynamic behavior of the model can be obtained by solving this system of linear differential equations (one equation of the above four can be eliminated because the fractions in the four states must sum to one). However the symmetry in the transitions leads to a significant simplification. If one defines $x_1 = u_1 + u_3$, $x_2 = u_2 + u_4$, $x_3 = u_1 - u_3$, $x_4 = u_2 - u_4$, then the system splits into two two-dimensional systems that can be solved very easily and analyzed in detail. We shall not pursue this here because, as we remark later, this scheme has limited value in the context of adaptation of the relay response of Dd.

In the remainder of this review we focus on the role of cAMP in Dd development through late aggregation, and we begin by discussing the biochemical aspects of signal transduction in the following section. Previous reviews on Dd are given in[17–24].

2 Signal transduction in *Dictyostelium discoideum*

2.1 Introduction

The social amoeba *Dictyostelium discoideum* exemplifies the exploitation of oscillatory signaling for self-organization and survival. These cells normally live in forest soil, where they feed on bacteria[25]. Upon

starvation, amoebae become chemotactically sensitive to cAMP and acquire competence to relay cAMP signals within a period of six hours[26]. After about eight hours, randomly located cells, called pacemakers, start to emit cAMP periodically[27], surrounding cells move towards the cAMP source and relay the cAMP signal to more distant cells. Eventually the entire population collects into mound shaped aggregates containing up to 10^5 cells. The mound elongates to form a slug, which topples over and migrates over the substratum. Meanwhile the cells start to differentiate into prestalk and prespore cells. Differentiation initially starts at random in the mound stage, but by a combination of cell sorting and positional signaling, the prestalk cells eventually end up in the anterior quarter of the slug, while the prespore cells occupy the remaining posterior part. When conditions for fruiting body formation are favorable, the slug tip is extended upwards, the anterior prestalk cells become immobilized in a central stalk tube, which the remaining cells use as a support for upward movement. When the stalk has reached a certain length the prespore cells mature into spores, which remain dormant until they are dispersed and meet with conditions favorable for growth.

The autonomous production and relay of cAMP pulses by starving cells results in a very efficient process of chemotactic aggregation, and cAMP oscillations subsequently organize the transformation of mounds into slugs, the migration of slugs over the substratum, and the culmination into fruiting bodies. These morphological changes are accompanied by a program of stage- and cell-type-specific gene expression, which ultimately causes amoebae to differentiate into accurately-regulated proportions of spore and stalk cells (cf. Figure 5). Extracellular cAMP also plays a crucial role in gene regulation during development. During aggregation, cAMP pulses strongly accelerate expression of components of the cAMP signaling system. During post-aggregative development cAMP directly induces entry into the spore differentiation pathway, and, by inducing the synthesis of a stalk-cell-inducing factor, DIF, cAMP is also indirectly responsible for the differentiation of stalk cells.

The highly allosteric regulation of cAMP synthesis by adenylyl cyclase and its degradation by cAMP phosphodiesterase (PDE) are at the core of oscillatory behavior. The progress in understanding the regulation of both enzymes at the biochemical level has been accompanied by the formulation of theoretical models describing the dynamics and potential for self-organization of the system. Adaptation of cAMP production

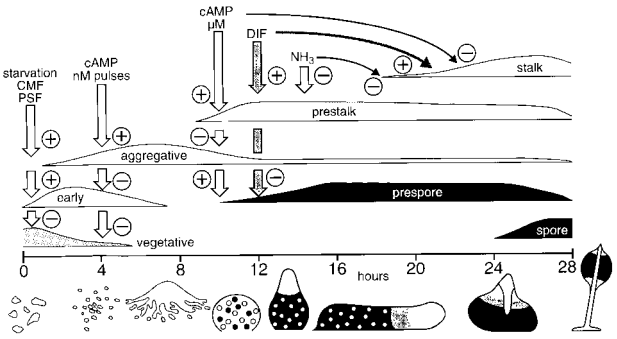

Figure 5. A schematic of the temporal pattern of activation of genes in the development of Dd.

is essential for oscillatory signaling and for relay during aggregation.* Molecular genetic approaches have recently extended our understanding of the complexity of adenylyl cyclase regulation and indicated that earlier theories for adaptation are no longer tenable[28]. In this section we review the current information on cAMP signaling in Dd and discuss mechanisms that have been proposed for adaptation of responses controlling oscillatory signaling and chemotaxis. In the following section we evaluate the validity of existing theoretical models for oscillatory signaling and present the biochemical framework of a model that is consistent with current data. We then review models in which cell movement and oscillatory signaling are incorporated to model the aggregation process.

*The response in Dd to an extracellular signal has many components that are described later. In view of this multiplicity one must carefully define what is meant by adaptation. The observables during the relay response are the intracellular cAMP, the secretion rate, the rate of cell translocation, etc. Early studies showed that the relay response, among others, returns to basal level in the face of constant cAMP stimuli, but this response is the end result of numerous intracellular steps. However, if the intracellular phosphodiesterase that degrades cAMP is not regulated then termination of the relay response requires that the rate of cAMP production returns to the basal level, and hence that either the activity of adenylyl cyclase or a component upstream of it adapts. The possible mechanisms for this adaptation are discussed later. Similar remarks apply to the other pathways from stimulus to response.

2.2 cAMP signal transduction

In higher organisms, a multitude of endocrine and paracrine signals usually activate a limited number of responses in target cells. In Dd a single extracellular signal, cAMP, activates almost all of the major recognized signaling pathways. cAMP is detected by at least four serpentine cAMP receptors (cARs), which show different affinities and different expression patterns during development. The high affinity receptors cAR1 and cAR3 are first expressed before and during aggregation, respectively[29–31]. The low affinity receptors cAR2 and cAR4 are expressed in prestalk cells after aggregation[32,33].

cAMP bound to cARs activates a number of rapid intracellular responses. On a time scale of seconds, cAMP induces excitation and adaptation of guanylyl cyclase. This results in transient accumulation of cGMP, which ultimately controls myosin phosphorylation and pseudopod extension in the chemotactic response[34–37]. On a time-scale of minutes, cAMP causes excitation and adaptation of adenylyl cyclase, resulting in synthesis and secretion of a cAMP pulse. This constitutes the relay response. In addition, cAMP raises intracellular Ca^{2+} levels directly by stimulating Ca^{2+} influx[38–40] and indirectly by activating a phospholipase C_γ (PLC). This enzyme catalyzes the conversion of phosphatidylinositolbisphosphate (PIP_2) into diacylglycerol (DAG) and inositol 1,4,5-trisphosphate (IP_3), and the latter induces Ca^{2+} mobilization[41–44]. In addition, cAMP transiently activates the MAP (mitogen-activated protein) kinase ERK2 with peak activity at 1 min[45,46].

Activation of adenylyl cyclase, guanylyl cyclase and ERK2 by nanomolar cAMP concentrations are mediated by cAR1 in the aggregation stage of development[47,45,46] but may well be mediated by other cARs at other stages of development. Several responses such as cAMP-mediated Ca^{2+} influx, cAMP relay, and the cGMP response were shown to be mediated by at least three of the four cARs (Kim, *et al.* , submitted).At least one response, the cAMP-induced Ca^{2+} influx was shown to be mediated by all four cARs[40,48]. cAMP activation of PLC occurs in the absence of both cAR1 and cAR3 in aggregative cells, and since cAR2 and cAR4 are not yet expressed at this stage, the possibility of a fifth cAR cannot be excluded. Adaptation of PLC is lost in cAR1 null mutants, which indicates that here cAR1 only mediates the inhibitory input[44,49].

In addition to short term responses, which may principally be involved in controlling chemotaxis and cAMP signaling, cAMP regulates the expression of almost all classes of developmentally-regulated genes. Vegetative and early genes are downregulated by cAMP, while genes associated with the aggregation process are induced by nanomolar cAMP pulses. Persistent stimulation with micromolar cAMP concentrations regulates expression of most postaggregative genes. Pharmacological studies have shown that all effects of extracellular cAMP are mediated by cARs[50–52] but due to functional redundancy of the different cARs, it has as yet proved difficult to associate individual cARs with specific gene induction events, except for induction of aggregative gene expression by cAMP pulses, which is mediated by cAR1[53].

Activation of target proteins by serpentine receptors is generally mediated by heterotrimeric G-proteins. These proteins consist of an α subunit that harbors a GTP/GDP binding domain as well as intrinsic GTPase activity, and a complex of a β and a γ subunit. The α subunit and the $\beta\gamma$ complex dissociate after ligand binding to receptors and each have the potential to regulate the activity of (different) target proteins. Most but not all responses mediated by cARs require G-proteins for further transduction. Eight different G_α genes have been identified, but for only two of those (G_2 and G_1) has a role in cAMP signal transduction been established. There is only a single G_β gene in Dictyostelium and G_β null mutants distinguish between G-protein dependent and independent processes[54]. Two G-protein-independent responses mediated by cARs have been identified: cAMP-induced influx of Ca^{2+} ions and cAMP-induced phosphorylation of cAR1[48,55]. G_2 plays a major role in cAMP signal transduction: its α subunits mediate activation of both guanylyl cyclase and PLC[56,44], while its $\beta\gamma$ subunits mediate activation of adenylyl cyclase.[57] G_1 is required for adaptation of PLC activation by cAMP[44] and possibly also for adaptation of guanylyl cyclase activation[58].

Activation of both adenylyl cyclase and guanylyl cyclase by G_2 is indirect; both require an interaction with distinct cytosolic factors[59,60]. The Cytosolic Regulator of Adenylyl Cyclase, CRAC, contains a pleckstrin homology (PH) domain that interacts with the G_β subunit. It is hypothesized that the dissociated $G_{\beta\gamma}$ complex, which is localized in the plasmamembrane, binds with free CRAC from the cytosol, and the complex then activates adenylyl cyclase[61,62]. Adenylyl cyclase activation is significantly reduced in null mutants for ERK2[63] and Ras-GEF, a guanine

nucleotide exchange factor for the monomeric G-protein Ras[64], indicating further complexities in regulation that are not yet understood. The cytosolic regulator of guanylyl cyclase is a cGMP binding protein, that activates guanylyl cyclase when not bound to cGMP, and inhibits the enzyme when bound to cGMP[65].

2.3 Excitation and desensitization pathways for cAMP-induced responses

For many cAMP-induced responses in Dd, desensitization of the response is as important as excitation. Desensitization describes the gradual cessation of the response during persistent stimulation, or a reduction in responsiveness to subsequent stimuli. Complete desensitization may consist of several components, such as loss of ligand binding activity due to sequestration or phosphorylation, without loss of receptor number, internalization and degradation of receptors (down-regulation) and uncoupling of receptors and target proteins (adaptation). Cells regain sensitivity if the stimulus is absent for a sufficient length of time. Degradation of the stimulus is achieved by an extracellular PDE that can either be secreted extracellularly or become anchored to the extracellular face of the membrane[66,67]. Dictyostelium PDE is under complex regulation at both the gene and the enzyme level. The PDE gene is controlled by three different promoters, each of which controls expression at different stages of development: (i.) a low level of expression during growth, (ii.) a high level of expression during aggregation, and (iii.) a moderate level of expression that is restricted to prestalk cells in slugs[68,69]. Post-translational modification of the PDE protein depends on extracellular cAMP levels, with high cAMP levels favoring the formation of the extracellular over the membrane-bound form[70]. PDE activity is furthermore regulated by a glycoprotein inhibitor, PDI, which is secreted by the cells during the first 8 hours of development. PDI can only inhibit the extracellular and not the membrane-bound form of the enzyme, by increasing its K_M from 5μM to 2 mM[71]. Expression of the PDI gene is inhibited by high cAMP levels[72].

Desensitization and re-sensitization of cells is essential for oscillatory cAMP signaling and for orientation of cells in chemotactic gradients. In addition, the expression of aggregative genes can only be induced by a series of cAMP pulses and not by continuous stimulation. The kinetics of excitation and adaptation of both adenylyl cyclase and guanyl cyclase

were studied in great detail in the 1980's by Devreotes and Van Haastert and their coworkers, respectively. These studies provide the biochemical description of the input-output behavior of the cells, but the components of the excitation and adaptation pathways and their kinetic interactions are still being characterized. We summarize the current knowledge of putative excitation and adaptation mechanisms in the following paragraphs.

2.4 Desensitization at the receptor level.

The kinetics of various events that occur at the receptor level are summarized in Table 1 and compared with the excitation and adaptation kinetics of adenylyl- and guanylyl cyclase. During prolonged stimulation with micromolar cAMP concentrations, cAR1 protein is down-regulated by internalization and degradation[73–76].

Down-regulation occurs with a half-time of 15-30 min and it takes several hours for the cAMP receptor to re-accumulate after the cAMP stimulus has been removed. This process is too slow to account for the transient kinetics of responses that occur at a second or minute time-scale, but may help cells to adjust themselves to the variations in signal amplitudes at low or high cell density or during the transition to multicellular aggregates, which is accompanied by cAR1 down-regulation[75].

cAMP also induces more subtle receptor modifications. Kinetic studies indicate the presence of two major subpopulations of cAR1, the rapidly dissociating A-sites (about 96% of total binding activity) and the slowly dissociating B-sites[77,84,85]. In down-regulated cells, the A sites are lost and cAMP can no longer activate adenylyl cyclase, but the B-sites and cAMP activation of guanylyl cyclase are still present, which suggests that the A-sites are responsible for adenylyl cyclase activation and the B-sites for guanylyl cyclase activation[74]. During stimulation with nM cAMP concentrations, the A-sites convert from a high affinity state A^H (K_D = 60 nM) to a low affinity state A^L (K_D = 450 nM) with a half-time of 9 s[77]. Similar alterations in affinity accompany spontaneous cAMP oscillations in suspension and can be induced with either GTP or GDP in cell lysates[86,87]. cAMP also induces a loss of ligand binding activity with a half-time of 1-3 min[88]. Additionally, cAMP receptors become phosphorylated with a half-time of 2.5 min[89,80]. After removal of the stimulus, receptors return to the unphosphorylated state with a half-time of 6 min. These kinetics correlate well with adaptation and deadaptation

Table 1. The rates of various receptor-level events in Dd

Response	Half-time	EC50 cAMP	Half-life reversion	References
Down-regulation	15-30 min	10 μM	1-2 h	[73,76]
A^H to A^L transition	9s	13 nM	2 min	[77]
Loss of ligand binding	1 min	25-50 nM		[78,79]
Phosphorylation cAR1	1-3 min	27 nM	4-6 min	[80]
Activation of AC	1 min	20-50 nM		[8,47]
Adaptation of AC	2-3 min	100 nM	3-4 min	[9,81,82]
Activation of GC	2s	10 nM		[83]
Adaptation of GC	2.4s	10 nM	1-2 min	[82,83]

of adenylyl cyclase (cf Table 1) and in view of the fact that activation of adenylyl cyclase by β-adrenergic receptors adapts in a similar fashion, phosphorylation was widely accepted to be the mechanism of adaptation. However, recent studies show that removal of all phosphorylation sites in cAR1 does not affect adaptation, although cAMP-induced loss of ligand binding no longer occurs[78,90]. Loss of ligand binding appeared to be due to a reduction in cAR1 affinity and may therefore represent the A^H to A^L transition[91,28], albeit that the rate of the A^H to A^L transition ($t_{1/2}$ = 9 s) is much faster than that of loss of ligand binding and cAR1 phosphorylation ($t_{1/2}$ = 1-3 min). Thus one can conclude that cAMP induces cAR1 phosphorylation and consequent reduction of cAR1 affinity, but neither phosphorylation nor the reduction in affinity are responsible for adaptation of adenylyl cyclase.

The remaining 4% of cAR1 binding activity constitutes the B-sites, which are considered to regulate guanylyl cyclase activation. During cAMP stimulation the B-sites interconvert into three forms with different off-rates, fast (F, 2.5 s), slow (S, 15 s) and super-slow (SS, 150s). cAMP binds to B^F, which converts to the B^S form with a half-time of 3s. B^S converts without detectable delay into the B^{SS} form, which slowly re-

turns to the B^F state. During stimulation with cAMP, the capacity of B^S to convert to B^{SS} declines with a half-time of 3 s, while recovery of the B^{SS} form after removal of cAMP occurs with a half- time of 75 s[84,85]. These kinetics agree with the adaptation and deadaptation kinetics of guanylyl cyclase[83,82]. The conversions in the B-sites form the framework for the cycle-adaptation model for guanylyl cyclase regulation (Figure 6): after cAMP (L) binding, the receptor (R) cycles from an inactive state RL (B^F) to an active state R*L (B^S) and activates the response during conversion to the desensitized state R^DL (B^{SS}), which then slowly converts to the inactive state RL[92] . Apart from the correlation in kinetics, there are no experimental data to support this model, and it is also not clear how adaptation is achieved in molecular terms. Nevertheless, as we shall discuss below, this model reproduces the dynamics of the cGMP response best of all the existing models.

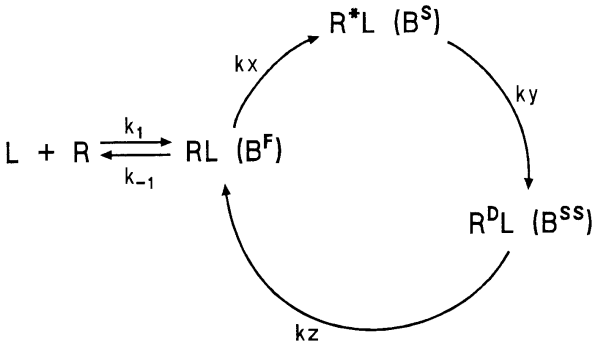

Figure 6. The cycle adaptation model for GC. After Valkema and van Haastert[92] .

To conclude, despite suggestive experimental evidence, adenylyl cyclase adaptation is not regulated at the level of receptor modification. This is a viable possibility in the case of guanylyl cyclase activation, but as we shall see below, additional processes contribute to its transient kinetics here.

2.5 Post-receptor desensitization

Phospholipase C Adaptation of PLC appears to be simple, possibly because it has been least intensively investigated. In Dd cells cAMP induces a transient accumulation of IP_3 that peaks at 5-15s[41,93]. In cell lysates, a cAMP- and GTP-γ-S-stimulated PLC activity can be detected[94], which is lost in $G_{\alpha 2}$ null mutants[44,56]. Remarkably, activation is retained in cAR1 null mutants and in cAR1/cAR3 double null mutants ([44] and Van Haastert, personal communication). Since neither cAR2 and cAR4 are expressed during aggregation, this suggests the existence of a fifth cAR, a thus-far elusive cARx. The partial chemotactic antagonist 3'NH-cAMP can inhibit, but not activate PLC, suggesting that it induces adaptation, but not excitation. The inhibitory effect of 3'NH-cAMP is lost in cAR1 and $G_{\alpha 1}$ null mutants[44]. Taken together, these data suggest that cAMP acting on cARx and $G_{\alpha 2}$ induces excitation of PLC, while cAMP acting on cAR1 and $G_{\alpha 1}$ induces adaptation by inhibiting PLC activity (cf Figure 7). PLC additionally requires Ca^{2+} for activity, which could be provided by the cAMP-induced Ca^{2+} influx or through autocatalytic feedback from the IP_3-induced Ca^{2+} release. It is at present not known whether the Ca^{2+} requirement plays a critical role in cAMP regulation of the enzyme[95].

Guanylyl cyclase Stimulation of cells with either cAMP or the bacterial chemoattractant folate induces a rapid transient accumulation of intracellular cGMP which peaks at 10s[96,97]. cAMP activation of guanylyl cyclase is lost in cAR1 null and in $G_{\alpha 2}$ null mutants[47,98,56]. Folate activation is lost in $G_{\alpha 4}$ null mutants, indicating that its activation pathway is distinct from that of cAMP[99]. This is confirmed by observations that prestimulation with cAMP desensitizes cells for a second cAMP stimulus, but not for a folate stimulus[83];[100]. Multiple mechanisms contribute to the transient kinetics of the response: Figure 8 (i.) cGMP is rapidly degraded by a cGMP-stimulated cGMP-phosphodiesterase (cGMP-PDE); in null mutants for this enzyme, the cGMP response is elevated and prolonged[34,35]. (ii.) Guanylyl cyclase activity is inhibited by Ca^{2+} with an IC_{50} of 200 nM[101]. Concentrations within this range are easily reached by Ca^{2+} influx or IP_3-induced Ca^{2+} mobilization. (iii.) Adaptation at the receptor level. Here a number of possibilities were explored: (a.) linear adaptation, where after ligand binding the receptor first enters into an activated and then a desensitized state, and goes back to the free state via

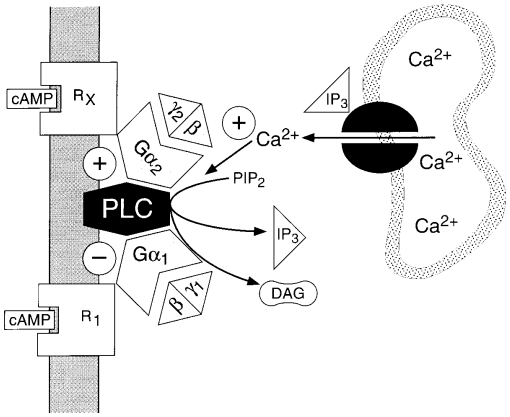

Figure 7. Excitation and adaptation of PLC. cAMP binding to cAMP receptor R_X induces dissociation of the stimulatory G-protein, G_2 into its α and $\beta\gamma$ subunits. The α subunit activates PLC, which catalyzes the production of IP_3 and DAG from PIP_2. IP_3 binds to Ca^{2+} channels in the endoplasmic reticulum, facilitating opening of the channels (see Tang *et al.*[12] for a review of models of this process), and Ca^{2+} ions exert positive feedback on PLC activity. The adaptation pathway is activated by cAMP binding to cAMP receptor R_1, which activates the inhibitory G-protein G_1 to inhibit PLC in an as yet unknown manner.

the same route. (b.) Box adaptation: both in the free and occupied state the receptor can inter-convert into two forms, all four forms displaying different activities[15], this scheme is represented in Figure 4. (c.) The cycle adaptation model, based on the inter-conversion of the B-sites (see Figure 6). Numerical values of the parameters of all reactions involved in activation of guanylyl cyclase and in the three modes of terminating the response were incorporated in a quantitative model to test the relative contributions of the three mechanisms. The model showed that inhibition of guanylyl cyclase activation by Ca^{2+} influx and Ca^{2+} mobilization, in combination with cGMP activation of cGMP-PDE cannot reproduce the rapid transient kinetics of the response. cGMP levels increase rapidly, but decline very slowly. All three schemes for adaptation at the receptor level showed transient kinetics, but only the cycle adaptation model could reproduce experimental data that the kinetics of the response are independent of the stimulus concentration[92].

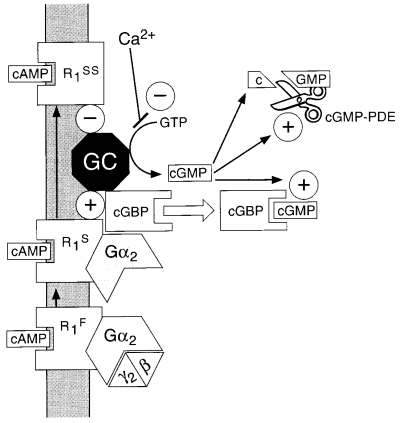

Figure 8. Excitation and adaptation of guanylyl cyclase. cAMP induces the inactive cAMP receptor form R_1F to convert into R_1^S, which induces dissociation of the stimulatory G-protein G_2. The $G_{\alpha 2}$ subunit, in combination with the cGMP binding protein, cGBP, activates guanylyl cyclase (GC) to produce cGMP. Multiple processes terminate the response: (i.) R_1^S converts to the desensitized receptor form R_1^{SS}, which inhibits GC in an unknown manner, (ii.) cGMP binds to the cGBP, causing cGBP to translocate from the membrane to the cytosol, which terminates activation of GC. (iii.) cGMP activates a cGMP dependent cGMP phosphodiesterase (cGMP-PDE), which rapidly degrades cGMP. (iv.) Ca^{2+}, mobilized by other cAMP activated signaling pathways, inhibits GC directly.

Recently a fourth potential mechanism for adaptation of guanylyl cyclase was uncovered. A cytosolic cGMP binding protein is required for guanylyl cyclase activation in its native state, but becomes an inhibitor of guanylyl cyclase, when bound to cGMP[65]. The quantitative contribution of this response to the three others has not yet been evaluated. Folate- and cAMP-induced cGMP responses are not additive, suggesting that both use the same guanylate cyclase pool. In combination with observations that cells that are adapted to folate can still respond to cAMP, this suggests that the major contribution to total desensitization is adaptation at the receptor level and not at the level of guanylyl cyclase itself[100].

Adenylyl cyclase cAMP induces cAMP production in intact cells which peaks at 2-3 min and returns to basal levels within 3-8 min[8]. Prestimulation with cAMP leaves cells desensitized to the same stimulus for a

couple of minutes[81]. Activation of adenylyl cyclase by cAMP is medi-

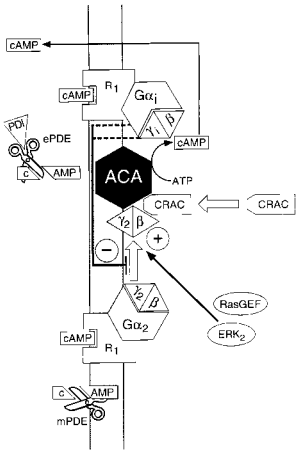

Figure 9. Excitation and adaptation of adenylyl cyclase. cAMP binding to cAMP receptor R_1 induces dissociation of G_2 into its α_2 and $\beta\gamma_2$ subunits. Dissociation exposes PH (pleckstrin homology) binding sites on $\beta\gamma_2$ which bind to the PH domain of CRAC. CRAC serves as an adaptor which links $\beta\gamma_2$ to adenylyl cyclase A (ACA), which is then activated. The Ras guanine nucleotide exchange factor, Ras-GEF has an essential, but as yet nebulous, role in ACA activation. cAMP is rapidly secreted to the exterior of the cell, where it is degraded by both an extracellular (ePDE) and membrane bound (mPDE) cyclic nucleotide phosphodiesterase activity. ePDE can be inhibited by a glycoprotein PDI that is secreted as long as cAMP levels are low. ACA activation is hypothesized to be terminated by R_1 activation of an inhibitory G protein G_i, whose α_i or $\beta\gamma_i$ subunits prevent or terminate dissociation of G_2.

ated by cAR1 and the $\beta\gamma$ subunits of G_2[47,57]. The liberated $\beta\gamma$ complex is considered to bind to the pleckstrin-homology domain of CRAC and to recruit CRAC from the cytosol to the plasmamembrane[61,62,102]. In other systems, target proteins that are activated by $\beta\gamma$'s usually harbor an intrinsic pleckstrin homology domain[103,104]. CRAC is therefore considered as an adaptor that links the Dd $\beta\gamma$'s to adenylyl cyclase. In ras-GEF null mutants, GTP-γ-S no longer generates CRAC binding sites, suggesting that ras-GEF is essential for formation of free $\beta\gamma$ subunits.

It is as yet far from clear how adaptation of adenylyl cyclase is achieved. Figures 9 10 summarize what is known. In cAR1 null mutants, adapta-

tion of adenylyl cyclase is lost, while excitation requires higher cAMP concentrations, because it can be taken over by the low levels of cAR3 that are present in the cells. This indicates that both excitation and adaptation are mediated by cAR1[105,47]. This would agree perfectly with the scheme for adaptation by receptor phosphorylation that was discussed above, which is now undermined by findings that cells with mutated receptors, that cannot be phosphorylated, adapt normally[90]. Other recent experiments also indicate that receptor modification is not sufficient to cause adaptation: GTP-γ-S activates G-proteins directly and bypasses the requirement for receptor activation. However, in cells that were prestimulated by cAMP, GTP-γ-S activation of adenylyl cyclase is lost[105]. It appeared that in prestimulated cells GTP-γ-S can no longer generate CRAC binding sites, which suggests that the occupied cARs interfere with the formation of free $\beta\gamma$s[62].

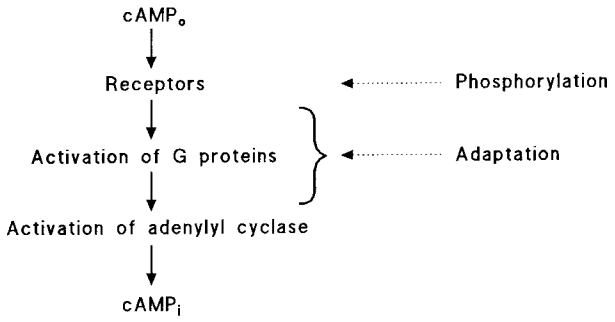

Figure 10. A schematic of the major steps in cAMP signaling at which various processes occur.

Experiments with pertussis toxin, an agent that causes ADP-ribosylation and inactivation of G-proteins in vertebrates, suggest that an inhibitory G- protein mediates adaptation of adenylyl cyclase. In pertussis-toxin-treated cells, cAMP production in response to a constant stimulus is no longer transient and a second response can be triggered shortly after an initial response has been evoked. It was concluded that in the presence of pertussis toxin, adaptation no longer occurred because the inhibitory G-protein was inactivated. Both receptor phosphorylation and activation and adaptation of guanylyl cyclase were normal in pertussis toxin treated cells[106,107]. There is as yet no candidate gene for an inhibitory G-protein,

since none of the eight cloned G-proteins carries the consensus sequence for ADP-ribosylation. The evidence for involvement of an inhibitory G-protein would be corroborated if it could be demonstrated that pertussis toxin would annihilate the inhibitory effect of cAMP prestimulation on the GTP-γ-S induced formation of CRAC binding sites. For the present, adaptation by an inhibitory G-protein remains an attractive possibility.

3 Models of signal transduction, relay and oscillations in *Dictyostelium discoideum*

There are several aspects to signal transduction and relay that every plausible model must capture. Firstly, the elegant experiments by Devreotes *et al.* [7–9] show that when the extracellular cAMP in a perfusion chamber undergoes a step increase, the transduction/relay system produces a pulse of cAMP in response and then adapts to the new constant extracellular level (cf the response predicted by the Tang-Othmer model shown in Figure 1(a): the experimental result is very similar). In addition, a system that is adapted to one stimulus level maintains sensitivity to further stimulation (cf Figure 1(b)). These results imply that a minimal model of the transduction/relay system in which the rates of change of intracellular state variables depend only on the present state of the system must incorporate at least two intracellular variables, one which adapts in the sense that it returns to its basal level after stimulation, and one variable which effects the adaptation but itself does not return to its pre-stimulation level. Certainly the primary intracellular variable should be cAMP, but the second intracellular variable in such a minimal model is not easily determined. The system discussed in the Introduction has some of the necessary features of a minimal model; there one can identify u_1 with cAMP and leave the identity of the second variable unspecified. As we noted earlier, this model is excitable but it also shows a graded response. It can however be too robust, depending on the function f. For example, if f is a linear function of the stimulus and excitation is fast relative to adaptation, then the response is essentially proportional to the stimulus. Thus a 10-fold step in the stimulus will produce an approximately 10-fold increase in the response, but this is not what is observed in Dd (cf 1(b)). Certainly there is always saturation in the transduction/relay system not exhibited by this simple scheme when f is a linear function,

but as we shall see later, it can be incorporated by making f a saturating function of the stimulus level.

Experimental results on the dynamics of cellular suspensions provide data for further tests of any model. Suspension experiments differ from perfusion experiments because the extracellular cAMP concentrations are not clamped, and thus self-stimulation of the cells can occur. One can predict on theoretical grounds that such a positive feedback loop may produce oscillations if coupled with a mechanism that terminates the response. If cyclic AMP is added to the suspension at a sufficiently high rate the oscillations are suppressed completely. This is consistent with the observations of Devreotes *et al.* [7–9] discussed previously, since the two experimental configurations are essentially the same in this case.

3.1 A comparison of existing models

Twenty years ago models of relay and oscillations in Dd were highly speculative because little data on the molecular interactions that govern oscillatory signaling were available. One of the earliest models[108] was based on positive feedback of the products of the enzymes adenylyl cyclase (cAMP) and ATP-pyrophosphohydrolase (5'AMP) on ATP degradation and cAMP synthesis, respectively. The model also included PDE and could generate periodic oscillations of cAMP synthesis with a period of 3-5 minutes. However in this model there was no role for extracellular cAMP; the oscillations were generated through interactions of the intracellular components. Thus this model could not display adaptation or other necessary features, and it was replaced by a model based on receptor-mediated positive feedback of cAMP on adenylyl cyclase activation[109,110]. In both models ATP depletion by cAMP production was required to sustain oscillatory behavior, but it is known that the production of nanomolar cAMP pulses has little effect on the millimolar ATP concentrations, that are produced by respiration, and thus these models are no longer viable. A more abstract two-component model which directly incorporates adaptation of cAMP production by making the rate of synthesis proportional to rate of change of extracellular cAMP, rather than to the level of extracellular cAMP itself, was formulated at about the same time[111]. Though it is far removed from the biochemistry as it is now known, this model is capable of reproducing several key aspects of Dd behavior.

Several second generation models were based on the observations by Devreotes and coworkers that the kinetics of adenylyl cyclase adaptation and deadaptation correlated well with those of cAR1 phosphorylation and dephosphorylation. As noted earlier, Knox *et al.* [15] formulated a model for adaptation (called the K-model hereafter) that was based on the assumption that in the presence of ligand, receptors can exist in four interconvertible states, each of which contributes with a certain weight to a downstream activity (cf Figure 4). Thus the 'physiological' response is given by

$$\mathcal{R} = \sum_{i=1}^{4} a_i u_i$$

where as before, u_i is the fraction in the i^{th} state. If an intracellular effector binds to each form of the receptor and the total amount of effector is constant, then the weight a_i is taken to be the affinity constant of the i^{th} receptor state for the effector. Thus this model assumes that the binding of effector occurs according to Figure 11. For Dd, the R^D and

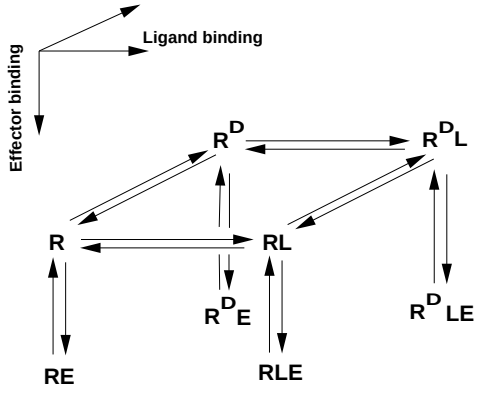

Figure 11. A minimal network associated with the K model.

R^DL forms represent the phoshorylated states of the receptor. The various rate constants for the interconversions and the dissociation constants of the R^D and R forms were experimentally determined[80,89] and used to calculate the weight factors, which were treated as association constants of the receptor with adenylyl cyclase. When simulated numerically, the model could generate activity in response to a change in extracellular

cAMP and adapt on an appropriate time scale. However, the assumption that the weights are simply the K_Ds for binding to the enzyme is a serious limitation; it is based on the assumption that the various forms of the receptor do not bind ligand when bound to effector, or in other words, that there are no horizontal transitions in the lower tier in Figure 11. Moreover, the analysis assumes implicitly that the various forms of the effector-receptor complex do not bind to other intracellular components, for otherwise these species are coupled to the intracellular species and the analysis presented is no longer valid. While this assumption is appropriate in the original context of ligand binding to membrane channels, it is less appropriate in the context of Dd ligand binding.

To formulate a model for oscillatory signaling, Barchilon and Segel[112] embedded the model for adaptation by receptor modification into the Goldbeter-Segel[109] model described above. Oscillations and signal relay could be generated, but only by using parameter values that deviated substantially from the experimentally-determined values[80]. Martiel and Goldbeter[113] used a modification of the K-model, and assumed that only the RL form can activate adenylyl cyclase. Since some form of positive cooperativity was required to generate oscillatory behavior, they further assumed that only a dimerized form of RL, in which two RL units first associate, could activate the enzyme. Intra- and extracellular PDE activity and cAMP secretion were also incorporated in the form used in the Goldbeter-Segel model. This model (hereafter referred to as the MG model) successfully simulates certain aspects of relay and oscillatory behavior of cells in a semi-quantitative fashion. While it can be tuned to predict the response to a single stimulus, it does not correctly reproduce the response to a sequence of step increases such as are used in the perfusion experiments[114]. Moreover, in contrast to experimental data[7], both the MG and K model show incomplete adaptation at low stimulus concentrations (see also[92]). However, these deficiencies might have been remedied and considering the fact that receptor modification was generally accepted as the cause of adaptation, the MG model was until recently widely used as the framework for models on aggregation behavior and slug morphogenesis[115–117]. However, in view of the experimental evidence discussed above the MG model is no longer valid for several reasons, the major ones being: (i.) receptor modification by phosphorylation is not essential for adaptation, and (ii.) adaptation of adenylyl cyclase occurs at the level of production of free $\beta\gamma$'s and not at the level of receptor

activation. Thus it is certainly necessary to incorporate G-proteins into any model that is to be biochemically-realistic.

At about the same time as the box adaptation models were proposed, Monk, Rapp and Othmer[118,4] formulated a model for adaptation that was based on inhibition of adenylyl cyclase by the cAMP induced Ca^{2+} influx and Ca^{2+} mobilization from internal stores. This model, as modified in Monk and Othmer[119], could reproduce full adaptation over a wide concentration range as well as repeated responses to a stepwise increase in stimulus concentration. Earlier data suggested that Ca^{2+} inhibits cAMP relay in Dd, and Ca^{2+} inhibition of mammalian adenylyl cyclases is well documented. However, recent experiments show no direct inhibitory effects of Ca^{2+} on Dd adenylyl cyclase[120] .

Caffeine inhibits cAMP-induced activation of Dd adenylyl cyclase and decreases the excitability of the cells[121]. To study whether cAMP production by adenylyl cyclase could be responsible for adaptation, cells were pretreated with caffeine, while being exposed to a first stimulus and then challenged with a second stimulus in the absence of caffeine. Despite the fact that no cAMP was synthesized in response to the first stimulus, the cells still adapted and could not respond to the second stimulus[9]. This indicates that adaptation is independent of adenylyl cyclase activation.

Evidence for the involvement of G-proteins in signal transduction led Tang and Othmer[5] to propose a model based on G-proteins. This model, which will be described in more detail later, involves two G-proteins: a stimulatory one, G_s, whose α subunit activates the cyclase and an inhibitory one, G_i, that competitively interferes with the stimulatory pathway to prevent activation of G_s. The TO model reproduces excitation and adaptation kinetics and relay quantitatively correctly, but since the competitive interference occurs at the level of the receptor, it cannot explain the recent observations on adenylyl cyclase regulation in cAR1 null mutants. However, with some minor alterations the model can be turned into a scheme that is consistent with the known biochemical steps. (i.) Recent data indicate that cAR1 mediates both excitation and adaptation of adenylyl cyclase[47]. This poses a problem for the TO model unless the association of the receptors with the other membrane components alters their affinity for G_s and/or G_i. Alternatively, if R_s and R_i are in fact the same unit then there is no reason why the activated G_i would preferentially bind to the receptor unless it is modified during ligand binding. The

same cAR for G_s and G_i activation is possible if, instead, G_i interferes with a process downstream of cAR. Since adaptation was shown to interfere with generation of CRAC binding sites, this could be the site of inhibition by G_i rather than at R_s. (ii.) It is assumed that the CRAC binding sites are the free $G_{2\beta\gamma}$s[62]. Since activation of G_is will also yield $G_{i\beta\gamma}$s, one must therefore assume that these are different from the $G_{2\beta\gamma}$s and cannot generate CRAC binding sites. This difference would have to reside in the γ subunit or in some post-translational modification of β. In Figure 12, we present the TO model and a modified form of the TO model (SO), that is consistent with current data. Here cAR1 activates both G_2

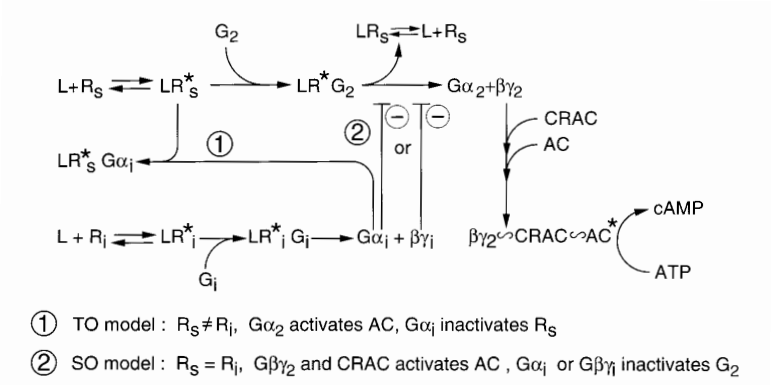

Figure 12. Models for regulation of adenylyl cyclase by stimulatory and inhibitory G-proteins. Occupancy of the stimulatory receptor R_s activates adenylyl cyclase AC via the G_β subunits of the G-protein G_2. Binding of cAMP to the inhibitory receptor produces an activated G-protein that interacts with R_s and prevents its activation of G_2. In the alternative SO model, R_s is the same species as R_i, the $G_{i\alpha}$ or $G_{i\beta\gamma}$ terminates dissociation of G_2.

and G_i and either the $G_{i\alpha}$ or $G_{i\beta\gamma}$ inhibits the activity of the $G_{2\beta\gamma s}$. This could for instance occur if either component of G_i would activate a GTPase activating protein (GAP), that would act on G_2 to accelerate GTP hydrolysis and reassociation with $G_{2\beta\gamma}$. GAPs, though formerly associated with inactivation of monomeric G-proteins, were recently shown to act on heterotrimeric G-proteins as well[122]. For G_i to inactivate dissociation of G_2, we have to assume that formation of the LR*G_i complex is slower than that of the LR*G_2 complex. Alternatively one could assume that the delay in G_i activation is the result of some form of cAR1 modi-

fication with G_i only binding to the modified form. Not all components, such as Ras-GEF, that are known to be involved in adenylyl cyclase activation are incorporated in this scheme. This would be very difficult since we do not know the function of these components in adenylyl cyclase activation. Since Ras-GEF seem to be required for the formation of CRAC binding sites, it could also be a putative target for G_i.

Ultimately the correct model can only be formulated after a complete elucidation of all the components of AC regulation and their dynamic interactions. The MG model, the RMO and MO models, and the TO models for oscillations in suspensions have been used as frameworks to model generation of cAMP waves in aggregation fields and slugs, and with incorporation of cell movement to model the processes of aggregation and slug morphogenesis. As described above, none of these models has the correct molecular background and it may yet take a while before all molecular interactions involved in adenylyl cyclase regulation are elucidated. Should work on oscillatory behavior be arrested until this distant goal is achieved? We think not. Wave propagation and cell aggregation reflect the behavior of the system at the supra-cellular level. Provided that the model faithfully reproduces the input-output behavior of the cells, it is at this level for most purposes not essential to know how that behavior is exactly produced.

3.2 Relay and oscillations in a toy model

It is often difficult, even in relatively simple models, to understand quantitatively how properties such as adaption arise in a model, and how changing the balance between different processes changes the dynamics. Therefore, before discussing a realistic model for adaptation and relay in Dd, we analyze a toy model that contains some of the essential features but is still very easy to understand. Consider the equations (6) for adaptive behavior given earlier, but modified so as to shift the basal level of u_1:

$$\begin{aligned} \frac{du_1}{d\tau} &= (f(S(\tau)) - (u_1 + u_2) + 10)/\tau_e \\ \frac{du_2}{d\tau} &= (f(S(\tau)) - u_2)/\tau_a . \end{aligned} \tag{8}$$

Given a suitable choice for $f(\cdot)$, the u_1 component shows adaptive behavior analogous to that of $cAMP_i$ in Dd. Let u_o stand for the $cAMP_o$: then

a suitable choice for the transduction function f is

$$f(S(\tau)) = \frac{au_o}{a_1 + u_o}.$$

One interpretation of this form is that the intracellular signal is proportional to the fraction of cAR1 receptors occupied with cAMP.

In order to use this system to gain insight into suspensions, we have to add an equation for the evolution of cAMP_o. This equation should describe the changes in cAMP_o due to secretion and to degradation by membrane-bound phosphodiesterase (mPDE) and extracellular phosphodiesterase (ePDE), and we do this as follows.

$$\frac{du_o}{d\tau} = (a_2 u_1 - \frac{a_3 u_o}{a_4 + u_o} - a_5 u_o^2)/\tau_c \tag{9}$$

The first term represents the change in cAMP_o due to secretion, while the last two describe degradation.

For a suitable choice of the parameters these three equations can mimic both the perfusion and suspension experiments for Dd. In Figure 13(a) we show the adaptive response of (8) to a step change in u_o, while in Figure 13(b) we show that the three-dimensional system consisting of (8) and (9) can be made oscillatory with a suitable choice of a_3. If the strength of the feedback loop is decreased sufficiently by increasing either a_3 or a_5 sufficiently, the system has a stable steady state and no periodic oscillations. Thus this simple system displays the essential characteristics of the relay and suspension behavior in Dd. Next we describe some of the behavior of the Dd model.

3.3 Relay and oscillations in the TO model

At present the TO model reproduces the input-output behavior of cells most accurately and is closest to a biochemically-correct model, and therefore we shall use it in our discussion of relay, oscillations, wave propagation and cell aggregation. The main steps in the signal transduction and cAMP production components of this model are shown in Figure 14. In the model there are three major pathways in the transduction of and adaptation to an extracellular cAMP signal (L) in perfusion experiments. In the stimulus pathway, cAMP binds to receptors R_s, and the complex LR_s catalyzes the activation of the stimulatory G-protein G'_s. This in turn binds with the inactive form of adenylyl cyclase (UC) and produces the activated form of adenylyl cyclase ($G'_s AC$).

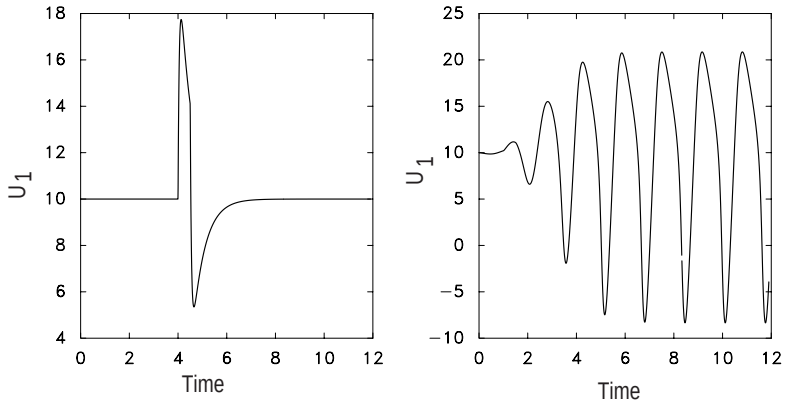

Figure 13. (a) The step response of (8). We impose a step change in u_o from 0 to 0.5 beginning at t=1. Parameter values: $a = 30., a_1 = 1., \tau_e = 0.05, \tau_a = 0.5$ In (b) we use the same parameters and in addition set $a_2 = 0.6, a_3 = 10., a_4 = 0.6, a_5 = 0.05, \tau_c = 0.25$.

A GTP-ase activity intrinsic to the α subunit of the G-protein terminates the activation. In the inhibitory pathway, an inhibitory G-protein G_i' is produced by analogous steps. However, the symmetry between the pathways is broken at this point, because G_i' binds with LR_s, and in this bound form LR_s cannot activate G_s. Finally in the pathway for the production and secretion of cAMP, the activated adenylyl cyclase ($G_s'AC$) catalyzes the turnover of ATP to intracellular cAMP ($cAMP_i$). $cAMP_i$ in turn is hydrolyzed by intracellular phosphodiesterase ($iPDE$) or is secreted into the extracellular medium($cAMP_o^*$). Here the '$*$' on $cAMP_o^*$ is to distinguish the secreted cAMP from the stimulatory cAMP in the perfusion solution, which is denoted by L. The biochemical reactions as well as kinetic parameters involved are given in Figure 14.

(i) The Stimulus Pathway

$$
\begin{aligned}
L + R_s &\underset{k_{-1}}{\overset{k_1}{\rightleftarrows}} LR_s \\
LR_s + G_s &\underset{k_{-2}}{\overset{k_2}{\rightleftarrows}} LR_sG_s \\
LR_sG_s + GTP &\xrightarrow{\hat{k}_3} LR_s + G'_s + GDP + \beta\gamma \\
G'_s + UC &\underset{k_{-4}}{\overset{k_4}{\rightleftarrows}} G'_sAC \\
G'_s &\xrightarrow{k_5} \alpha_sGDP + P_i \\
G'_sAC &\xrightarrow{k_5} \alpha_sGDP + UC + P_i \\
\alpha_sGDP + \beta\gamma &\xrightarrow{k_6} G_s
\end{aligned}
$$

(ii) The Inhibitory Pathway

$$
\begin{aligned}
L + R_i &\underset{h_{-1}}{\overset{h_1}{\rightleftarrows}} LR_i \\
LR_i + G_i &\underset{h_{-2}}{\overset{h_2}{\rightleftarrows}} LR_iG_i \\
LR_iG_i + GTP &\xrightarrow{\hat{h}_3} LR_i + G'_i + GDP + \beta\gamma \\
G'_i + LR_s &\underset{h_{-4}}{\overset{h_4}{\rightleftarrows}} LR_sG'_i \\
G'_i &\xrightarrow{h_5} \alpha_iGDP + P_i \\
LR_sG'_i &\xrightarrow{h_6} H + R_s + G'_i \\
LR_sG'_i &\xrightarrow{h_5} LR_s + \alpha_iGDP + P_i \\
\alpha_iGDP + \beta\gamma &\xrightarrow{h_7} G_i
\end{aligned}
$$

(iii) The Production and Secretion of Intracellular cAMP

$$
\begin{aligned}
G'_sAC + ATP &\underset{l_{-1}}{\overset{l_1}{\rightleftarrows}} G'_sAC - ATP \\
G'_sAC - ATP &\xrightarrow{l_2} cAMP_i + G'_sAC + PP_i \\
cAMP_i + iPDE &\underset{l_{-3}}{\overset{l_3}{\rightleftarrows}} cAMP_i - iPDE \\
cAMP_i - iPDE &\xrightarrow{l_4} AMP + iPDE \\
cAMP_i &\xrightarrow{l_5} cAMP_o^*
\end{aligned}
$$

Figure 14. The kinetic steps in the Tang-Othmer model

These steps are applicable in the context of perfusion experiments; additional steps must be added to account for cAMP degradation in the extracellular medium in the context of suspension experiments. The interested reader is referred to the original papers for details[5,123].

If it was necessary to retain differential equations for all species in this scheme there would be a very large number of equations and it would be difficult to obtain qualitative insights into the system. Fortunately however, parameter estimates show that some steps are fast compared to others. As a result, one can reduce the governing equations for well-mixed suspensions to five primary variables, which are shown in Figure 15, using the mathematical technique of singular perturbations (which is related to the pseudo-steady-state hypothesis (PSSH) for fast reactions) . Details of how this reduction is done can be found in the original papers, where the reduction was done in two steps, first to eight variables[5]

and then to five[123]. In the reduced scheme shown in Figure 15 there are four internal variables, compared with the minimal number of two as discussed earlier. For perfusion experiments the extracellular cAMP is a specified function of time and the system reduces to four equations. The components of primary interest in the following equations are the intra- and extracellular cAMP, whose concentrations are denoted by C_i and C_o, respectively. The variables w_i, i = 1,2,3 represent intermediate species in the signal transduction pathway, as shown in Figure 15. In the following equations Greek letters and lower case c's represent constants. The definitions of the following parameters differ from those used earlier[123]: $L_5 = (l_{-5} + l_5^*)/(l_5[ATP])$, $\Gamma_5 = \gamma_5/(1 + L_5) = 2.4$, $L_7 = l_1/(l_{-1} + l_2)$ and $\Gamma_7 = 1 + L_7 = 1.091$; the remaining parameter values are the same as those in Tang and Othmer[123]. Many of the parameters in this model can be obtained from the literature, but the remainder must be estimated.

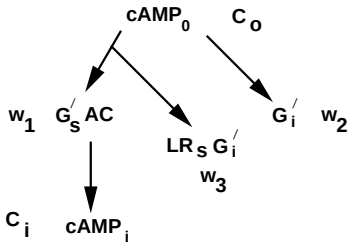

Figure 15. The reduced network for the five primary variables in the TO scheme. The symbols C_i , C_o and w_i i = 1,2,3 beside a species corresponds to the symbol used in the equations at (10).

$$
\begin{aligned}
\frac{dw_1}{d\tau} &= \alpha_4 u_2(1 - w_1) - w_1 \\
\frac{dw_2}{d\tau} &= \beta_2\beta_3 c_2 u_4(1 - w_2 - c_3 w_3) - \beta_5 w_2 + \beta_6 c_3 w_3 - c_3\beta_4 u_1 w_2 \\
\frac{dw_3}{d\tau} &= -(\beta_5 + \beta_6) w_3 + \beta_4 u_1 w_2 \qquad (10) \\
\frac{dC_i}{d\tau} &= \gamma_1\gamma_2 w_1 + \Gamma_5(1 - \Gamma_7 w_1) - \gamma_4 \frac{C_i}{C_i + \gamma_3} - sr(C_i) \\
\frac{dC_o}{d\tau} &= \frac{\rho}{1 - \rho}\left(sr(C_i) - \gamma_7 \frac{C_o}{C_o + \gamma_6} - \gamma_9 \frac{C_o}{C_o + \gamma_8} \right).
\end{aligned}
$$

To illustrate the interpretation of terms in these equations, consider the fourth equation, that for the change in cAMP$_i$. The first term represents the production of cAMP$_i$ via the activated cyclase, the second term represents the basal production of cAMP$_i$, and the third term represents the rate at which cAMP$_i$ is secreted. As a result of applying the PSSH, some rapidly-varying variables are related to others via algebraic equations. Most are eliminated completely, but it is convenient to retain some of these quantities for the purpose of explaining how the system functions. They are the fraction of R$_s$ bound, the amount of activated G$_s$, and the fraction of R$_i$ bound, which in dimensionless form are given by

$$u_1 = \frac{\alpha_0 C_o + (\beta_5 - \alpha_0 C_o) w_3}{\alpha_1 + \alpha_0 C_o + \beta_4 w_2} \qquad u_2 = \frac{\alpha_2 \alpha_3 c_1 u_1 (1 - w_1)}{1 + \alpha_4 + \alpha_2 \alpha_3 c_1 u_1 - \alpha_4 w_1}$$

$$u_4 = \frac{\beta_0 C_o}{\beta_1 + \beta_0 C_o}.$$

A qualitative description of how this system responds to stimuli is as follows. Suppose first that cAMP$_o$ is clamped, and that the system is adapted to a given level of cAMP$_o$. A change in cAMP$_o$ is reflected in the stimulatory (inhibitory) pathway via a change in the term $\alpha_o C_o$ ($\beta_o C_o$) that appears in the fraction u_1 (u_4) of stimulatory (inhibitory) receptors bound with ligand. On the stimulatory side, this input is immediately reflected in a change in u_2 (G'_s) because the activation is fast. This increases the amount of activated cyclase (w_1), and this in turn produces more $cAMP_i$ and the relay response. Simultaneously, but on a slightly slower time scale, the inhibitory pathway activates the inhibitory G-protein G_i , which competitively interferes with the production of G'_s, and hence the activation of the cyclase. This interference then leads to adaptation in the model, and the combination of relay and adaptation qualitatively explains the response in the context of perfusion experiments. When cAMP$_o$ is not clamped a positive feedback loop is created via the secretion of cAMP$_i$. Depending on how it is tuned, this feedback system leads either to amplification of a pulse of cAMP$_o$ or to sustained oscillations. Using experimentally-determined parameters where possible, and estimates for the remaining parameters, this system predicts a time course of cAMP levels and secretion rates that agrees both qualitatively and quantitatively with experimentally-observed results in perfusion and suspension experiments.

In Figure 1 we show the response to a single step change and to a four-step increase in cAMP$_o$ in a simulated perfusion experiment, using the TO model[123]. The response shown there is based on experimental parameters where they are known, and one sees that the system does not adapt fully at large stimuli. However this can be corrected by a simple modification of the dynamics. In Figure 16 we show the response when the speed of the inhibitory channel is reduced by a factor of 10 and the sensitivity to cAMP$_o$, as reflected in α_o and β_o, is reduced. One sees there that adaptation is very good at all stimulus levels, both for cAMP$_i$ and the secretion rate. Clearly the relative peak heights change as compared with Figure 1, but the results shown are still well within the experimentally-observed range. In any case, the cAMP and secretion responses peak at about 1 min after stimulation, which is as observed experimentally[124].

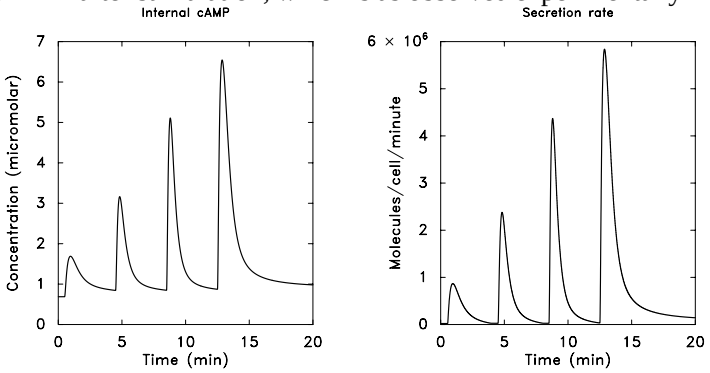

Figure 16. The cAMP$_i$ (a) and secretion rate (b) predicted by the TO model when the dynamics are modified as described in the text. The total secretion over 20 minutes for the rate shown in (b) is 1.42×10^7 molecules.

To understand how the dynamics may vary with the developmental stage of the cell, we note that there are several parameters which are known to vary with the developmental stage (cf. section 2). Following starvation the sensitivity to cAMP$_o$ increases, and in the model this is reflected by an increase in the parameter γ_2[123]. Three qualitatively-distinct types of dynamics have been found in numerical simulations of suspensions for different values of γ_2. When γ_2 is small the system is not excitable, as judged by the amplification of a cAMP pulse. As γ_2 increases the cells become excitable and hence relay competent. Finally a stable oscillation arises when γ_2 exceeds a critical value, and the sta-

ble oscillatory response persists over a wide range of γ_2. This behavior matches the experimentally-observed stages of Dd cells.

For a fixed γ_2, the intensity of the response to a stimulus is determined by the strength and duration of that stimulus, *i.e.*, the response is graded. In Figure 17 we show the responses for fixed $\gamma_2 = 0.175$ and different concentrations in the stimulus. At stimulus levels of 0.001μM/min, 0.005μM/min, 0.01μM/min, and 0.1μM /min, the corresponding maximum extracellular cAMP levels reached are 0.09μM, 0.38μM, 0.62μM, and 1.09μM. From this we see that although this system is excitable in the usual sense, the threshold for cAMP stimuli is not sharp; as the intensity of the stimulus increases the secretion rate and hence the extracellular cAMP increases in a graded manner. This happens in other systems as well. For instance, in cardiac myocytes calcium stimuli open RyR channels in the sarcoplasmic reticulum membrane. While they are open, these channels release stored calcium into the cytoplasm, which increases in a graded manner in response to stimuli[125,11].

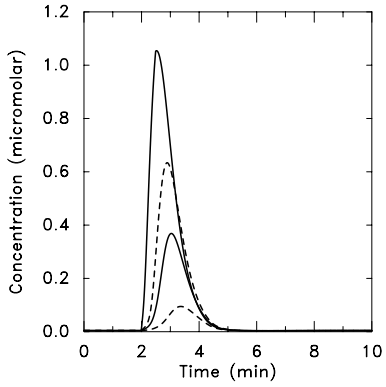

Figure 17. Graded responses of extracellular cAMP for different levels of the cAMP stimulus. Square wave stimuli of extracellular cAMP of four different amplitudes are applied at $t = 2$ min for 0.5 min duration. No clear threshold exists for the system. The amplitudes of stimuli are 0.001 (dashed line), 0.005 (solid line) 0.01 (dashed line), and 0.1 (solid line). $\gamma_2 = 0.175$ in all cases.

As cells age the amount of adenylyl cyclase expressed increases, and for sufficiently large γ_2 a suspension oscillates periodically, as is shown in Figure 18(a). In this figure the time delay between a peak of the intra-

cellular cAMP and the extracellular cAMP is about 0.5 minutes, which agrees with the experimental results reported in[126,127]. The amplitudes of the oscillations are in the same range as the experimental data, which are shown in Figure 18(b). Of course the period of the oscillations varies

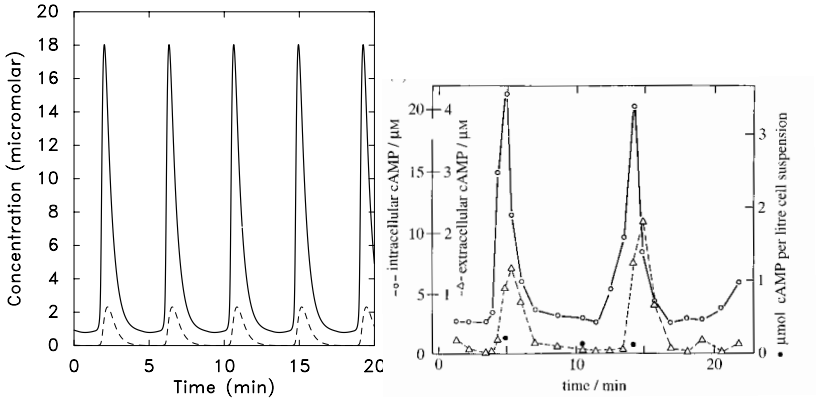

Figure 18. (a) Periodic oscillations in a numerical simulation of suspension experiments for $\gamma_2 = 0.4$. Solid line: intracellular cAMP; dashed line: extracellular cAMP. (b) Experimental measurements of intracellular $(\circ)$ and extracellular $(\triangle)$ cAMP concentration. Redrawn from Figure 2 of Gerisch and Wick[126].

as the parameters in the model are changed, and in Figure 19 we show this variation for two of the most important parameters, the excitability (as measured by γ_2), and the density of the cells in suspension. One sees in Figure 19(b) that the period decreases significantly at higher densities. Although it has not been checked explicitly, similar density dependence probably exists in aggregation fields as well.

3.4 Stochastic effects in signal detection

The preceding models all assume that the system is deterministic, but certainly the number of cAMP molecules near a cell fluctuates, hence the number of bound receptors and downstream components all fluctuate. In this section we address the importance of fluctuations on the extracellular side of the signal detection/transduction pathway.

For concreteness we represent a cell as a cylinder of radius $r_o = 5.5\mu$ and 2μ high, immersed in a fluid layer of that height. To determine

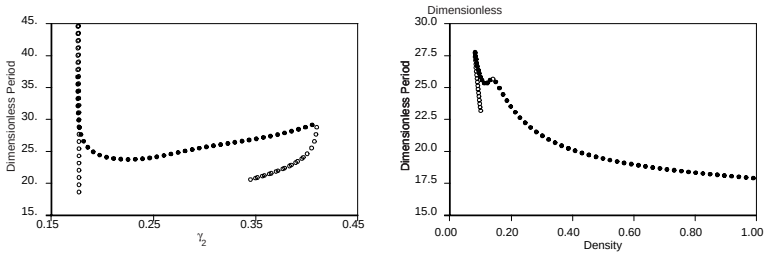

Figure 19. (a) The dimensionless period of the oscillatory solutions as a function of the excitability parameter γ_2. (b) The dependence of the period on the cell density for a fixed $\gamma_2 = 0.3$. Filled circles denote stable solutions and open circles denote unstable solutions. To convert dimensionless time to minutes divide by 3.75

whether fluctuations in the number of cAMP molecules are significant we have to decide what an appropriate sampling volume is for a cell. For instance, if we assume that a cell samples a distance r_o from its lateral surface then the volume sampled is $570\mu^3$ and at a concentration of $10^{-10}M$ there are only 34 molecules in this volume. Is this a realistic sampling volume? This depends on how quickly a receptor can 'process' a molecule it binds. For a cAR1 receptor the off rate is ~ 0.45 sec^{-1} [77], and therefore the mean lifetime of the bound state is ~ 2 sec. A molecule that begins a random walk in the cylindrical shell between r_o and r_1 has a mean lifetime in that shell that is determined by r_1, and a better estimate of the sampling volume is to choose r_1 so that the mean lifetime in the shell is equal to the mean lifetime of the bound receptor. This choice means that on average a molecule remains in the shell long enough so that the receptor will be free at least once during the molecule's sojourn through the shell. How do we compute r_1?

In their paper on the physics of signal detection by cells, Berg and Purcell[128] do essentially this problem, and one finds that the ratio $\xi \equiv \dfrac{r_1}{r_o}$ satisfies the equation

$$\frac{8D\tau_B}{r_o^2} + 3 = 4\frac{\ln \xi}{\xi^2 - 1} + \xi^2 \tag{11}$$

where D is the diffusion coefficient of cAMP and τ_B is the lifetime of the bound receptor*. If we assume that τ_B = 2 sec, $D = 10^{-6}$cm^2/sec

*When rearranged, this expression gives the mean lifetime of a particle in the cylindrical

(a conservative estimate) and $r_o = 5.5\mu$, then we find that the solution of (11) is

$$\xi \sim 7.5$$

i.e. $r_1 \sim 7.5\, r_o$. Thus the sampling volume is about 55 times the volume of the cell. At a cAMP concentration of $10^{-10}M$ there are ~ 620 molecules in this volume, while at $10^{-6}M$ there are $\sim 6 \times 10^6$ molecules in this volume.

How important are the fluctuations in the number of cAMP molecules and the number of bound receptors? The binding step is

$$cAMP + R \underset{k_{-1}}{\overset{k_1}{\rightleftharpoons}} cAMP - R \tag{12}$$

and it is estimated that there are between 5×10^4 and 1×10^5 receptors per cell[79]. Suppose we assume there are 10^5 receptors. Then at the lowest concentration there are about 160 receptors per molecule in the sampling volume, while at $10^{-6}M$ there are 10 cAMP molecules per receptor. In the former case one can treat the number of unbound receptors as a constant, since at most about 1% are bound, while in the latter case the number of free cAMP molecules can be treated as a constant.

These two extremes allow for a simplified treatment of the birth-death process defined by the binding reaction (12), in that either R or cAMP can be considered constant, thereby reducing the second-order stochastic process to a first-order process[†]. Suppose that R is large compared to cAMP; then the steady state probability that a cAMP molecule is bound is given by

$$p_c = \frac{k_1 R_0}{k_{-1} + k_1 R_0}$$

where R_0 is the total number of receptors, and thus the probability that a

shell between r_o and r_1, assuming that there is no flux at the inner boundary, zero concentration at the outer boundary, and a uniform concentration in the vertical direction. In effect, the boundary condition at the outer cylinder means that any particle that hits this boundary is lost forever.

[†]The measured on-rate for cAMP binding, $\sim 7.5 \times 10^6$/M-sec[77], is one to two orders of magnitude below the rate expected for a diffusion-limited reaction[129]. Thus the controlling rate step is the binding of cAMP to cAR1.

receptor is bound is given by

$$p_r = \frac{k_1 N_0}{k_{-1} + k_1 R_0}.$$

where N_0 is the total number of cAMP molecules. If we assume that the receptors are independent, then the number of cAMP molecules bound, and hence the number of receptors occupied is binomially distributed with mean $\mu = N_0 p_c$ and variance $\sigma^2 = N_0 p_c (1 - p_c)$. Therefore the coefficient of variation is

$$\frac{\sqrt{\sigma^2}}{\mu} = \frac{1}{\sqrt{N_0}} \frac{(1 - p_c)}{p_c}.$$

When $N_0 \sim 600$ the fluctuations may be significant, but they are certainly insignificant when $N_0 = 10^6$. If the binding is strong enough they may even be insignificant at $10^{-10} M$. The intermediate cases, in which the concentration of receptors and free cAMP molecules are comparable, and which are the most important, requires a more detailed analysis that has not yet been done. Nonequilibrium effects and the effects of diffusion limitations are discussed by several authors[130–132].

4 Microscopic and macroscopic aspects of Dd aggregation

Aggregation following starvation begins when individual cells or groups of cells begin to release cAMP periodically. Nearby cells sense this signal and respond to it either by moving toward the source of the signal, or by both relaying the signal and moving toward its source, depending on whether they are only competent for chemotaxis or competent for both relay and chemotaxis. If relay-competent Dd cells are spread over an agar surface, two-dimensional waves of extracellular and intracellular cAMP can be observed[133–135]. The waves of extracellular cAMP travel across the field in the form of either target patterns (expanding concentric waves), or spiral waves with rotating cores. Different types of interacting wave patterns, such as interacting target patterns and coexisting spiral waves of the same or of the opposite rotation, are found experimentally. Several examples of this are shown in Figure 20. The extracellular cAMP wave rises from a level of less than ~ 0.001 μM to a peak value of $0.1 - 1$ μM in a medium with a cell density of 10^6 cells $\cdot$ cm^{-2}. In either a spiral wave or a concentric wave, the distance

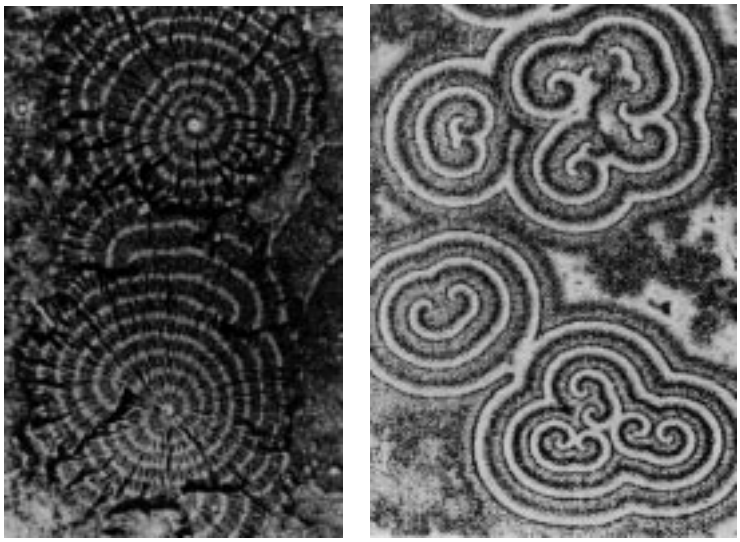

Figure 20. Examples of the wave patterns observed during the aggregation of Dd. In (a) the light bands represent cells that are moving while the dark bands represent stationary cells. From Newell[134] (with permission). (b) From Siegert and Weijer[121] (with permission).

between two traveling fronts is $1-4$mm. The speed of these waves is $\sim 300-600\ \mu\text{m}\cdot\text{min}^{-1}$, and the time between two successive wave fronts is 6-10 minutes[133,136]. The traveling cAMP waves serve as the chemotactic signal to induce aggregation of the cells, which move toward the center at about $10-15\ \mu\text{m}/\text{min}$ [137–139].

Given an accurate description of the input-output behavior of individual cells, one can address a number of questions concerning signal propagation and cell movement in aggregation. Several that will be discussed here are as follows.

1. Can individual cells be pacemakers and initiate traveling waves under normal conditions of early aggregation, or is it necessary for two or more cells to come into close proximity in order to initiate a wave?

2. What determines whether the traveling waves of cAMP_o are axisymmetric target patterns or spiral waves?

3. What are the details of the signal seen by a cell (front-to-back cAMP ratio, etc), how do cells orient themselves in a traveling wave, and how do they solve the 'back-of-the-wave' problem? Do cells measure spatial gradients, temporal gradients, both, or neither in determining how to move?

4. How accurately must cells determine the optimal direction of movement, or said otherwise, how sloppy can they be in the choice of direction and still aggregate effectively?

5. How should the rules for individual movement, primarily the choice of direction and speed of movement, be incorporated in a continuum description of aggregation?

We begin with the first of these in the following section.

4.1 Pacemakers in aggregation fields

One aspect of understanding aggregation concerns the origin of the pacemaker sites in aggregation fields. The proportion of cells that can signal autonomously saturates at a small fraction of the total population about 21 hours after starvation begins[27]. In wild type populations it has been estimated that 0.01% to 0.1% of a population becomes a pacemaker[27], and whether or not a cell becomes a pacemaker may depend on its position in the cell cycle when starvation begins[140]. At present it is not known whether the pacemakers consist of single cells or whether it is necessary that small clumps of cells form before pacemaker activity can begin. From a theoretical standpoint the question is whether a model predicts that a single cell in the plane can generate periodic waves of cyclic AMP. Whether or not this is possible depends on the relative importance of degradation by extracellular phosphodiesterase, diffusion from the cell, and the rate of secretion of cyclic AMP. One expects that if diffusion and extracellular degradation are very slow the cell will simply adapt to the level of cyclic AMP at the cell surface and it will not generate waves. At the other extreme, if extracellular degradation and diffusion are rapid the level of extracellular cyclic AMP can be maintained uniformly low, and again one expects no periodic release of cAMP. However, if the combined effect of extracellular degradation and diffusion is moderate, there may be sufficient self-stimulation, followed by adaptation and decay of extracellular cyclic AMP, to lead to periodic emission of waves.

In DeYoung *et al.*[141] it is shown, using the MO model for the intracellular dynamics, that a single cell can serve as a pacemaker in the sense that it releases cAMP periodically. Since this model provides a good description of the input-output behavior of cells, and since the question of whether a single cell oscillates relies only on this and not on the details of the intracellular dynamics, one expects that in reality a single cell in a low-density aggregation field can release cAMP periodically, but this has not been established experimentally.

This theoretical prediction shows that a single cell can function as a pacemaker in the sense that it attracts cells within the chemotactic range, irrespective of whether those cells relay the signal, but it does not prove that a single cell can elicit the traveling waves that characterize long-range signaling. For the latter it is necessary that both the frequency and the amplitude of the periodic stimulus lie in the correct range. Thus we must digress briefly to review some of the experimental results concerning relay in aggregation fields. Firstly, assuming that each cyclic AMP signal from the pacemaker initiates a traveling target pattern wave, the period of the pacemaker should be the same as the period for target patterns close to the center. Alcantara and Monk[142] report periods of 3-10 minutes, and these periods are also consistent with observations of spiral waves reported in[133]. The results given in DeYoung *et al.*[141] show that the period predicted by the model is in the range of 5 - 10 minutes, except near the onset of oscillations, which agrees well with the observations. Secondly, it is observed that below a certain critical density in the range of $\sim 2.5 - 4 \times 10^4$ cells/cm^2 [143,144] there is no long range signaling and the aggregation field decomposes into many small territories. Thus there is a maximum cell-cell separation above which signal relay cannot occur. From critical density measurements Gingle[143] and Cohen and Robertson[145] estimate this distance to be about 75μ. Alcantara and Monk report a somewhat smaller distance of 57μ on the basis of time lapse photography.

The existence of an upper limit to the spacing for relay stems from the fact that when the cAMP concentration at the cell surface is too low the cell will not produce a sufficiently large pulse of cyclic AMP. This effect is also predicted by either the MO or the TO model, which for the latter is shown in Figure 17. Assuming that a cell relays once the signal exceeds a certain magnitude, regardless of the time above threshold, Gingle[143] estimates that the ratio of the critical concentration for relay to the total

amount of cyclic AMP emitted by a cell in a relay burst is between 0.9 and 1.9 $\times 10^5$ cm^{-3}. Using the estimate that a single cell emits 10^7 molecules during relay[146], we obtain an estimate for the critical concentration of approximately 3×10^{-9} M.

A more direct measurement of sensitivity to external stimuli is provided by the perfusion experiments of Devreotes, et al.[8] where a small but measurable secretion response is obtained with a stimulus as low as 10^{-10} M cyclic AMP, although a half maximal relay response is not observed until the stimulating concentration is about 5×10^{-8} M. These experiments are designed to minimize the influence of free and membrane bound phosphodiesterase, so Devreotes, et al.'s results can be interpreted as showing that a signal of at least a 10^{-10} M is needed at the cell surface for relay. In aggregation fields membrane-bound phosphodiesterase degrades the signal and greatly alters the external cyclic AMP profile close to the cell[147], and for this reason we cannot use Devreotes' results as a direct measure of the critical average concentration for relay in aggregation.

Another unknown aspect of the stimulus-response coupling is the magnitude-duration relationship for threshold signals. Devreotes and Steck[8] report that the maximal relay response occurs about 1-2 minutes after stimulus, which provides an upper limit to the time a stimulus must be held in order to provoke a full response. Alcantara and Monk[142] report a delay of about 12 seconds between the stimulation of a cell by a wave and the onset of the relay response, while Cohen and Robertson[145] estimate that the delay is approximately 15 seconds.

In Figure 21(a) the maximum concentration of extracellular cyclic AMP during one period is shown as a function of the distance from the cell center for various values of ePDE, the diffusible form of the extracellular PDE. These curves are obtained using the MO model, in which the parameter V_{PE} is a measure of the ePDE activity, the nominal value of which is 5000. In the figure we see that the maximum concentration exceeds 10^{-9}M up to a distance of 50μ for all values of ePDE shown, and exceeds this level as far as 75μ if $V_{PE} \leq 30000$. In Figure 21(b) we show the temporal profiles of the cyclic AMP concentration 60μ from the cell center for several values of the ePDE concentration. From this figure one can estimate the signal duration above a fixed level for different values of V_{PE} and the distance from the cell. For instance, the cyclic AMP concen-

tration at 60μ from the cell exceeds 10^{-10}M for 30 seconds for all values of V_{PE} shown. According to our discussion in the previous paragraph, the concentrations at 75μ are at the low end of the range of concentrations that will induce relay, but at 60μ they are significantly higher. Thus the predicted signaling range of a single cell is approximately $60 - 75\mu$, which is in the experimentally-observed range.

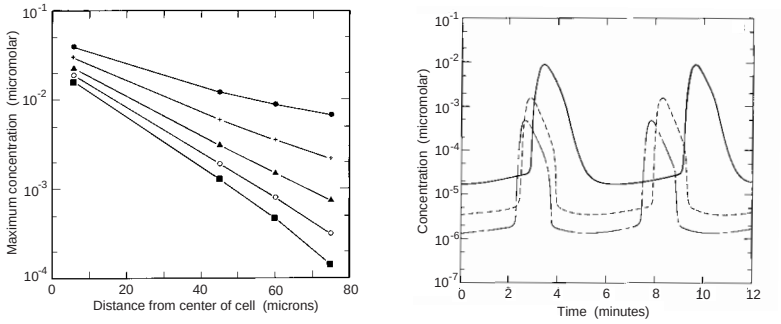

Figure 21. (a) The maximum concentration as a function of distance for different activity levels of ePDE. The curves are for 1, 3, 6, 9 and 12 times the nominal ePDE activity. (b) The concentration as a function of time 60 μ from the cell surface for the nominal value of ePDE activity (solid line), six times the nominal value (dashed line), and twelve times the nominal value (chain line). (Modified from DeYoung *et al.*[141].)

In summary we can say that the MO model (and undoubtedly others) predicts that a single cell can induce relay signaling in fields of relay competent cells. Moreover, the signaling range and period of the single cell pacemaker are in good agreement with experimental observations. This prediction is consistent with the results of Glazer and Newell[144], who found that fields of non-relaying cells could be induced to form small aggregates by seeding the fields with wild type cells. Glazer and Newell estimate that as many as one in five wild-type cells can serve as aggregation centers, but of course they could not test whether single cells induce long-range relaying.

4.2 Traveling waves in the absence of cell motion

4.3 Cell-based *vs* continuum models

Earlier models of Dd aggregation fields can be grouped into two major categories: those that treat the cells as discrete units and those which use a continuum description for the cell density. Although both types of models have given some insight into the aggregation process, they all have limitations which preclude a detailed analysis of the questions we raised earlier. The models developed by Parnas and Segel[148], MacKay[149] and Vasieva *et al.*[150] fall into the first category. The first two of these are similar in that in each the cells are treated as black boxes, which when stimulated, output a fixed amount of cAMP. No description of signal transduction, cAMP production, or adaptation is incorporated, but diffusion of cAMP is taken into account. The model of Parnas and Segel is in one space dimension and can only address the questions of how the cell decides when to move and, in a very simplistic manner, which direction the cell moves. MacKay's model is two dimensional and can reproduce the observed streaming patterns, the effect of two competing pacemakers and can generate spiral waves. These models are a first step in the modeling process, but the rules are formal and not based on a mechanistic description of signal detection, transduction, cAMP production, and cAMP secretion. In more recent modeling by Vasieva *et al.*[150] the diffusion of cAMP is not even incorporated; instead a cellular automaton model with rules that determine which neighbors are activated is used . They are able to reproduce streaming patterns and find self-sustaining sources of excitation, but because the model is purely formal, little can be said about its relevance to Dd aggregation.

The models developed by Keller and Segel[151], Nanjundiah[152], Levine and Reynolds[153]; Vasiev *et al.*[154] and by Höfer *et al.*[155] fall into the second category. The Keller-Segal and Nanjundiah models use formal kinetics since little was known about cAMP dynamics at the time they were formulated. Keller and Segel propose that aggregation is the result of a diffusive instability that develops in the aggregation field, but there is clear experimental evidence that aggregation is initiated and controlled by individual pacemaker cells or small groups of cells. In particular, their analysis predicts that spatial inhomogeneities of the size of the entire field grow most rapidly, and this is not observed. Instead, as we discussed

above, the prevailing opinion is that aggregation results from randomly-located pacemaker cells that arise during maturation of the cells. Nanjundiah uses a similar model to analyze the onset of streaming in aggregation, a topic that will be discussed later. The Levine and Reynolds and Höfer *et al.* models are based on a modified form of the MG model for cAMP production and signaling, whereas Vasieva *et al.* use a modified FitzHugh-Nagumo model for these processes. When the MG model is used the parameters which describe the behavior in suspensions must be changed by orders of magnitude to reproduce the observed waves[156], but there is no suggestion in the literature that such changes are realistic. The FitzHugh-Nagumo model incorporates none of what is known about signal transduction and cAMP production in Dd. Furthermore, since Höfer *et al.*[155] and Levine and Reynolds[153] use continuum chemotaxis equations to describe cell motion, additional assumptions are needed to incorporate adaptation of the tactic component of the movement, as will be discussed later.

The attraction of continuum models is that it is somewhat easier to obtain analytical insights from continuum descriptions with simplified local dynamics, and the computational algorithms needed to simulate the evolution are relatively simple. In the following section we present some results for waves in one and two space dimensions, using the TO model, under the assumption that the cells are immobilized. Thus these results apply very early in aggregation when cell movement is not yet significant. Results from a model that incorporates cell motion and exhibits the patterns of aggregation seen experimentally will be discussed later.

4.4 Traveling waves in one and two space dimensions

We consider both a one-dimensional and a two-dimensional spatial domain, and in order to obtain a simple mathematical model, we make the following assumptions.

- There are sufficient cells present in the medium so that the field can be considered as a continuum and the cells represented by a continuous density function. In the absence of movement this density function is constant throughout the domain.
- The concentrations of $ePDE$ and $mPDE$ are uniform in space and time, and are also represented by a density function.

- Extracellular cAMP is the only diffusible chemical in the system.
- The cell density ρ is constant and uniform throughout the domain; the cells are supposed to be immobile.

Under these assumptions, the governing equation for cAMP$_o$ is

$$\frac{\partial C_o}{\partial \tau} = D\Delta C_o + \frac{\rho}{1-\rho}\left(sr(C_i) - \frac{\gamma_7 C_o}{C_o+\gamma_6} - \frac{\gamma_9 C_o}{C_o+\gamma_8}\right) \quad (13)$$

where D is the dimensionless diffusion coefficient for cAMP and Δ is the Laplace operator, which reflects the diffusive transport, for the domain in question. The dimensional diffusion coefficient D_o has been measured as 4.4-5.0 $\times$ 10^{-6} cm^2·s^{-1} [157–159] in aqueous solution, but we will use D = 2.5 $\times$ 10^{-6} cm^2· s^{-1} in our calculations since it is expected to be lower in the presence of cells. The dimensionless diffusion coefficient is defined as $D \equiv D_o/k_5L^2$ where L is a characteristic dimension of the system. The remaining equations are the same ordinary differential equations as the first four equations given in (10), except that all the variables are functions of both time t and space x. We will use a homogeneous Neumann (no-flux) boundary condition in all simulations, which corresponds to cells spread on an agar surface embedded in a Petri dish.

The density of cells is typically around 10^5 cells·cm^{-2} in wave propagation experiments. The lower limit of the density for propagation is $\sim$ 2.5 $\times$ 10^4 cells ·cm^{-2}, and the largest density used is $\sim$ 10^6 cells · cm^{-2} [133,142]. If one uses the conversion procedure given in Monk and Othmer[114], this gives a range for the dimensionless density ρ of 0.031 to 1.25. A value for ρ higher than 1 simply means that more than one layer of cells is present on average, and depends of course on the assumptions made in the conversion. The standard value we use in the following simulations is $\rho = 0.14$, or 1.12×10^5 cells cm^{-2}, except where otherwise noted.

First consider a circular disk of radius 1 cm, which we denote [0,1] in dimensionless form. As we saw in the context of suspensions, the parameters γ_2 and ρ have a significant affect on the dynamics, and the same can be expected in aggregation fields. In the results discussed below we choose the parameters as in the standard TO model[123], except for γ_2, which is specified as follows. In the disk of radius [0,.05] we set $\gamma_2 = 0.4$ to make cells there pacemakers, were they to be placed in a suspension

at the same density. In the annulus of radius between 0.10 and 1.0 we set γ_2 so as to make the cells there excitable, and we then interpolate between these regions with a cubic spline* Thus the pacemaker region initiates waves periodically, and if the medium is sufficiently excitable they propagate throughout the disk.

The wave speed as a function of the excitability, as reflected by γ_2, is shown in Table 2 for two values of the diffusion coefficient. For $\rho \leq\sim 0.155$ waves fail to propagate, and for $\rho \geq\sim 0.177$ the entire medium is oscillatory. Alcantara and Monk[142] report speeds in the range

Table 2. The wave speed as a function of γ_2 for two values of the cAMP diffusion coefficient

Speed microns/min			
γ_2	D = 2.5×10^{-6}	D = 5.0×10^{-6}	Ratio
0.157	0	0	-
0.158	0	297	-
0.159	188	319	1.70
0.160	225	329	1.43
0.165	218	400	1.42
0.170	312	588	1.87
0.1725	329	615	1.87
0.175	338	625	1.85

of $200 - 400\mu$m/min for the first wave through a medium and lower speeds for later waves, while Siegert and Weijer report speeds in the range $300 - 600\mu$m/min[136]. As the cells progress in development the wave speed increases, and this is reflected in the model by the change in γ_2: as γ_2 increases, the system becomes more excitable and can support more rapidly propagating waves. The values given in Table 2 reflect the steady state wave speed for the given parameters, which is achieved after

*In the results in the following table we use a smooth variation of parameters to avoid possible artifacts of discontinuities in relation to wave block.

several waves have passed through the medium. In cases where propagation fails, the medium may propagate a single wave and then block succeeding waves. In the last column of the table we show the ratio of the speed for $D = 5.0 \times 10^{-6}$ cm^2/sec to that at $D = 2.5 \times 10^{-6}$ cm^2/sec.

A scaling argument applied to the equation

$$\frac{\partial u}{\partial t} = D\Delta u - \lambda f(u) \tag{14}$$

shows that the quantity $\sqrt{D\lambda}$ is a characteristic speed, and as a result, one may expect roughly square root dependence on the diffusion coefficient. If the nonlinearity is $f = (u - u_1)(u - u_2)(u - u_3)$ (the so-called bistable nonlinearity) the speed of a traveling front in one space dimension is given by

$$c = \sqrt{\frac{D\lambda}{2}}(u_1 + u_3 - 2u_2). \tag{15}$$

One sees in the table that at intermediate values of γ_2 the speed follows a 'square-root of D' law, but at higher γ the speed increases almost in proportion to D. The lower cutoff for propagation increases with D and therefore the first ratio in the table is not meaningful in this regard.

The density of cells in the aggregation field also has a significant effect on the speed, as is shown in Figure 22. The lower limit for propagation is $\rho \sim 0.05$, which corresponds to a cell density of about 4×10^4 cells/cm^2. This is higher than the lowest observed cutoff for propagation, but agrees with Glazer and Newell's observations[144]. This cutoff does not depend significantly on the diffusion coefficient, nor does it change significantly if the number of grid points used in the numerical computations is doubled. An analysis of how the waves fail show that they propagate for a short distance from the pacemaker, but then die out because relay fails. A comparison of (14) and (13) would suggest that the speed varies with the density as $\sqrt{\rho/(1-\rho)}$, but this does not predict propagation block at a finite density. Qualitatively a more appropriate dependence is $\sqrt{\rho - \rho_0}$, where ρ_0 is the density at which waves are blocked. One also sees that there is a maximum in the wave speed as a function of density at $\rho \sim 0.6$, which is not predicted by the 'square root of density' dependence of the speed. Such density dependence was observed by Alcantara and Monk[142], but the experimentally-observed maximum occurs at a lower

density than in the model. Of course the speed at high densities may not be physically realistic since the underlying model takes no account of cell-cell interactions.

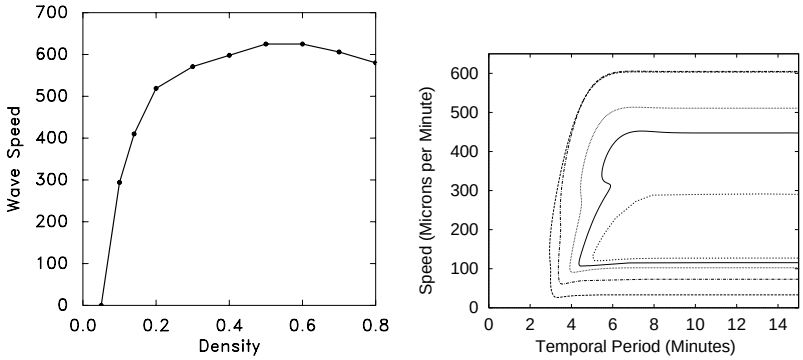

Figure 22. (a) The wave speed as a function of the density for $\gamma_2 = 0.175$. To convert the density to cells per cm^2 multiply the numbers on the abcissa by 8×10^5. (b) The dispersion curves for the TO model for $\gamma_2 = 0.175$ and different densities. The curves shown are for ρ = 0.8, 0.4, 0.2, 0.14 and 0.1 from left to right. The waves are stable on those portions of the curves on which the speed is an increasing function of the period. The curves for $\rho = 0.4$ and $\rho = 0.8$ cross at a speed of about 500 microns/minute.

It is known that the period/speed characteristics of both the pacemaker-initiated waves described here and the spiral waves to be discussed later lie close to the dispersion curve for periodic traveling waves[114] (cf Figure 22(b)), and thus some insight into the effect of density on wave propagation is obtained by calculating these dispersion curves for different densities. The dispersion curves are computed according to the procedure described elsewhere[160,114], and the results for five distinct densities are shown in Figure 22(b). The range of periods of naturally-occurring pacemakers is 3-10 minutes, and under the conditions used here the periods are in the range of 4-8 minutes. One sees in that figure that a high density field can propagate higher frequency waves than low density fields, and are thus more likely to propagate every wave initiated by a pacemaker, rather than gating the waves. In particular, one sees that at $\rho = 0.8$ a wave speed of 300 microns/min corresponds to a temporal period of about 3.5 mins, whereas at a density of 0.1 the medium will not propagate a wave

of that speed. It should also be noted that for a small interval of periods there are two stable traveling waves for densities around $\rho = 0.14$.

In the previous discussion the traveling waves were stimulated by a pacemaker, but in an excitable medium waves can be generated by a steady source as well. In Figure 23 we show the extracellular cAMP along a radius of the disk for two situations: one in which the central core is a pacemaker and the other in which the central core secretes cAMP at a high steady rate. In Figure 23(a) the disk of radius 0.05 is a pacemaker and the remainder of the unit disk is excitable. The pacemaker region generates an oscillation of maximum external cAMP $\sim 1.0\mu M$, and this triggers a wave in the excitable region with a peak cAMP concentration far from the center, averaged over the intra- and extracellular phases, of $\sim 0.34\mu$M, which is in the range reported by Tomchik and Devreotes[133] for spiral waves. At higher cell densities the amplitude of extracellular cAMP increases significantly, just as in suspensions. If we increase γ_2 further so that the 'pacemaker' region is no longer oscillatory, but instead releases cAMP at a high rate, then the steady source triggers waves in the excitable region (Figure 23(b)). These results show that travel-

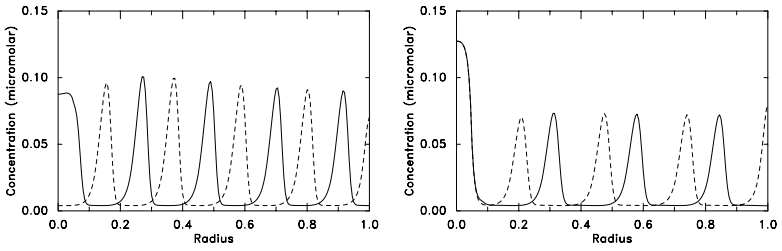

Figure 23. The extracellular cAMP concentration along a radius through an outwardly-propagating target pattern. In (a) the central disk is a pacemaker and the curves represent the wave at time t (solid line) and $t + 2$ (dashed line). The wave has a temporal period of 6.62 minutes, a spatial period of 0.216 cm and a speed of 325 microns/minute. In (b) $\gamma_2 = 0.6$ in the central disk, which leads to a high, steady production of cAMP. Periodic waves are initiated at a radius of about 0.1, and have a temporal period of 7.8 minutes, a spatial period of 0.27 cm and a speed of 346 microns/minute. The solid and dashed lines in (b) are the cAMP concentration at t and $t + 2$. The shape and duration of the extracellular waves should be compared with that shown in Tomchik and Devreotes[133].

ing waves can be elicited either by a an oscillatory pacemaker or by a large time-independent input of cAMP. This coincides with observations

by Durston[161], who suggested that in later aggregation the center of an aggregate emits cAMP at a high steady rate.

Another aspect of interest concerns the interaction of pacemakers of different frequencies. In Figure 24(a) we show a contour plot of the cAMP level lines in the $x - t$ plane for a system in which a fast pacemaker is turned on after a slow one has had sufficient time to organize the entire field. In the figure there is a slow pacemaker at the five central grid points of 200 total grid points. This pacemaker has parameters $\beta_2 = 0.2, \beta_5 = 0.1, \gamma_2 = 0.4, \gamma_6 = 1.16$, and $\gamma_9 = 9.17$ and others standard, which gives a period of ~ 18.2 minutes. After 20 minutes a faster pacemaker is turned on at the single grid point at $x = 0.125$. One sees in Figure 24(a) that the faster pacemaker dominates in the interval [0, 0.5], but waves that emanate there rarely propagate through the slower pacemaker. At $x = 0.75$ (Figure 24(b)) the wave is very erratic, perhaps chaotic. The pattern of interaction that results depends very heavily on the strength of the slower pacemaker. For instance, if the slower pacemaker occupies only one grid point at the center it will be completely entrained by the faster pacemaker.

It is possible that the foregoing results on wave blocking are artifacts that stem from the fact that the domain is one dimensional. One might anticipate that in two space dimensions the fastest pacemaker dominates far from other pacemakers, even though it may not suppress slower ones. However, the situation can be more complicated, as is shown in Figure 25. There we show three oscillating centers interacting in a 1 cm x 1 cm domain. The fastest pacemaker is centered around $(0.5, 0.67)$ and has a period of 4.8 min. The two slower pacemakers are centered at $(0.33, 0.33)$ (period = 11.6 min) and $(0.33, 0.67)$ (period = 18.2 min), respectively. The radii for all three pacemakers is 0.05. One sees in panel (a) that the slower pacemakers may or may not break the waves emanating from the fastest pacemaker, depending on when they fire. The broken wave shown in panel (b) begins to curl up and initiate a double spiral later, but the next wave from the fast pacemaker kills the nascent spiral (not shown). However, if the fast pacemaker were turned off at the appropriate time, perhaps because of cell movement, the broken wave would form a fully-developed spiral. Other mechanisms of spiral generation will be discussed in a later section.

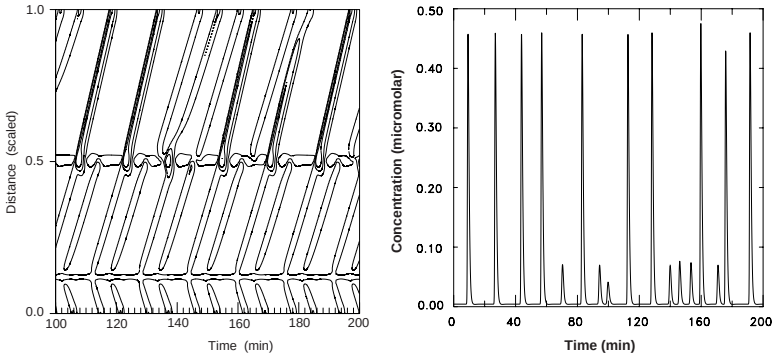

Figure 24. Phase locking and gating of waves. There is a slow pacemaker of period ~ 18.2 minutes at five grids points centered around $x = 0.5$. For the first 20 minutes this is the only pacemaker, but then a faster pacemaker (period ~ 7.2 minutes) situated at the single point $x = 0.125$ is turned on. In (a) we show the contours of extracellular cAMP in the $x - t$ plane for t between 100 and 200 minutes. In (b) we show the extracellular cAMP concentration at $x = 0.75$, where the local dynamics are excitable, for the entire time of the experiment. The first three waves at $x = 0.75$ have the period of the central pacemaker, but thereafter the pattern becomes erratic.

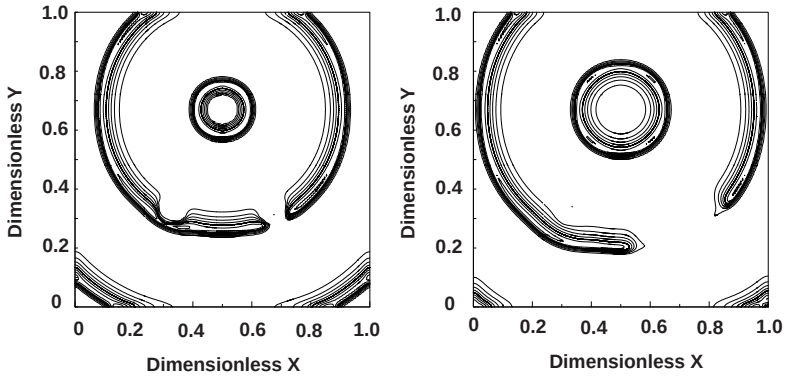

Figure 25. Phase locking of pacemakers in two space dimensions. Waves from a fast pacemaker located at $(0.5, 0.67)$ interact with two slower pacemakers located at $(0.33, 0.33)$ and $(0.33, 0.67)$, respectively (a) T = 11 mins. (b) T = 20 mins.

In Figure 26 we show a stable spiral wave computed on a 1.5 cm $\times$ 1.5 cm domain, using parameters which make the medium excitable but

not oscillatory. In this figure there are no pacemakers in the system, and the wave was initiated by using a broken plane wave for initial data in a narrow strip extending halfway across the region, while setting the remainder of the region to the rest state. The period of this spiral is approximately 5.8 min and the wave speed is 460μm/min far from the center, which gives a spatial wave length of about 2.3 mm. The radius of the core is $\sim$0.1 mm. These results are in the range of experimental results obtained by Gross *et al.* [162], by Tomchik and Devreotes[133], and Siegert and Weijer[136].

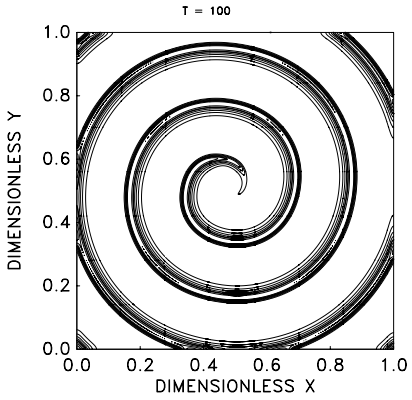

Figure 26. An example of a single spiral in a field of immobilized cells (from Tang and Othmer[123]).

The spiral appears to move rigidly around a fixed point in the aggregation field. At present there is no adequate theoretical framework for predicting the period and geometry of such a rigidly rotating spiral, although computational[114] and experimental[162] evidence indicates that the period of a spiral is usually lower than that of target patterns in the same medium. A linear theory, based on equations of the form

$$\begin{aligned} \epsilon \frac{\partial u}{\partial t} &= \epsilon^2 D \Delta u + f(u,v) \\ \frac{\partial v}{\partial t} &= g(u,v) \end{aligned}$$

where u and v are scalar functions of time and space and ϵ is a small parameter, was proposed by Zykov[163] and analyzed by a number of authors[164,165]. In these studies, f and g are assumed to be such that the

local dynamics are excitable, as in the Fitzhugh-Nagumo equations. The aim of the theoretical analysis is to infer properties of spiral waves from known properties of one dimensional waves, and in particular, from the dispersion relation. Consider a contour $u(\mathbf{x},t) = \overline{u}$ where $\overline{u}$ is fixed. At each time this contour is a curve $C(t)$ with a curvature denoted by $\kappa(\mathbf{x},t)$ and a normal velocity denoted $V_n(\mathbf{x},t)$. The main prediction of the linear theory is that, for bounded curvature the leading term in the expansion of V_n in powers of ϵ is

$$V_n = \overline{V_n} + \epsilon D\kappa. \tag{16}$$

Far from the center of the spiral $\kappa \to 0$ and therefore $V_n \to \overline{V_n}$. However in this limit the wave motion is asymptotically planar and thus one expects $\overline{V_n}$ to lie on the dispersion relation for one dimensional waves. Unfortunately, there is at present no way of determining $\overline{V_n}$ *a priori*.

The relation (16) has been tested numerically for the MO model (the details of how this is done can be found in the original paper[114]) and some of the results are shown in Figure 27. In (d) the quantity $\overline{V_n} = V_n - D\kappa$, which is the normal velocity corrected for curvature (the factor ϵ is absorbed into the diffusion constant). When the linear theory holds this line will be horizontal. Clearly the linear theory does hold for arc lengths less than about 0.4 and for arc lengths greater than about 0.55. That the linear theory does not hold around the center of the spiral is not surprising, since the curvature is large there. Perhaps more surprising is the fact that the linear approximation works well at the back of the wave much closer to the center than on the front of the wave. Further work is needed to clarify conditions under which the linear theory is applicable.

Another situation in which the curvature of the wavefront might play an important role is when axisymmetric waves in two space dimensions are initiated from a localized source. From (16) one sees that if this relation for the normal velocity holds then a wave initiated at a stimulation site may be blocked if the curvature is too large (*i. e.* if the radius of the site is too small). The role of curvature in cAMP waves in Dd has been studied experimentally by Foerster *et al.*[135], who measured the normal velocity of an outward propagating circular wave. Their data is re-plotted in Figure 28, and if the straight line fit to it is extrapolated to zero normal velocity, it predicts a critical radius for block of about 185 μ. If this extrapolation were valid then a single pacemaker, or even a group of pacemakers lying in a disk of radius less than 185 μ, could not initiate a

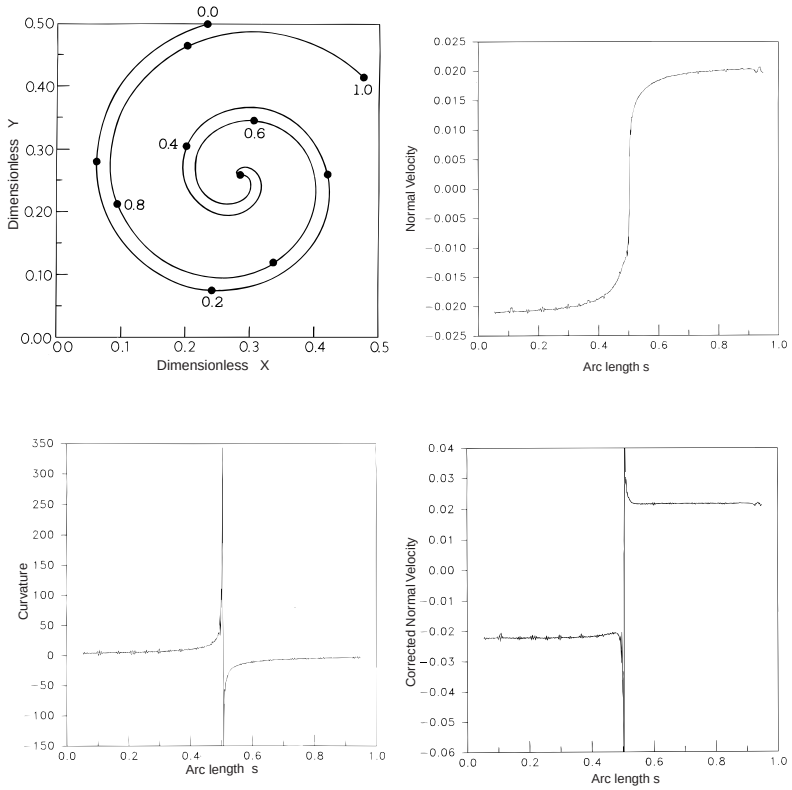

Figure 27. The curvature and normal velocity for the 1×10^{-8}M cyclic AMP concentration contour of the spiral computed using the MO model[114]. In (a) we show this contour in a 0.5cm $\times$ 0.5cm square of the aggregation field. The marks • and the associated numbers indicate the arc length along the curve, which has been normalized so that the total arc length of the curve is one. The normal velocity (b) and curvature (c) of the contour as a function of arc length along the contour. The small oscillations in this and (b) correlate with points at which the contour is parallel to the finite difference grid. (d) The normal velocity corrected for curvature via (16). From Monk and Othmer[114].

wave. However, this contradicts both the earlier theoretical work and the experimental observations, and shows again that further work on the role of curvature in propagation is needed.

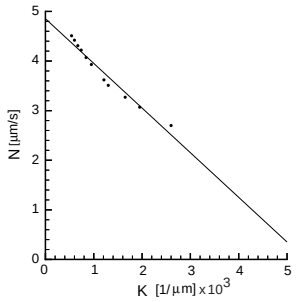

Figure 28. A plot of the normal velocity as a function of the curvature for outward propagating waves, using the data in Figure 4 of Foerster *et al.*[135]. The x-intercept of a straight-line fit to this data predicts a critical radius of 185 microns. It is clear that a straight-line fit is inappropriate, even over the limited range of the data, but at present higher-order terms in the expansion (16) that could account for the deviation from a straight line have not been computed.

In addition to target patterns and single spirals, another wave pattern commonly-observed experimentally is a pair of coexisting co- or counter-rotating spiral waves (cf. Figure 20(b)). Such waves can be reproduced with the foregoing model, either by the mechanism discussed earlier, or by using appropriate initial data. However, it is not understood how the various types of spirals are initiated in the laboratory. The large proportion of spiral waves observed in experiments may be due to variations in the parameters between cells and other inhomogeneities in the medium, or to interaction between pacemakers (cf. Figure 25), rather than any special initial conditions. The cell density may not be uniform, the developmental stage of cells may be different, the cell population may not be homogeneous genetically, and of course the cells are mobile. Computations discussed later, in which the cells are allowed to aggregate, show that it is possible to initiate spirals under those conditions, even when cells are identical.

Various other mathematical models of the single cell dynamics have been used for the purpose of simulating the observed 2-dimensional wave patterns[166,114,135,115]. All can produce qualitatively correct results for suitable parameter choices, and Monk and Othmer[114] showed that if a model represents the stimulus-response behavior of an individual cell correctly, then the wave patterns will also be reproduced.

4.5 Cell motion and aggregation

Thus far we have discussed signal detection, transduction, relay and wave propagation in aggregation fields of immobilized cells, but of course some form of directed or non-random cell movement is essential for aggregation. This leads to another aspect of signal detection and transduction, which is whether, and if so how, cells can extract directional information from an extracellular field. For instance, the motion of flagellated bacteria such as *E. coli* consists of a series of more-or-less straight runs, punctuated by tumbles during which cells choose a new direction. These bacteria move at a fixed speed, but they extend their run length when moving up the gradient of an attractant. Since they are small they probably cannot discriminate spatial differences in the concentration of an attractant on the scale of a cell length, and they simply choose a new direction more or less at random[167,168]. The propensity of a flagellum to rotate clockwise or counterclockwise, and hence the probability of a run or tumble, is biased by an intracellular signal whose level is determined by inputs from all receptors, and thus reflects an average signal over the cell surface[6]. However, it is conceivable that larger cells such as Dd are able to extract directional information from the extracellular cAMP distribution. Since the cAMP distribution is a scalar field, directional information can only be obtained from this field by *effectively* taking measurements at two points in space, but how might this be done?

Signal detection and response for the purpose of movement control involves the same general steps as shown in Figure 2, except for the last step of signal relay. In the present context the internal response consists of changes in the velocity of motion, which may involve both changes in direction and in speed, and perhaps changes in the frequency at which a cell makes a decision as to whether to change velocity[†]. We have already indicated that *E. coli* alters the frequency of directional changes as a function of the stimulus level, and later we discuss similar evidence for Dd. For the present, a simple but quite accurate description of motion is obtained if we ignore any random component of movement, neglect acceleration, and assume that the velocity changes only at discrete points

[†] Strictly speaking, there is no unique velocity by which to characterize motion of a cell, since it deforms as it moves and there is frequently significant relative motion of various parts[169]. However when cells translocate, as opposed to merely quivering in place, the motion is usually described in terms of the motion of the centroid, and we follow this convention.

in time. Under these assumptions the trajectory of a cell comprises a sequence of straight-line paths punctuated by turns or changes of speed. Within this descriptive framework one can distinguish two major types of responses to the cAMP field; those for which the response depends only on the local scalar field, perhaps averaged over the cell surface, and those that depend on local directional information. Any of the former is classified as a *kinesis* and any of the latter as a *taxis*[‡]. According to this classification, the bacterial response to a spatially nonuniform signal is a chemokinesis[§]. On the other hand, a Dd cell changes direction in proportion to the disparity between its present direction and the local cAMP gradient (see below) and changes speed as well; thus the Dd response comprises both chemotaxis and chemokinesis.

In the absence of cAMP stimuli Dd cells extend pseudopods in random directions, perhaps as a method for determining a favorable direction, and aggregation competent cells respond to cAMP stimuli with characteristic changes in their morphology. The first response is suppression of existing pseudopods and rounding up of the cell (the 'cringe response'), which occurs within about 20 secs and lasts about 30 secs. Under uniform elevation of the ambient cAMP this is followed by extension of pseudopods in various directions, and an increase in the motility[138,171]. A localized application of cAMP elicits the cringe response followed by a localized extension of a pseudopod near the point of application of the stimulus[172]. This type of stimulus is similar to what a cell experiences in a cAMP wave.

Cells also respond to static gradients of cAMP. Fisher *et al.*[139] show that cells move faster up a cAMP gradient than down, and that the majority of turns made by a cell are spontaneous (although there is a slight depression in the frequency of turns when the cell moves up the gradient). However, the magnitude and direction of a turn is strongly influenced by the gradient in that there is a strong tendency to lock onto the gradient[¶]. Furthermore, chemotaxis is not affected by the absence of relay (treating

[‡]These terms are used with varying degrees of precision in the literature; see Alt and Hoffman[170] for a detailed taxonomy of the terminology used to describe changes in motive behavior in response to stimuli.

[§]Sometimes described as a *klinokinesis*, since the response involves a change in the frequency of turning, whereas a change in the speed is called an *orthokinesis*[170].

[¶]That chemotaxis is involved is disputed by Vicker[173], who believes that accumulation of cells in static gradients is due to ortho- and klinokinesis.

cells with caffeine suppresses relay[174] but has no effect on their chemotactic ability[139]). The ability of larger cells such as Dd to apparently 'measure' concentration differences over the length of the cell body has lead to various proposals as to how this might be done, some of which are discussed later. First however we discuss a discrete cell description of aggregation in which movement is governed by formal rules and several continuum descriptions in which movement is described phenomenologically.

4.6 Discrete and continuum models of cell aggregation

4.7 A discrete cell model for aggregation

A mixed discrete/continuum model in which the cells are treated as individual units and the extracellular cAMP is described by a continuum reaction-diffusion equation has been developed[175]. A detailed description of signal transduction and adaptation is possible in such a model, and movement rules based on the intracellular dynamics can be explored. Such a model comprises two main parts: (i) the mechanism for signal transduction and cAMP relay response, for which the TO model is used, and (ii) the cell movement rules. The equations for the intracellular dynamics of the i^{th} cell can be written as a system of the form

$$\frac{d\mathbf{w}^i}{d\tau} = \mathbf{G}^i(\mathbf{w}^i, C_o), \tag{17}$$

where $\mathbf{w}^i$ is a vector whose components w_j^i, j = 1,$\cdots$,4, represent the intracellular quantities in the TO model for the i^{th} cell, and C_o represents extracellular cAMP. In this model the cells are treated as discrete points, and thus the analog of (13) is the partial differential equation

$$\begin{aligned}\frac{\partial C_o(\mathbf{x},\tau)}{\partial \tau} &= \Delta_1 \nabla^2 C_o(\mathbf{x},\tau) - \hat{\gamma_9}\frac{C_o(\mathbf{x},\tau)}{C_o(\mathbf{x},\tau)+\gamma_8} \\ &\quad + \sum_{i=1}^{N} \frac{V_c}{V_o}\delta(\mathbf{x}-\mathbf{x}_i)\left(sr(w_4^i) - \gamma_7\frac{C_o(\mathbf{x},\tau)}{C_o(\mathbf{x},\tau)+\gamma_6}\right)\end{aligned} \tag{18}$$

Here $\mathbf{x}_i$ denotes the position of the i^{th} cell, the first term represents diffusion of cAMP, the second represents the degradation of cAMP by extracellular phosphodiesterase, and the summation represents the localized sources and sinks of cAMP at the cells.

The second component of the model involves the cell movement rules, which determine when motion is initiated, how the direction is determined, and how long movement persists[‖]. In reality only the probability of each step is determined, but in the simulations the following deterministic rules are used[175]: (i) the cell moves in the direction of the gradient of cAMP when the motion was started; (ii) the cell moves at a speed of 30 microns per minute[142]. Various rules for initiating movement and determining its duration were explored. As is shown in Dallon and Othmer[175], formal rules based on a fixed duration of movement can produce aggregation. However, if the duration is too short aggregation does not occur, but by adding other mechanisms such as directional persistence the problem can be corrected. For example, when the duration is set at 20 seconds, which is an experimentally-observed turning time[177], the cells do not aggregate successfully. By adding cell polarization[178] or a memory of recently-encountered gradients, the aggregation patterns are restored. Because the cAMP signal a cell sees is very rough, the cell may move away from the aggregation center, and the simulations indicate that the cell must commit to a direction for a sufficient length of time to successfully aggregate.

However formal rules based on a fixed duration of movement ignore experimental facts described earlier because there is no coupling between the intra- or extracellular environment and the duration of movement. For example, if the profile of the cAMP wave is altered due to changes in parameters, a rule based on fixed durations might predict that cells continue to move after the wave has passed. One cannot rule out this possibility, and we show an example later of how this might apply for a certain mutant. However the choice of duration is probably determined by one or more intracellular variables, and an outline of a detailed model of how cells might choose the direction of motion and the length of a 'run' will be described later. Such a model has not been analyzed as yet, and it would probably be computationally prohibitive to include it in the simulations at present. Instead, more realistic rules based on internal variables were developed as follows[175]. It is known that cAMP activates the cGMP pathway via G proteins in addition to activating the cAMP production pathway[179]. It is also known that cGMP is near the beginning of the chemotactic response pathway and that cGMP produc-

[‖] van Duijn and van Haastert[176] have shown that locomotion and orientation are controlled separately in Dd.

tion adapts to the cAMP stimulus on a time scale of about 10-15 seconds. If cGMP adapts to extracellular cAMP levels then downstream components will also adapt, perhaps on a longer time scale, except in unusual circumstances. Thus it is assumed in the model that there is a downstream 'motion controller', the identity of which is not known. However, it must be used in such a way that the cell moves only when cAMP is increasing, for it is known that wild-type cells only move in the rising phase of the cAMP wave. In the absence of detailed information about the controller dynamics, we used as a stand-in a quantity in the cAMP pathway that has the appropriate time course. This mechanism is biologically more realistic than the *ad hoc* rules and it gives results which match very well with experimental results (cf. Figure 29(a)). This rule shows how a cell can respond to temporally-increasing cAMP levels by predicating motion on a threshold of an intracellular variable, and it also solves the 'back-of-the-wave' problem, in that a cell does not respond to the receding cAMP wave after it passes, even though it sees a positive gradient on the back side of the wave. These simulation results support the conclusion reached by Soll *et al.*[180], that cells seem to orient during the beginning of the wave of cAMP and then move in a relatively blind fashion. The simulations also show that aggregation is very robust with respect to the accuracy with which the correct direction must be selected. For example, Figure 29(c) shows cells can aggregate successfully, albeit more slowly, as long as the cells choose their direction within the correct half space determined by the gradient and a line orthogonal to it[175]. When there are many pacemakers the aggregation field breaks up into a number of smaller fields, although certainly not equal in number to the number of pacemakers present (cf. Figure 29(d)). These computations show that single cells can be pacemakers, in agreement with the theoretical analysis described earlier, but they also show that many of these pacemakers will be entrained by others. Whether or not an individual pacemaker can continue to oscillate in the face of periodic signals from other sources is a function of how large an aggregate it has recruited, and hence how strong a signal it emits, differences between its frequency and that of other sources, and the initial distribution of cells. As yet there is no theoretical analysis that enables one to predict when it will survive, but it is an important question because the answer would shed light on the breakup of waves by pacemakers and hence on the origin of spirals. This will be discussed further in a later section.

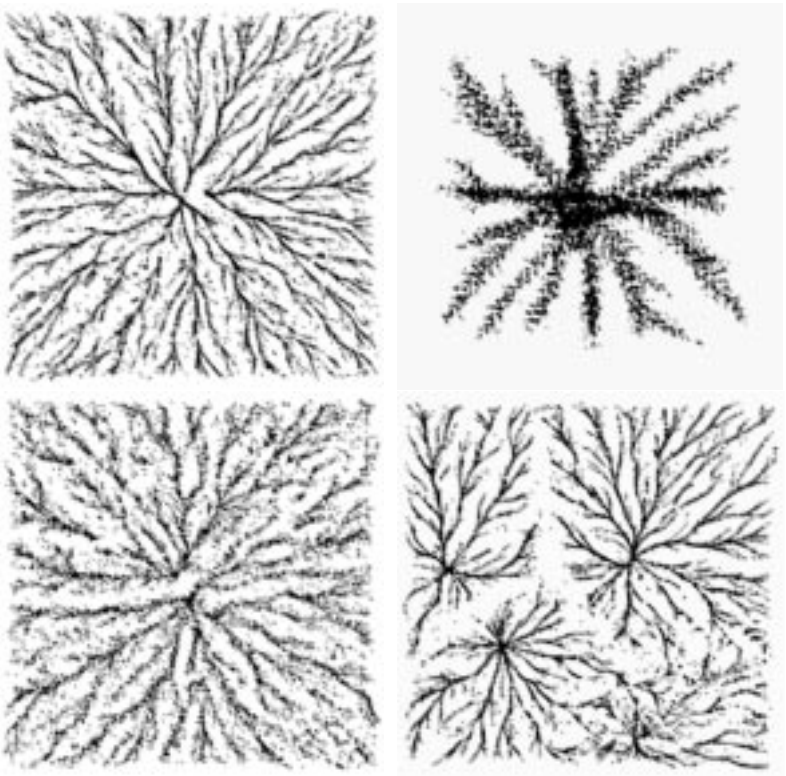

Figure 29. Examples of the aggregation patterns which form using the discrete cell model. In (a) cell movement is governed by an internal variable that adapts, in (b) cells move for 500 seconds to simulate the streamer mutants[34,181] and in (c) the direction of movement is randomly perturbed by up to 90 degrees from the direction of the local gradient. In (a), (b) and (c) there is a single pacemaking region in the center, but in (d) there are 0.1% pacemakers randomly-placed in the aggregation field initially, and cells move according to the rules in (a). All simulations are shown at 150 minutes, the domain is 1 centimeter by 1 centimeter with 200 grid points in each direction, and the number of cells used corresponds to a volumetric density of about 0.2. (From Dallon and Othmer[175].

4.8 Continuum descriptions of chemotaxis

Many theoretical analyses of chemotaxis begin by supposing that the movement of cells released at a point in a uniform environment can be

described as an uncorrelated, unbiased random walk of noninteracting particles on a sufficiently long time scale. In an appropriate continuum limit the cell density ρ, measured in units of cells/L^n, where L denotes length and n=1,2 or 3, satisfies the diffusion equation

$$\frac{\partial \rho}{\partial \tau} = D_c \Delta \rho. \tag{19}$$

Here D_c is the diffusion coefficient of cells, and as before, Δ is the Laplace operator. In this equation the cell flux is given by

$$\mathbf{j} = -D_c \nabla \rho, \tag{20}$$

where ∇ denotes the gradient operator. The flux has units of cells/(L^{n-1}-time), and thus unit-wise it is a density times a velocity. If we define the average particle velocity via the relation $\mathbf{j} = \rho \mathbf{u}$ then we see that for pure diffusive spread

$$\mathbf{u} = -D_c \frac{\nabla \rho}{\rho} = -D_c \nabla \ln \rho. \tag{21}$$

In the presence of an attractant the simplest description of cell motion is obtained by adding to the diffusive flux a directed component to obtain

$$\mathbf{j} = -D_c \nabla \rho + \rho \mathbf{u}_c \tag{22}$$

where $\mathbf{u}_c$ is the macroscopic chemotactic velocity. The taxis is positive or negative according as $\mathbf{u}_c$ is parallel or anti-parallel to the direction of increase of the chemotactic substance.

In the absence of cell division or death the resulting evolution equation for the density is

$$\frac{\partial \rho}{\partial \tau} = \nabla \cdot (D_c \nabla \rho - \rho \mathbf{u}_c), \tag{23}$$

and this is frequently called a chemotactic equation. In addition to this equation, the density must satisfy the conservation condition

$$\int_\Omega \rho(\mathbf{x}, t) d\mathbf{x} = \int_\Omega \rho(\mathbf{x}, 0) d\mathbf{x} \tag{24}$$

where Ω is the aggregation field. Unless the distribution of the chemotactic substance is fixed, (23) must be augmented by an evolution equation

for this substance and perhaps other internal variables. In the context of Dd aggregation these additional equations are the same as those for wave propagation in an immobilized field, except that the cell density depends on both space and time.

The earliest derivation that relates the chemotactic velocity to properties of individual cells is apparently due to Patlak[182], who used kinetic theory arguments to express $\mathbf{u}_c$ in terms of averages of the velocities and run times of individual cells. His formulation also led to a variable diffusion coefficient. Alt[183] has also pursued the kinetic theory approach and has shown how to relate the chemotactic velocity to the gradient of an attractant or repellent whose concentration is c. He finds that (in our notation) the flux is approximately given by

$$\begin{aligned} \mathbf{j} &= -D_c \nabla \rho + \rho \chi(c) \nabla c \qquad (25) \\ &= -D_c \nabla \rho + \rho \Delta \Phi(c) \qquad (26) \end{aligned}$$

where Φ is a primitive of χ. The function $\chi(c)$ is called the chemotactic sensitivity, and the chemotactic velocity is given by

$$\mathbf{u}_c = \chi(c) \nabla c = \nabla \Phi(c). \qquad (27)$$

When $\chi > 0$ the tactic component of the flux is in the direction of ∇c and the taxis is positive.

Since Patlak's derivation, other more phenomenological approaches to the derivation of the chemotactic sensitivity or chemotactic velocity have been taken. For example, Keller and Segel[184] postulated that the chemotactic velocity is given by (27) and later [151] related the chemotactic sensitivity to the frequency of reversals of a particle moving along the real line. Nanjundiah[152] considers several forms for the sensitivity, Segel[185] incorporated receptor dynamics into the Keller-Segel model, and Pate and Othmer[186] derived the velocity in terms of forces exerted by the cell. Starting from Newton's law for the motion of a point particle, neglecting inertial effects, and assuming that the motive force exerted by a cell is a function of the attractant concentration, they showed how the chemotactic sensitivity is related to the rate of change of the force with attractant concentration. In this formulation the dependence of the flux on the gradient of the attractant arises from the difference in the force exerted in different directions due to different attractant concentrations. Experimental support for this comes from work of Finney*et al.*[178], who show that as many

pseudopods are produced down-gradient as up, but those up-gradient are more successful in generating cell movement.

There have been many studies of chemotaxis equations in which the chemotactic species is diffusible. Nanjundiah[152] was apparently the first to suggest that aggregation could be viewed as the development of a singularity. This viewpoint was developed by Childress and Percus[187], and there have been many studies of these equations since then[188–191]. Othmer and Stevens[192] studied the aggregation of myxobacteria such as *Myxococcus xanthus*, whose life cycle is quite similar that of Dd, and found that when the chemotactic substance is non-diffusible, a variety of stable, spatially nonuniform solutions (*i. e.* , solutions which show aggregation) may exist for different choices of the chemotactic sensitivity. This work shows that within the framework of models based on a continuum density function, stable aggregation can occur with only local modulation of the transition rates, that is, without long range signaling via a diffusible chemical.

The above descriptions are continuum descriptions in that they can only be expected to hold in the presence of slow variations in the attractant concentration and the cell density. However, none of these descriptions incorporate adaptation into the chemotactic response, but there are several ways in which this can be done. For instance, one could simply postulate that the flux relation takes the form

$$\mathbf{j} = -D_c \nabla \rho + \rho \chi(c_t) \nabla c \tag{28}$$

where c_t denotes the time derivative of c. If $\chi(0) = 0$ then this relation predicts that the chemotactic component of the flux vanishes when the attractant field is time-invariant. A generalization of this in which c_t is replaced by an intermediate variable has been used by Höfer *et al.*[193], who show that such a model produces aggregation patterns very similar to those shown in Figure 29.

A significant problem in deriving equations such as (25) is to how translate microscopic responses of individual cells to the continuum level, and one approach to this problem that incorporates more of the microscopic details builds on the kinetic theory approach used earlier[182,183,194]. The diffusion equation can be derived as the limit of a random jump process, called a space jump process, in which the particle takes fixed jumps in space at fixed time intervals, by letting the space step size h and the

time step δt go to zero in such a way that the ratio $h^2/\delta t$ is a constant, namely D_c. Chemotaxis can be incorporated in this approach, but an alternative stochastic process that may be more appropriate than the space jump process to describe the motion of Dd cells is called the velocity-jump process[183,194]. In this process the velocity, rather than the spatial position, changes by random jumps. The prototypical organisms whose motion can be described as a velocity jump process are the flagellated bacteria, the best studied of which is *E. coli.* As we mentioned earlier, *E. coli* alternates two basic behavioral modes, a more or less linear motion called a run, and a highly erratic motion called tumbling, the purpose of which is to reorient the cell. Run times are typically much longer than the time spent tumbling, and when bacteria move in a favorable direction (*i.e.*, either in the direction of foodstuffs or away from harmful substances) the run times are increased further. During a run the bacteria move at approximately constant speed in the most recently chosen direction. New directions are generated during tumbles, and when bacteria move in an unfavorable direction the run length decreases and the relative frequency of tumbling increases. The distribution of new directions is not quite uniform on the unit sphere; it has a some bias in the direction of the preceding run. The effect of alternating these two modes of behavior, and in particular, of increasing the run length when moving in a favorable direction, is that a bacterium executes a three-dimensional random walk with drift in a favorable direction when observed on a sufficiently long time scale[168,195,196].

The chemotactic motion of Dd is more complicated, in that Dd cells change both the direction and the speed in the presence of cAMP[139]. As we indicated earlier, the directional changes are not randomly chosen, but rather, are chosen so as to align the cell with the direction of the stimulus. In the following paragraphs we describe a formulation that is sufficiently general to include these behaviors, as well as the involvement of internal cell variables in the description of motion. Details of this approach are given elsewhere[194,197].

We suppose that the internal dynamics that describe signal detection, transduction, processing and response are described by the system

$$\frac{d\mathbf{c}}{dt} = \mathbf{g}(\mathbf{c}, C_o). \tag{29}$$

where $\mathbf{c}$ is the vector of internal variables (concentrations, etc) and C_o

is the chemotactic substance (C_o is extracellular cAMP for Dd aggregation). In the TO model there are four internal concentration variables in the cAMP transduction pathway, but for describing chemotaxis one would have to formulate a model for the cGMP pathway. The form of this system can be very general but it should always have the 'adaptive' property that the steady-state value of the appropriate internal variable (the 'response regulator') is independent of the stimulus, and that the steady state is globally attracting with respect to the positive cone of R^m. A simple system which models the essential features of an adaptive system was given earlier.

In cases such as bacterial chemotaxis the cells do not significantly alter the signal, they only react to it. However Dd amoeba modify the chemotactic field when they relay the signal, and for such systems one has to augment (29) by an evolution equation for C_o. If transport is only via diffusion then this equation takes the form

$$\frac{\partial C_o}{\partial t} = D\Delta C_0 + f(\rho(\mathbf{x}, t), \mathbf{c}, C_o). \tag{30}$$

Let $p(\mathbf{x}, \mathbf{v}, \mathbf{c}, t)$ be the density function for individuals in a $2n + m$-dimensional phase space with coordinates $(\mathbf{x}, \mathbf{v}, \mathbf{c})$ where $\mathbf{v}$, which takes values in R^n, is the velocity. Then $p(\mathbf{x}, \mathbf{v}, \mathbf{c}, t)\, d\mathbf{x}\, d\mathbf{v}\, d\mathbf{c}$ is the number density of individuals with position between $\mathbf{x}$ and $\mathbf{x} + d\mathbf{x}$, velocity between $\mathbf{v}$ and $\mathbf{v} + d\mathbf{v}$, and internal state between $\mathbf{c}$ and $\mathbf{c} + d\mathbf{c}$. The quantity

$$\rho(\mathbf{x}, t) = \int p(\mathbf{x}, \mathbf{v}, \mathbf{c}, t)\, d\mathbf{v}\, d\mathbf{c} \tag{31}$$

is the density of individuals at $\mathbf{x}$, whatever their velocity and internal state. If we neglect external forces such as gravity then the evolution of p is governed by the partial differential equation

$$\frac{\partial p}{\partial t} + \nabla_{\mathbf{x}} \cdot \mathbf{v}p + \nabla_{\mathbf{c}} \cdot \dot{\mathbf{c}}p = \mathcal{R}, \tag{32}$$

where $\mathcal{R}$ is the rate of change of p due the random choice of velocity. In view of (29) this can be written in the equivalent form

$$\frac{\partial p}{\partial t} + \nabla_{\mathbf{x}} \cdot \mathbf{v}p + \nabla_{\mathbf{c}} \cdot \mathbf{g}p = \mathcal{R}. \tag{33}$$

We assume that the only contribution to the right-hand side arises from a process that generates random velocity changes, and we suppose that this process is a Poisson process of intensity λ, where λ may depend upon the internal variables, or at least on the response regulator**. Thus λ^{-1} is a mean run length time between the random choices of direction. In the case of Dd λ decreases slightly when the cell moves upgradient. The net rate at which individuals enter the phase-space volume at $(\mathbf{x}, \mathbf{v}, \mathbf{c})$ is given by

$$-\lambda p + \lambda \int T(\mathbf{v}, \mathbf{v}') p(\mathbf{x}, \mathbf{v}', \mathbf{c}, t)\, d\mathbf{v}'. \tag{34}$$

The kernel $T(\mathbf{v}, \mathbf{v}')$ gives the probability of a change in velocity from $\mathbf{v}'$ to $\mathbf{v}$, given that a reorientation occurs, and therefore $T(\mathbf{v}, \mathbf{v}')$ is non-negative and normalized so that $\int T(\mathbf{v}, \mathbf{v}')\, d\mathbf{v} = 1$. This normalization condition expresses the fact that no individuals are lost during the process of changing velocity.

In light of the foregoing assumptions, (33) becomes

$$\frac{\partial p}{\partial t} + \nabla_{\mathbf{x}} \cdot \mathbf{v} p + \mathbf{g} \cdot \nabla_{\mathbf{c}} p = -\lambda p - (\nabla_{\mathbf{c}} \cdot \mathbf{g})\, p + \lambda \int T(\mathbf{v}, \mathbf{v}') p(\mathbf{x}, \mathbf{v}', t)\, d\mathbf{v}'. \tag{35}$$

From this one sees that the dependence on the internal state adds both a drift term with velocity $\mathbf{g}$ and a source or sink of strength $\nabla_{\mathbf{c}} \cdot \mathbf{g}$. Since $\mathbf{g}$ depends on the stimulus $C_o(\mathbf{x})$ this velocity and source strength depend explicitly on the spatial position.

For most purposes one does not need the distribution p, but only its first few velocity moments. The first two are the number density $\rho(\mathbf{x}, t)$ introduced previously, and the macroscopic chemotactic velocity $\mathbf{u}_c(\mathbf{x}, t)$, which is defined by

$$\rho(\mathbf{x}, t) \mathbf{u}_c(\mathbf{x}, t) \equiv \int p(\mathbf{x}, \mathbf{v}, t) \mathbf{v}\, d\mathbf{v}\, d\mathbf{c}. \tag{36}$$

** Recent data suggest that this is an oversimplification; cells do not choose new directions via a Poisson process. Instead there appears to be an intrinsic periodicity to the extension of pseudopods, at least in un-stimulated amoeba[198,199]. Such behaviors can be taken into account by introducing other state variables, but we shall not pursue this here.

If we integrate (35) over $\mathbf{v}$ and $\mathbf{c}$ we find that ρ satisfies the conservation equation

$$\frac{\partial n}{\partial t} + \nabla_{\mathbf{x}} \cdot \rho \mathbf{u}_c = 0. \tag{37}$$

The problem is to relate the chemotactic velocity $\mathbf{u}_c$ to more fundamental quantities such as the internal and external state and to perhaps derive flux relations such as (25). This has not been done for any realistic problem that incorporates internal state variables since the analysis is difficult, but an indication of what is to be expected, using the cartoon model of adaptation described earlier, is given in Othmer[197]. We can however describe a simpler system that applies when the external gradient of cAMP is fixed, as in the experiments of Fisher *et al.*[139]. This analysis suggests that Vicker's[173] conclusion concerning aggregation in a static gradient is partially correct.

Suppose that a particle moves along the x-axis at a speed $s^{\pm}(x)$ that depends on x and its direction of travel, as in the experiments cited earlier, and that at random instants of time it reverses direction. Further, suppose that this "velocity-reversing" process is a Poisson process with constant intensity λ, *i.e.* the rate of reversal per unit time is λ. Further, let $p^{\pm}(x,t)$ be the probability density of particles that are at (x,t) and are moving to the right (+) and left (-). Then $p^{\pm}(x,t)$ satisfy the equations

$$\begin{aligned} \frac{\partial p^+}{\partial t} + \frac{\partial (s^+ p^+)}{\partial x} &= -\lambda p^+ + \lambda p^- \\ \frac{\partial p^-}{\partial t} - \frac{\partial (s^- p^-)}{\partial x} &= \lambda p^+ - \lambda p^-. \end{aligned} \tag{38}$$

These equations are obtained from (35) when there are no internal variables and only two velocities. The probability that a particle is at (x,t) is $p(x,t) \equiv p^+(x,t) + p^-(x,t)$, and the probability flux is $j \equiv (s^+ p^+ - s^- p^-)$. These satisfy the equations

$$\begin{aligned} \frac{\partial p}{\partial t} + \frac{\partial j}{\partial x} &= 0 \\ \frac{\partial j}{\partial t} + \lambda j &= -s^+ \frac{\partial}{\partial x}(s^+ p^+) - s^- \frac{\partial}{\partial x}(s^- p^-) + \lambda (s^+ p^- - s^- p^+) \end{aligned} \tag{39}$$

and the initial conditions $p(x,0) = p_0(x),\ j(x,0) = j_0(x)$, where p_0 and j_0 are determined from the initial distribution of p^+ and p^-. When the speed is constant the resulting model was first analyzed by Goldstein[200], and subsequently by Kac[201], McKean[202], Segel[203] and Othmer *et al.*[194].

Suppose we consider the system (39) on the interval (0,1) and impose Neumann (no-flux) boundary conditions at both ends. We wish to know under what conditions, if any, these equations have time-independent, nonconstant solutions for $p^\pm$ when $s^\pm$ are not constants. Under steady state conditions the first equation implies that j is a constant, and the boundary conditions imply that $j \equiv 0$. Therefore $s^+p^+ = s^-p^-$, and the second equation reduces to

$$\frac{\partial}{\partial x}(s^+p^+) = \lambda p^+ \frac{s^+ - s^-}{s^-} = \lambda s^+ p^+ \frac{s^+ - s^-}{s^+ s^-}. \tag{40}$$

This is a first order equation for p^+ whose solution is

$$p^+(x) = \frac{s^+(0)p^+(0)}{s^+(x)} e^{\lambda \int_0^x \frac{s^+ - s^-}{s^+ s^-} d\xi} \equiv p^+(0)F^+(x), \tag{41}$$

and therefore the condition of vanishing flux gives p^- as

$$p^-(x) = \frac{s^+(0)p^+(0)}{s^-(x)} e^{\lambda \int_0^x \frac{s^+ - s^-}{s^+ s^-} d\xi} \equiv p^+(0)F^-(x). \tag{42}$$

The constant $p^+(0)$ is determined by the global conservation condition

$$\int_0^1 (p^+(\xi) + p^-(\xi))d\xi = p^+(0) \int_0^1 (F^+(\xi) + F^-(\xi))d\xi = N, \tag{43}$$

where N is the total number of cells in the unit interval. The details of the spatial distribution depend on the functional form of the speeds $s^\pm$, but in any case we have

$$p(x) \equiv p^+(x) + p^-(x) = \left(\frac{N s^+(0)}{\int_0^1 (F^+(\xi) + F^-(\xi))d\xi} \right) \left(\frac{1}{s^+(x)} + \frac{1}{s^-(x)} \right)$$

$$\times \exp\left[\lambda \int_0^x \frac{s^+ - s^-}{s^+ s^-} d\xi \right], \tag{44}$$

and therefore

$$p'(x) = -A_o \left[\frac{s^+(x)'}{(s^+(x))^2} + \frac{s^-(x)'}{(s^-(x))^2} + \lambda \left(\frac{1}{(s^+(x))^2} - \frac{1}{(s^-(x))^2} \right) \right]$$

$$\times \exp \left[\lambda \int_0^x \frac{s^+ - s^-}{s^+ s^-} d\xi \right], \tag{45}$$

where A_o represents the quantity in the first parentheses in (44). From this one can determine how the distribution of $s^\pm$ affects the distribution of p. In particular, if $s^\pm$ are not constant then $p^\pm$ are also nonconstant. This is most easily seen if $s^+(x) = s^-(x)$, for then it follows directly from (44) that cells accumulate at the minima of the speed distribution. In any case, this simple model shows that cells can aggregate in a time-independent gradient by only modifying their speed. It is also easy to show that they cannot accumulate if the speed is constant but the turning rate λ is a function of x (*i. e.* if only local information is used to determine the rate of turning). However, they can aggregate if the turning rate is not constant and also depends on the direction of motion. Thus orthokinesis is sufficient to produce steady state aggregation irrespective of whether or not it is directionally biased. In contrast, klinokinesis is not if the turning rate is unbiased, but it is if the turning rate is directionally biased.

5 The chemotactic signal

The preceding descriptions are either macroscopic and phenomenological, or microscopic but still treat cells as point particles. Thus neither approach can address a number of basic questions about cell movement in aggregation and in the slug, including the microscopic issues of how a cell decides when to move, how it determines the direction in which to move, and how long it moves. A number of proposals as to how a cell orients have been made, and they can be classified into one of the following.

- A spatial gradient sensing mechanism, in which the cell measures the concentration difference or the difference in the number of occupied receptors between front and back[204–206,23].
- The differential force mechanism described earlier, which leads to

an expression for the macroscopic chemotactic sensitivity in terms of the sensitivity of the force exerted to the level of attractant[186,207].

- The 'pseudo-spatial' mechanism in which cells extend pseudopods and convert the spatial gradient in attractant sensed into a temporal rate of change of attractant[208].
- A spatio-temporal threshold mechanism, in which the orientation is determined by an internal gradient that is created by the spatial variation of the extracellular attractant. If there is adaptation in the chemotatic signal transduction pathway, then the internal gradient will decay, even in the presence of a steady external gradient, unless cells move. Internal gradients are known to exist in newt eosinophils where the development of a calcium gradient is necessary for cell polarization[209,210].

These mechanisms are clearly not all independent, and advocates of one or the other are more or less specific as to how cells 'measure' spatial gradients or temporal changes. Indeed it would be more appropriate to classify the mechanisms in terms of what characteristics of the signal determine the response, thereby removing the necessity for measurement by the cell. Numerous experiments[205,177,172,139,173] have been designed to determine which of these mechanisms are used to determine how to move, *e. g.* whether it is the local spatial or a temporal gradient, but the results are inconclusive, in part because the spatio-temporal characteristics of the signal seen by a cell are not known. Later we discuss some results obtained from a mathematical model for signaling between two relay-competent cells based on a geometrically-realistic representation of the cells. The model accurately reflects the spatial and temporal scales in signaling and the spatial localization of key enzymes, and thus the solutions of the governing equations should accurately reflect the spatial characteristics of the signal near the cell membrane, as well as in the cytoplasm. First however we discuss previous theoretical work aimed at understanding which mechanism is used.

5.1 Previous analyses of the chemotactic signal

Previous theoretical analyses of signaling ignore the membrane bound phosphodiesterase completely[211,212] or distribute the phosphodiesterase activity uniformly in space[213,113,119,5]. Models of aggregation have also

either ignored the mPDE[149,157,153,154,214], distribute the phosphodiesterase activity uniformly in space[148,193] or ignore the cAMP dynamics completely[150]. While the approach of distributing the phosphodiesterase activity uniformly in space may represent the average rate of degradation adequately, it does not yield the detailed spatial distribution of attractant in the immediate neighborhood of a cell.

Some of the earliest experimental support for the hypothesis that cells respond to the spatial gradient stems from the work of Mato *et al.*[204]. These authors used the chemotactic drop assay, in which drops of cAMP are placed near a droplet of cell suspension containing about 500 cells, and the distances at which 50% of the cells respond for a given cAMP concentration are measured. A log-log plot of the number of cAMP molecules *vs* the threshold distance yields an approximately straight line in Mato *et al.* 's experiments, the best fit slope of which is 1/4.25. The authors interpret this to mean that cells probably respond to the spatial gradient, and to understand how they reach this conclusion and why other interpretations are also possible, we present some of their theoretical analysis.

Consider the half-space $z \leq 0$ in three dimensions and suppose that N molecules are released instantaneously at the origin at $t = 0$. If there are no reactions that degrade this substance then the distribution at any later time is given by

$$c(r,t) = \frac{2N}{(4\pi Dt)^{\frac{3}{2}}} e^{-r^2/4Dt} \tag{46}$$

where D is the diffusion coefficient and r is the distance from the origin. Mato *et al.* measured the threshold distance for 50% response of amoeba in the droplet as a function of the concentration in the cAMP drop, which is interpreted as measuring a threshold r in (46) for different values of N. At any fixed distance $r > 0$ the cAMP concentration, the local gradient, and the local rate of change of cAMP in time all go through a maximum as a function of time, but they do so at different times, and the relationship between r and N when this occurs is different for the three quantities. One readily finds that

$$\frac{\partial c}{\partial r} = c(r,t) \left[\frac{-r}{2Dt} \right] \tag{47}$$

$$\frac{\partial c}{\partial t} = c(r,t)\left[-\frac{3}{2t} + \frac{r^2}{4Dt^2}\right] \tag{48}$$

$$\frac{\partial}{\partial t}\left(\frac{\partial c}{\partial r}\right) = -\frac{r}{2Dt}\left[\frac{\partial c}{\partial t} - \frac{c(r,t)}{t}\right] \tag{49}$$

and

$$\frac{\partial}{\partial t}\left(\frac{\partial c}{\partial t}\right) = c(r,t)\left[\frac{r^4}{16D^2t^4} - \frac{5}{4}\frac{r^2}{Dt^3} + \frac{15}{4t^2}\right]. \tag{50}$$

From these one finds that the maxima of c, $\partial c/\partial r$ and $\partial c/\partial t$ with respect to t occur at

$$t_1 = \frac{r^2}{6D} \sim 0.167\frac{r^2}{D} \tag{51}$$

$$t_2 = \frac{r^2}{10D} = 0.1\frac{r^2}{D} \tag{52}$$

and

$$t_3 = (5-\sqrt{10})\frac{r^2}{30D} \sim 0.06126\frac{r^2}{D} \tag{53}$$

respectively. Thus a cell sees the maximum rate of change in time first, then the maximum spatial gradient, and finally the maximum concentration. These are used to interpret the experimental data as follows.

If the time to a maximum of c, $\partial c/\partial r$ and $\partial c/\partial t$, respectively, is substituted into the foregoing expression for that quantity, one obtains the following dependence of the maximum values on the amount released and the distance from the source.

$$c(r,t)_{max} = \frac{0.66N}{r^3} \tag{54}$$

$$|\frac{\partial c}{\partial r}|_{max} = \frac{0.5827N}{r^4} \tag{55}$$

and

$$\left(\frac{\partial c}{\partial t}\right)_{max} = \frac{0.947ND}{r^5} \tag{56}$$

Note that only the maximum of the time rate of change depends explicitly on the diffusion coefficient.

If d is the distance at which 50% of the amoeba respond for a given N, then (54)-(56) define threshold values for the concentration, spatial gradient and temporal rate of change, respectively. Let $d_{min} = 0.95mm$ and $N_{min} = 10^{-14}$ be the smallest threshold distance at the smallest number of molecules used in the experiments; then one can normalize the data and obtain the following expression from (55).

$$\frac{d}{d_{min}} = \frac{1}{4} log \frac{N}{N_{min}} + \frac{1}{4} log \frac{0.5827 N_{min}}{\nabla C^* \cdot d_{min}^4}$$

Here ∇C^* is the threshold gradient for a 50% response. Similar expressions can be derived for the other quantities, but the coefficients are different. A straight line fit to a log-log plot of the experimentally-obtained normalized threshold distance versus the normalized amount released yields the reciprocal of the exponent of the r dependence. Mato *et al.* find that the slope is 1/4.25 for their experimental data, which is closer to the value of 1/4 for the maximum gradient than the value 1/5 for the maximum rate of change in time. On this basis they conclude that a cell responds to the spatial gradient. However this conclusion is predicated on the assumption that diffusion occurs in a half space, whereas in reality the system is a layer of finite thickness. If one recomputes the solution for diffusion in a vanishingly thin layer (*i. e.* in two space dimensions) one finds that the maximum rate of change is proportional to r^{-4} ! Thus one could also interpret the results as showing that the cells respond to the temporal gradient, since the exponent of the r dependence for the actual system will roughly lie between 4 and 5.* Further insight into how a cell decides to move can only be gained by knowing the details of the signal it sees, and a model that provides them is described in the next section.

5.2 A model for cell-cell signaling and orientation

Relay-competent cells must quickly decide on the direction in which to move after receiving a signal, since they will relay the signal and thus obliterate any directional information in the extracellular cAMP distribution. It is known that the cGMP pathway, which is important in

*In fact, the solution for a layer of finite thickness involves an infinite series and the $N - r$ relationship is not easy to extract. Thus the argument is somewhat heuristic.

controlling the cell motion[83,215,34], responds on a faster time scale than does the cAMP pathway, and that the intracelllular cGMP peaks about 10-15 seconds after stimulation[92]. In order to gain some insight into the mechanism by which the cell determines a direction to move, we first analyze the interactions between the various extracellular processes in the early stages of signaling. In the model presented here cells are endowed with specified volumes and boundaries, and thus the model should provide a realistic description of the signal seen by a cell. Such information is essential for understanding what aspects of the spatio-temporal signal trigger the chemotactic response. By adapting the TO model, which provides a good input-output relation for individual cells, the numerically-computed signal should closely approximate the signal seen by an aggregation-competent cell.

As shown in Figure 30, the cells are modeled as cylinders on the plane, and diffusion and degradation of cAMP occurs both within each cell and in the region exterior to the cells. Signal transduction and cAMP production occur at the boundary of each cell, and secretion occurs across that boundary. In this section one cell functions as the signaler by releasing

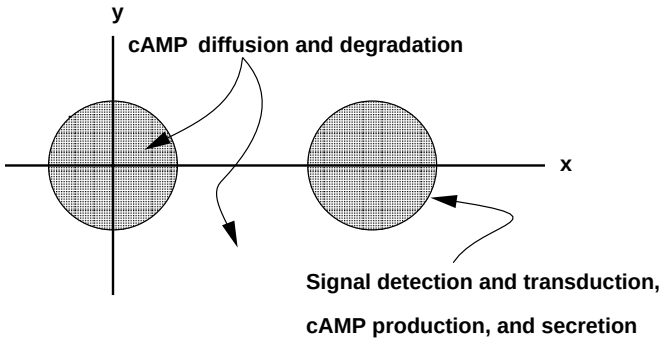

Figure 30. A top view of the geometric arrangement of the two cells and the processes that are incorporated in the model. All concentrations are assumed to be uniform in the vertical direction.

cAMP with a specified time course, and the other cell serves as the receiver but does not release cAMP. This is a realistic model for the early stages since a single cell can be a pacemaker[141], and each cell relays the signal. A more detailed model in which both cells are active is developed in Dallon and Othmer[216].

To determine the cAMP concentration in the region exterior to the cells, we must solve the reaction-diffusion equation

$$\frac{\partial w_5}{\partial \tau} = D_1 \nabla^2 w_5 - \hat{\gamma_9} \frac{w_5}{w_5 + \gamma_8} \tag{57}$$

exterior to the cells, with boundary conditions

$$-D_1 \hat{\mathbf{n}} \cdot \nabla w_5 = -\gamma_7 \frac{w_5}{w_5 + \gamma_6} \tag{58}$$

on $\partial\Omega_1$ and

$$-D_1 \hat{\mathbf{n}}^2 \cdot \nabla w_5 = \frac{V_c}{k_5 [\mathrm{iPDE}]_T A_c r_0} K F(t) - H(t-2) \left(\gamma_7 \frac{w_5}{w_5 + \gamma_6} \right) \tag{59}$$

on $\partial\Omega_2$. Here $\partial\Omega_i$ is the boundary of the i^{th} cell, $\hat{\mathbf{n}}^i$ is a vector normal to $\partial\Omega_i$ with respect to the exterior domain and $K^{-1} = V_c \times$ Avogadro's number. The function $F(t)$ takes into account not only the release of cAMP by the signaling cell, but also enzymatic degradation by mPDE on the cell surface. It is taken to be a piecewise linear function defined by

$$F(t) = \begin{cases} F_m t & 0 \leq t < 1 \\ F_m (2-t) & 1 \leq t \leq 2 \\ 0 & \text{otherwise} \end{cases} \tag{60}$$

where t is in minutes and F_m is set at 2×10^7 molecules per cell per minute [217,126]. The signaling is turned on for two minutes because this is the nominal signaling period in response to a step change in extracellular cAMP. H is the Heaviside function, which is defined as

$$H(t) = \begin{cases} 0 & t < 0 \\ 1 & t \geq 0 \end{cases} \tag{61}$$

Because F takes into account the degradation by mPDE, the effect of mPDE must be turned on separately when the signal is terminated at $t = 2$ minutes, which accounts for the term involving $H(t)$.

5.3 Numerical Results

Attenuation of the cAMP signal transmitted from a signaling cell to a receiver is due to both diffusive spread of the signal and hydrolysis due to the phosphodiesterase present. The interplay of these factors is complex, particularly when the distance between signaler and receiver is also varied. This was first shown in a model with no intracellular dynamics developed by Pate, et al. [147]. We first consider diffusive signaling between two cells in the presence of mPDE and the absence of ePDE (the effects of ePDE are small in most cases[216]). The value of the effective Michaelis constant for mPDE, which we denote K_{mPDE}, has a reported range of 0.5μM to 20.0μM[218,219]. At the lowest affinity reported ($K_{mPDE} = 20.0\mu M$) $\gamma_6 = 11.6$, while at the highest reported affinity ($K_{mPDE} = 0.5\mu M$) $\gamma_6 = 0.29$. The use of these values will produce chemical profiles which bracket the true profiles seen by a cell. In addition, the low-affinity results should closely approximate the profiles when mPDE is completely blocked.

In the following figures the center-to-center spacing between the signaling and receiving cells is 30 microns, which is approximately half the maximum separation at which aggregation by long-range signaling occurs[143,220]. Figure 31 displays the concentration profile 12 seconds after

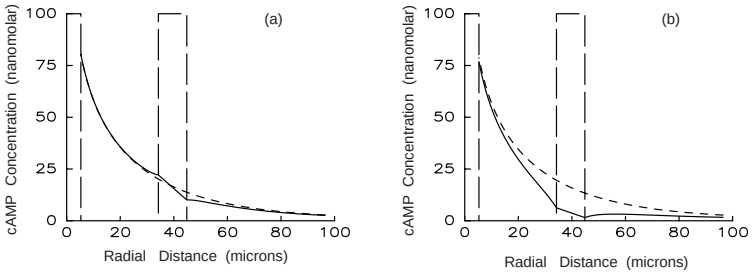

Figure 31. The concentration profile of cAMP when one cell is signaling and the receiver is inactive. The large dashed rectangles represent the cells: signaling cell on the left and the receiver on the right. In (a) $\gamma_6 = 11.6$, while in (b) $\gamma_6 = 0.29$. All the profiles shown are at 12 seconds after the onset of signaling. The solid line is the cAMP concentration along the radius passing through the center of the receiver, and the dashed line is the cAMP concentration in the antipodal direction.

the start of the 2 minute secretion period. The time at which to display

the profiles was chosen for two reasons: (a) cells can certainly orient within 20 seconds after receiving a stimulus[177] (and faster in some reports), which indicates that the choice of direction is made in this time frame, and (b) the cGMP signal, which is involved in chemotaxis, peaks about 10-15 seconds after stimulation.

In Figure 31 the solid curve gives the concentration profile along the half-line extending from the center of the signaling cell through the center of the receiving cell, while the dashed line shows the profile along the antipodal direction. Although the cAMP concentration is ultimately monotonically decreasing in both directions, there are distinct differences locally due to the presence of the receiving cell. In Figure 31(a) the local cAMP gradient is decreased in magnitude near the receiver as compared to the opposite direction. Due to the "diffusive shadow" created by the receiving cell, both the difference between the front and rear concentrations and the front/rear ratio of cAMP concentrations increases over that of the unperturbed field in the same spatial region. (Front will always refer to that point on the receiving cell closest to the signaling cell, rear to the point furthest away.) Thus the mere presence of the receiving cell amplifies any chemotactic signal based on a front-to-back concentration difference when compared with the field generated by the signaling cell alone.

To understand the effect of mPDE on the profiles we reduce the effective Michaelis constant to $K_{mPDE} = 0.5\mu$M, which makes $\gamma_6 = 0.29$. In comparing Figure 31(a) with Figure 31(b), we see that the cAMP levels are everywhere lowered in the latter due to increased enzymatic degradation, and there is a distinctive sharpening of the cAMP spatial gradient between the signaling and receiving cell (solid line), as was suggested previously on the basis of a less detailed model[221]. In fact the concentration at the receiving cell has been decreased by more than a factor of 2 as compared to either the concentration in the antipodal direction or to the concentration at the receiving cell in the presence of lower mPDE activity. Thus the presence of mPDE can have a major effect on the cAMP profiles, both at a fixed time, and as we shall see shortly, on the temporal profiles.

The effect of mPDE may extend a substantial distance from the receiving cell, as is shown by the level curves in Figure 32. One can see that the concentration level lines are nearly circular when the affinity of

mPDE is low (panel (a)), but in the high-affinity case the level sets are severely distorted (panel (b)). In fact, in the latter case the receiving cell is located at a local minimum of the cAMP concentration: the concentration increases significantly in the direction normal to the boundary of the receiving cell at all points on the boundary. This is further emphasized

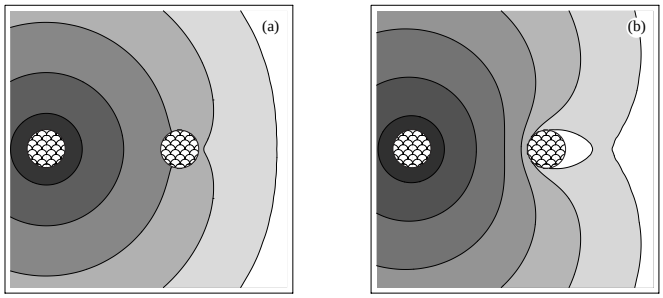

Figure 32. A contour plot of the cAMP concentration in an 85 micron square region 12 seconds after the onset of signaling. The cells are 30 microns apart, the signaling cell is the circle on the left and the receiving cell is the circle on the right. In panel (a) $K_{mPDE} = 20.0\mu M$ and in panel (b) $K_{mPDE} = 0.5\mu M$. The contours in (a) from highest (dark) to lowest are $10^{1.75}$ nM, $10^{1.50}$ nM, $10^{1.25}$ nM, 10 nM, $10^{0.75}$ nM and in (b) they are the same with one additional contour of $10^{0.5}$ nM.

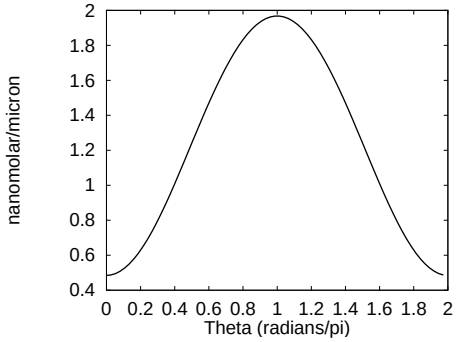

Figure 33. The derivative of cAMP concentration with respect to the outward normal at the surface of the receiving cell for $K_{mPDE} = 0.5\mu M$. The signaling cell is in the direction Theta = 1.0

by the graph in Figure 33, which shows that the spatial gradient in cAMP

concentration normal to the receiving cell surface is everywhere positive, with a maximum value in the direction of the signaling cell. This is easily understood given the presence of mPDE on the cell membrane, but had been overlooked prior to the work of Pate et al.[147]. It should be noted that the maximum gradient seen by the receiver, which is $\sim 2 \times 10^3$ nM/mm, is far larger than either the static gradients of ~ 10nM/mm used experimentally[139] or the average gradient of ~ 100 nM/mm in an aggregation wave[123].

To better characterize the cAMP signal at the receiving cell, we show the front (solid line) and rear (dashed line) cAMP concentrations at the receiving cell as a function of time in Figure 34, and the front/rear cAMP ratio as a function of time in Figure 35.

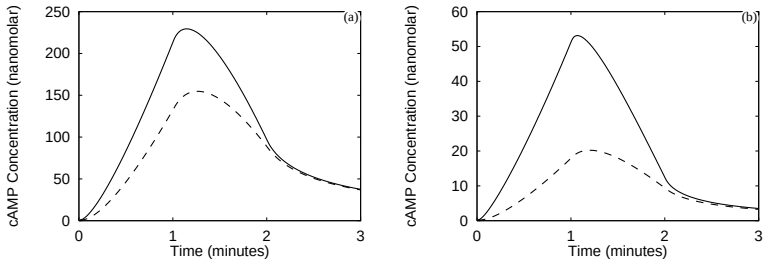

Figure 34. The concentration of cAMP plotted as a function of time for the same conditions as apply to Figure 32. The solid line corresponds to the concentration at the front of the cell, and the dashed line denotes the concentration at the back of the cell. Note the difference in the scales for the cAMP concentration in the two panels.

The detailed information given in these figures on the spatio-temporal cAMP signal seen by a cell may shed light on the precise nature of the chemotactic signal. The characteristics of the solution shown in the figures, as well as the front-to-rear ratio of the rate of change of cAMP, have been suggested by one or more authors to be important in determining the chemotactic response. However it is very unlikely that the ratio of the rates of change at front and back is used. Dallon and Othmer[216] show that this ratio is essentially constant during the early phase of signaling, and peaks *when both rates of change are negative*. Moreover, the peak occurs far too late to provide reliable information for orientation.

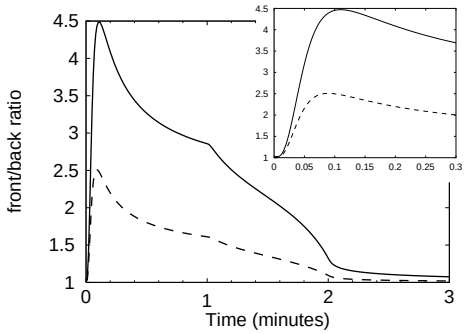

Figure 35. The ratio of front and back cAMP concentrations at the receiving cell's surface for the time plots in Figure 34. The solid line is the ratio $K_{mPDE} = 0.5\mu M$ and the dashed line is the ratio for $K_{mPDE} = 20.0\mu M$. The inset shows the short-time behavior of the ratios.

Earlier we described two other mechanisms that might plausibly be used, a spatial gradient sensing mechanism, in which the cell measures the concentration difference or the difference in the number of occupied receptors between front and back[204–206,23], and a 'pseudo-spatial' mechanism in which cells extend pseudopods and convert the spatial gradient in attractant sensed into a temporal rate of change of attractant[208]. However, Figures 31, 32 and 33 show that in the presence of significant mPDE activity the cell sees an increase in the attractant in *every* direction. This result does not preclude the use of either mechanism, but the problem of choosing a direction in which to move becomes harder for the cell and thus orientation becomes less reliable. Using either of these mechanisms, the problem is not to choose between favorable and unfavorable directions, as would be the case in the presence of a monotonic concentration profile across the cell, but rather that of selecting the best direction when all are favorable.

It is evident from a comparison of (a) and (b) of Figures 31 and 34 that the increased affinity of mPDE leads to a decrease in the absolute front-to-rear concentration difference across the receiving cell by a factor of two over that with a lower affinity mPDE. However, the peak front-to-back *ratio* of cAMP increases by a factor of nearly two when compared to that which exists for the low affinity mPDE (*cf.* Figure 35). Thus, this ratio provides a better signal characteristic to use for initiating the

chemotactic response than the local gradient at the surface[211]. Moreover, it is clear that this extracellular cAMP ratio can be transduced into an intracellular gradient of a species such as cGMP, and this can provide the directional information needed by a cell for orientation[†]. This mechanism also frees the cell of the problem associated with the fact that the cAMP concentration near the cell is increasing outwardly in all directions. Furthermore, the front/back ratio peaks at about 7 secs (cf. inset in Figure 35), which enables the cell to choose a direction for movement before it swamps the signal with the relay response.

These results suggest that mPDE may increase the efficiency of orientation by amplifying the front/back ratio of extracellular cAMP, and hence the steepness of an intracellular gradient of cGMP or other components in the chemotactic pathway. However the results also show that this is not necessary, particularly if the intracellular transduction steps amplify the end-to-end differences significantly. This could be done, for example, by a highly cooperative step in the chemotactic pathway.

Chemotaxis, and the extraction of directional information from a noisy signal that it requires, is used by many other types of cells, and a great deal of work has been done toward understanding the effects of noise in the signal. This and other aspects of signal detection have been reviewed by numerous authors[222–226].

6 Mechanisms for the generation of spirals and streams in aggregation

6.1 Formation of spiral waves

Spiral waves are the dominant pattern of aggregation in many laboratory experiments, but it is not understood how they arise *in vivo*. As we showed earlier, in the continuum description they can be initiated by using special initial conditions, but they can also arise spontaneously in the discrete cell model. Using a random initial cell density, Dallon and Othmer[175] found that they are generated by a pacemaker that initiates axisymmetric (target pattern) waves which then break up into a spiral when

[†]Computational results[216] demonstrate that intracellular cAMP exhibits a significant gradient, and since it responds more slowly than cGMP, the same is undoubtedly true for cGMP or other species that respond more rapidly than cAMP.

they encounter a low density region. They discovered that spirals do not form when the initial density is too low, but they do form at a sufficiently high density ($\rho \geq 0.4$) (cf figure 36). Laboratory experiments also suggest that the average density is an important factor in the formation of spirals[227], and the computational experiments support these findings. To understand the density effect one must understand two aspects: (i) how spiral waves are initiated, and (ii) when can they coexist with a pacemaker.

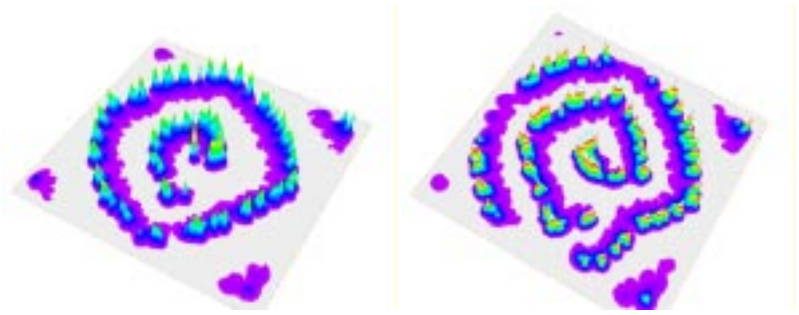

Figure 36. The cAMP wave for a simulation in which a spiral wave arises spontaneously in a field with a pacemaker at the center. In (a) $t = 95$ and the pacemaker fires before the spiral wave arrives. In (b) $t = 110$ and the spiral has entrained the pacemaker, at least temporarily. (From Dallon and Othmer[175].)

Durston[161] was one of the first to consider theoretically how waves can be broken during aggregation, and Lee *et al.* [227] observe that spirals form at disrupted wave fronts that arise from wave-wave interactions and from inhomogeneities in the system. However it is not understood why density is an important factor in determining whether or not spirals will form. In the simulations shown in Figure 36 wave-wave interactions are not important, since there is only one pacemaking region. At low average densities a local low density region usually elongates in the direction of propagation as streams form on either side of the region. Initially the cAMP wave will start to curl as it travels around the region on both sides, but then the two pieces rejoin at the rear to form a distorted, yet connected wave front. At higher average densities the computational results suggest that passive spread of cAMP through the low density region is rapid enough to trigger a wave on the downstream side of the low density region before the main wave reaches that side. Initiation of

this secondary wave can then alter the cAMP environment sufficiently to break the primary wave and form a spiral. A natural question is why this process depends on the average density, and the explanation is as follows. At sufficiently low average densities the passive spread of cAMP never produces a superthreshold signal at the downstream side and the primary wave rejoins smoothly there, but at sufficiently high densities the passive spread can trigger a secondary wave. Long-range spread of cAMP through the low density region is possible because of the smaller effect of mPDE there. While this provides a qualitative explanation for the origin of spirals, further work is needed to quantify the effect and to determine whether this is an important mechanism for break-up (others are given below).

Once a wave is broken and a spiral is formed, it must be able to coexist with a pacemaker, at least for a period of time, unless the pacemaker dies. It has been shown previously that a pacemaker can coexist with a spiral wave indefinitely in other excitable systems[10], but no theoretical explanation of this was given. It is known that for both pacemaker-initiated waves and spiral waves, their speed and period is such that the combination lies close to the dispersion curve for periodic traveling waves (Figure 22(b)), and thus some insight into the effect of density on coexistence is obtained by comparing the dispersion curves for different densities given in Figure 22(b).

The range of periods of naturally-occurring pacemakers is 3-10 minutes, and under the conditions used here the periods are in the range of 4-6 minutes. As a result, one can see from this figure that a high density field is more likely to propagate every wave initiated by a pacemaker, rather than gating the waves. Secondly, it is clear that higher density fields propagate stable waves over a much wider range of speed for pacemaker periods in the range used here, and thus coexistence between distinct types of waves is more likely at high densities. In particular, a spiral wave and an axisymmetric wave are more likely to coexist for some time in a high-density field. Such coexistence is essential to provide time for a spiral to develop in a field forced by a pacemaker. Once it is fully developed, it may or may not completely entrain the pacemaker. An alternative to coexistence is that the pacemaker dies when the local cell density grows too large, something which we have observed in computational experiments.

There are several other possible mechanisms that may lead to the for-

mation of spiral waves. It is known that cells may become pacemakers as aggregation proceeds, and therefore there is a possibility that randomly-located pacemakers may release pulses of cAMP and thereby break a traveling wavefront. This is unlikely to happen after waves are well-established in the field, because a single cell does not release enough cAMP to disrupt a well-established wave. However, this may be important in early aggregation when the waves are not yet well-established and the competition between pacemakers already produces partial fragmentation of waves. This idea could be tested by random additions of cAMP pulses to an early aggregation field, something which is more easily done using a computational model than in the laboratory.

Another recent suggestion for the origin of spirals that relies on random variations in early aggregation is due to Palsson and Cox[117]. These authors add spatial and temporal noise to the levels of the cAMP phosphodiesterase inhibitor in order to create local pacemakers that break wavefronts and create spirals. In their approach, which is formally identical to that in the preceding paragraph, a local increase in PDI, the inihibitor of PDE, gives rise to a cAMP pulse, and since the cells do not all secrete PDI at the same time, this can explain the random spontaneous cAMP pulses that are observed, and which may break wavefronts. Heterogeneity of cell parameters has also been suggested as a mechanism of spiral formation[228].

Finally, Levine *et al.* [229] postulate a third mechanism for the origin of spiral waves based on what they call genetic feedback. It is known that in early aggregation several genes are induced by nanomolar pulses of cAMP (cf. Figure 5), and Levine *et al.* assume that the excitability of a cell changes with time according to a first-order equation of the form

$$\frac{dE}{dt} = -\alpha E + \beta C_o \tag{62}$$

where E is the excitability and C_o is the extracellular cAMP concentration. Thus during a transient increase of cAMP the excitability increases, but after the cAMP level decreases the excitability decays to a level set by the basal cAMP level (which in reality depends on the excitability, but in the model only the threshold cAMP level for secretion depends on the excitability). The authors prescribe rules for the cAMP production and secretion and simulate the resulting equations. They find that the use of (62) in conjunction with an equation for cAMP dynamics can

produce large-scale spirals, whereas uniform increases in the excitability of all cells produces a more fragmented aggregation field that contains many spirals. However their model seems implausible since it requires that the excitability vary on a time-scale of minutes, and in particular, that it increases in a cell that experiences the temporal cAMP profile characteristic of a traveling wave. This is incompatible with the observation that stimulatory effects of a series of cAMP pulses on gene expression occur with a half-time of several hours[53].

Thus there is no experimentally-established mechanism for spiral wave formation, but there are several plausible theoretical suggestions, all of which rely on random variations in the aggregation field, either in the cell density, or in parameters that can locally produce pacemakers that disrupt wavefronts. Further work is needed to more rigorously establish the mechanisms, both from the experimental and the theoretical side.

6.2 The origin of streaming

The final aspect to be discussed concerns the origin of streams during aggregation. In Figure 37 we show the distribution of cells at two times. It is clear in the right panel that the streams first develop close to the pacemaker, and then grow outward. Also noteworthy is the branching pattern in the streams, and in particular, that there is no dominant length scale in the streams: streams form at every length scale and their structure may be approximately fractal. In this section we discuss several theoretical mechanisms proposed to explain their formation.

It is easy to produce an heuristic argument that shows why the uniform cell distribution should be unstable to sufficiently large disturbances. Cells move in the direction of higher cAMP and produce it as well; therefore a disturbance that creates a large enough density or cAMP nonuniformity will induce cell movement and this will in turn reinforce the nonuniformity. Moreover, the variations in density or concentration will be reinforced with each passing cAMP wave. Thus there is no doubt that large variations in density can lead to streaming; where current theories differ is whether the uniform distribution is stable or unstable to small disturbances. Dallon and Othmer[175] provide computational evidence that a perfectly uniform initial distribution of identical cells will not develop streams, and they give several heuristic reasons to assist in understanding these results. Firstly, it is known that there is a diffusional component to

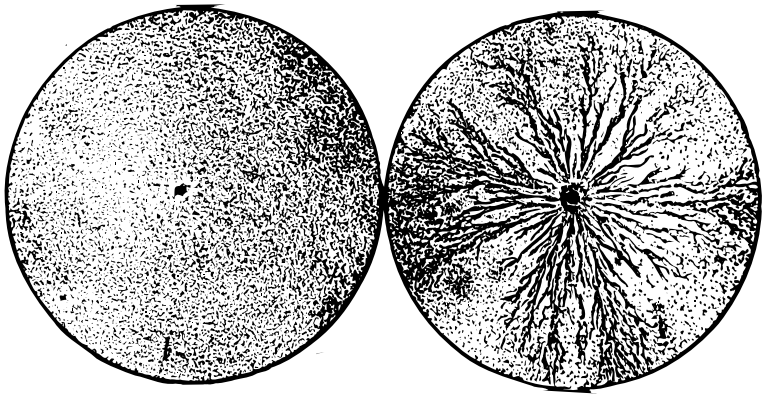

Figure 37. The evolution of streams during aggregation. The top panel shows an early, relatively-uniform field with a pacemaker at the center, and the bottom panel shows the development of streams at a later stage. Note that the streams are most pronounced near the pacemaker, and that there is little stream formation near the boundary of the dish. (From Raper[230].)

cell motion, and this will tend to stabilize the uniform distribution. Diffusion is not explicitly included in the model, but it can be shown that the numerical procedure introduces it via the truncation errors. Secondly, it is known that the transduction pathway to the locomotory machinery adapts to the extracellular cAMP signal, and this fact is included in their model. As a result of adaptation, disturbances that vary slowly over time will not be amplified by cell movement. Finally, there is a threshold in the cAMP gradient of $\sim 10\ nM/mm$[231] below which the cells do not chemotact. These three factors, diffusion, adaptation and a threshold, all mitigate against amplification of small disturbances, and Dallon and Othmer[175] conjecture that the streams result from a finite-amplitude instability. This is currently under investigation[232].

Other numerical evidence that supports their conjecture is as follows. In a simulation with a uniform initial cell density of 0.2, streaming occurs after a period two to three times longer than when a random initial density is used. In order to test for edge effects a simulation on a cylinder with a central (axially) band of pacemaker cells was done. The initial conditions were uniform around the cylinder and cells within 0.05 cm of the center were made oscillatory. In this simulation the cells moved toward the center line, uniformly in the transverse direction, for at least

100 minutes, *i. e.* , there was no streaming before this time. After this time the pacemaker region begins to break up, which causes streaming in the nearby field. The far field structure remains largely unaffected for at least 50 minutes more. Thus they conclude that linear instabilities, if they exist at all, do not effect the aggregation patterns on a time scale that is relevant to aggregation under normal conditions.

This conclusion differs from the conclusion reached by others using a continuum description of the cell density. Levine and Reynolds[153] find that for a different model streaming is due to a linear instability in the governing equations. These authors use a continuum description and show that planar traveling waves can be unstable to perturbations of wavelength greater than approximately 8 mm, but stable otherwise. They conclude that a streaming instability can occur, but their results show that it is a very long wavelength instability and thus would probably not be seen on the scale of normal aggregation patterns. Moreover, in the mechanism they suggest the growing modes are not stationary in space, but rather, they propagate outward with the cAMP waves as their amplitude increases. Thus the maximum growth will be seen at the outer boundary of the domain, which implies that streams will develop first near the outer boundary. However, as we pointed out earlier, streaming develops first in the center and later at the periphery.

Vasiev *et al.*[154], who also use a continuum model for the cell density, conclude that a necessary condition for the development of streams is that the initial density be nonuniform. However, they did not addresses the question as to whether or not the uniform distribution is stable to small amplitude disturbances. These authors suggest that the major factor in stream formation is a change in the speed of the cAMP wave as density varies. As can be seen in Figure 22(a), the speed increases with density, at least up to moderate densities (in Vasiev *et al.* 's model the speed is monotonic increasing for all densities), and this may be an important factor. Höfer and Maini[233] incorporate this idea and the curvature-velocity relationship given in (16) into a simplified model on which some analysis can be done.* They also conclude that plane cAMP waves can become unstable to transverse perturbations, but as in the Reynolds-Levine analy-

*It should be noted that these authors incorporate the ϵ in that equation into the diffusion coefficient, which is therefore a scaled version of the true diffusion coefficient.

sis, the disturbances propagate outward as they grow and thus the largest amplitude will be seen on the outer boundary.

Thus the existing simplified models make predictions that are at variance with the experimental observations and with the computational results obtained using a discrete cell model, and further work is needed to resolve this issue.

7 Conclusion

Much less is understood about the later stages of development, including the formation of the mound, the migration of the slug, pattern formation, cell sorting and regulation during migration, and the formation of the fruiting body. Some important problems for future study are the following.

1. **Understanding adenylyl cyclase regulation** At present there is still uncertainty concerning the detailed molecular interactions that produce adaptation of adenylyl cyclase. Here, more experimental data are required before a biochemically correct model for oscillatory signaling can be formulated.

2. **Understanding cell locomotion and orientation in response to chemotactic stimuli** The chemotactic signal is ultimately translated into cytoskeletal rearrangements, that lead to pseudopod extension and cell locomotion[234–236]. cAMP affects the state of myosin phosphorylation through the cGMP signaling pathway[36,37]; regulation of guanylyl cyclase is complex and shows at least three levels of desensitization[92]. Since desensitization involves both rapidly (Ca^{2+}, cGMP) and slowly diffusing (cytosolic proteins that regulate guanylyl cyclase activity) molecules[101,65], integration of this input could provide the cells with spatio-temporal information on the chemoattractant gradient (*cf.* Section 4). cAMP also regulates actin polymerization by an as yet unknown signaling pathway. Clearly, much experimental work is still required to identify both the signal transduction and cytoskeletal components of the chemotactic response and to understand their interactions. Even when all molecular components are identified, the highly complex network that specifies their interactions interaction can probably only be under-

stood by a quantitative approach. Single cell models of the type developed by Bottino[237] will be useful in this respect since models of actin polymerization can be incorporated.

3. **Understanding cAMP signaling after aggregation** A fairly large body of evidence indicates that oscillatory cAMP signaling continues after aggregation and controls the morphogenetic cell movement that leads to formation of migrating slugs and culminating fruiting bodies. The apical tip of mounds and slugs, which has the properties of a classical embryological organizer, is thought to exert this function in Dictyostelium by acting as an autonomous cAMP oscillator. At the onset of multicellular development one essentially goes from two-dimensional to three dimensional wave patterns, the latter confined to hemispherical mounds and cylindrical slugs. Advanced imaging techniques show optical density waves shaped armed spiral patterns similar to spiral cAMP waves in aggregation fields[238]. Cells appear to respond to these waves with rotary movement around the aggregate center. Interrupted cell movement reminiscent of chemotaxis to cAMP pulses was observed in slug posteriors, whereas rotary movement is the predominant movement pattern in slug anteriors[239,240]. It was concluded that during slug formation the two-dimensional spiral evolves into a three -dimensional scroll wave at the slug tip, which degenerates into a planar wave at the posterior, due to reduced excitability in this region. These three-dimensional wave patterns could be generated in a cylindrically-shaped 'computational slug' using the MG model[241], but the diameter used was much larger than it is in reality, and thus it is not clear whether existing modesl will predict that scroll waves can exist in a slug. Further, in slugs the major components of the cAMP signaling system, such as cAMP receptors, adenylyl cyclase and extracellular PDE are quite substantially downregulated after aggregation[242,75,243]. This downregulation may reflect the fact that much higher cAMP levels can be achieved with lower cAMP output by individual cells, due to the high cell density in aggregates. The high affinity cAMP receptor cAR1, which is present in large numbers in aggregating cells, decreases significantly after aggregates have formed, and the intermediate affinity receptor cAR3 and low affinity receptors cAR2 and cAR4 are now expressed in different domains in the slug[244]. All cARs can potentially mediate

excitation and adaptation of adenylyl cyclase, and so may regulate this enzyme during postaggregative development (Kim, J.Y., Borleis, J. and Devreotes, P.N. submitted). One can only speculate as to whether this actually occurs and what the effects of coupling adenylyl cyclase to lower affinity cARs might be. Future studies are required to establish to what extent current models for oscillatory cAMP signaling in early development can reproduce the cell movement patterns observed during multicellular developments and if not, what adjustments are required. In parallel, experimental data on the input/output behavior of the cAMP signaling system and the biochemical characteristics of its components should be collected to determine whether such adjustments are realistic.

4. **Understanding cell movement in streams, mounds and slugs** Little as we understand the translation of chemotactic signals into directed movement of individual cells, there are additional problems in understanding cell movement in multicellular structures. A major question is whether cells use the same system for locomotion, *i. e.* pseudopod extension and retraction of the rear end. Cell tracking of a few labeled cells in streams and mounds shows that this is probably the case [245–249,238]. During aggregation cells become progressively more adhesive and a possible role of cell adhesion in cell movement should be considered. Cell adhesion may e.g. be important to generate traction, and there is probably also a function for the muccopolysaccharide sheath in generating traction and maintaining structural integrity. From the modeling standpoint one question is whether the motion of the slug can be described adequately by continuum models such as are used by Vasiev *et al.*[250]. A further question is how the 'rules' for the motion of individual cells should be incorporated into continuum models?

4. **Interactions between cell movement and cell differentiation** In the period just after starvation, cell differentiation is essentially linear and cells differ only with respect to the extent in which they express markers of preaggregative development. After aggregates have formed, intercellular signaling induces the cells to differentiate into two distinct differentiation pathways. On one hand, extracellular cAMP produced by oscillatory signaling triggers prespore differentiation and synthesis of morphogens such as the stalk inducing factor DIF. On the other, the differentiation state of the cells has

a profound effect on its signaling properties. The components of the cAMP signaling system are drastically downregulated, particularly in prespore cells[243]. The differentiated cells sort by differential chemotaxis, and by so doing they create separate domains with different signaling properties. This in turn will affect cell movement and further differentiation and maturation of the differentiated cell types. In order to completely understand Dictyostelium development at the molecular level, this complex network has to be experimentally mapped and theoretically understood. This is clearly not within easy reach, but some progress has been made[251]. In view of the fact that current molecular genetic approaches are rapidly uncovering hitherto unknown components of signaling systems, whose function and interactions are more easily understood because of the excellent experimental accessibility of the system, a complete understanding of Dictyostelium may be obtained within the not too distant future.

ACKNOWLEDGMENTS

We thank J. J. Blum, Thomas Höfer, Vidyanand Nanjundiah, Lee Segel and Peter J. M. van Haastert for their critical reading of the manuscript and many suggestions for improvements.

Hans G. Othmer*
Department of Mathematics
University of Utah
Salt Lake City, UT, 84112

Pauline Schaap
Cell Biology Unit
University of Leiden
2300 RA Leiden
The Netherlands

*Supported in part by NIH Grant #GM 29123

I. Literature cited

[1] Parker, S. P, ed. (1994) *Dictionary of Scientific and Technical Terms* (McGraw-Hill, Inc., New York).

[2] Koutalos, Y & Yau, K. Y. (1996) *TINS* **19**, 73–81.

[3] Goldbeter, A & Koshland Jr, D. E. (1982) *J. Mol. Biol.* **161**, 395–416.

[4] Othmer, H. G, Monk, P. B, & Rapp, P. E. (1985) *Math. Biosci.* **77**, 77–139.

[5] Tang, Y & Othmer, H. G. (1994) *Math. Biosci.* **120**, 25–76.

[6] Spiro, P. A, Parkinson, J. S, & Othmer, H. G. (1997) *PNAS* **94**, 7263–7268.

[7] Devreotes, P. N, Derstine, P. L, & Steck, T. L. (1979) *J. Cell Biol.* **80**, 291–299.

[8] Devreotes, P. N & Steck, T. L. (1979) *J. Cell Biol.* **80**, 300–309.

[9] Theibert, A & Devreotes, P. N. (1983) *J. Cell Biol.* **97**, 173–177.

[10] Othmer, H. G & Tang, Y. (1993) in *Experimental and Theoretical Adv. Pattern Formation*, eds. Othmer, H. G, Maini, P. K, & Murray, J. D. (Plenum Press), pp. 277–313.

[11] Tang, Y & Othmer, H. (1994) *Biophys. J.* **67**, 2223–2235.

[12] Tang, Y, Stephenson, J. L, & Othmer, H. G. (1996) *Biophys. Jour.* **70**, 246–263.

[13] Katz, B & Thesleff, S. (1957) *J. Physiol.* **138**, 63–80.

[14] Gero, A. (1983) *J. Theor. Biol.* **103**, 137–162.

[15] Knox, B. E, Devreotes, P. N, Goldbeter, A, & Segel, L. A. (1986) *PNAS* **83**, 2345–2349.

[16] Segel, L. A, Goldbeter, A, Devreotes, P. N, & Knox, B. E. (1986) *J. Theor. Biol.* **120**, 151–179.

[17] Gerisch, G. (1968) *Curr. Top. Dev. Biol.* **3**, 157–197.

[18] Newell, P. C. (1971) *Essays in Biochem.* **7**, 87–126.

[19] Loomis, W. F. (1979) *Dev. Biol.* **70**, 1–12.

[20] Devreotes, P. N. (1982) in *The Development of* Dictyostelium discoideum, ed. Loomis, W. F. (Academic Press, New York, USA), pp. 117–168.

[21] Gerisch, G. (1982) *Ann. Rev of Physiol.* **44**, 535–552.

[22] Schaap, P & Wang, M. (1984) *Dev. Biol.* **105**, 470–478.

[23] McRobbie, S. J. (1986) *Crit. Revs in Microbiol.* **13**, 335–375.

[24] Gross, J. D. (1994) *Microbiological reviews* **58**, 330–351.

[25] Bonner, J. T. (1982) *The Development of* Dictyostelium, ed. Loomis, W. (Academic Press), pp. 1–33.

[26] Gingle, A. R & Robertson, A. (1976) *J. Cell Sci.* **20**, 21–27.

[27] Raman, R. K, Hashimoto, Y, Cohen, M. H, & Robertson, A. (1976) *J. Cell. Sci.* **21**, 243–259.

[28] Parent, C. A & Devreotes, P. N. (1996) *Ann. Rev of Biochem.* **65**, 411–440.

[29] Klein, P. S, Sun, T. J, Saxe III, C. L, Kimmel, A. R, Johnson, R. L, & Devreotes, P. N. (1988) *Science* **241**, 1467–1472.

[30] Johnsson, R. L, Saxe, III, C. L, Gollop, R, Kimmel, A. R, & Devreotes, P. N. (1993) *Genes & Dev.* **7**, 273–282.

[31] Yu, Y & Saxe III, C. L. (1996) *Dev. Biol.* **173**, 353–356.

[32] Saxe III, C. L, Yu, Y, Jones, C, Bauman, A, & Haynes, C. (1996) *Dev. Biol.* **174**, 202–213.

[33] Louis, J. M, Ginsburg, G. T, & Kimmel, A. R. (1994) *Genes & Dev.* **8**, 2086–2096.

[34] Ross, F. M & Newell, P. C. (1981) *J. Gen. Microbiol.* **127**, 339–350.

[35] Van Haastert, P. J. M, Wit, R. J. W. D, Grijpma, Y, & Konijn, T. M. (1982) *PNAS* **79**, 6270–6274.

[36] Liu, G & Newell, P. C. (1991) *J. Cell Sci.* **98**, 483–490.

[37] Liu, G, Kuwayama, H, Ishida, S, & Newell, P. C. (1993) *J. Cell Sci.* **106**, 591–596.

[38] Wick, U, Malchow, D, & Gerisch, G. (1978) *Cell biology international reports* **2**, 71–79.

[39] Bumann, J, Wurster, B, & Malchow, D. (1984) *J. Cell Biol.* **98**, 173–178.

[40] Milne, J. L & Coukell, M. B. (1991) *J. Cell Biol.* **112**, 103–110.

[41] Europe-Finner, G. N & Newell, P. C. (1986) *Biochim Biophys Acta* **887**, 335–340.

[42] Europe-Finner, G. N & Newell, P. C. (1987) *J. Cell Sci.* **87**, 221–229.

[43] Flaadt, H, Jaworski, E, Schlatterer, C, & Malchow, D. (1993) *J. Cell Sci.* **105**, 255–261.

[44] Bominaar, A. A & Van Haastert, P. J. M. (1994) *Biochem. J.* **297**, 189–193.

[45] Knetsch, M. L. W, Epskamp, S. J. P, Schenk, P. W, Wang, Y, Segall, J. E, & Snaar-Jagalska, B. E. (1996) *The EMBO J.* **15**, 3361–3368.

[46] Maeda, M, Aubry, L, Insall, R, Gaskins, C, Devreotes, P. N, & Firtel, R. A. (1996) *J. Biol. Chem.* **271**, 3351–3354.

[47] Insall, R. H, Soede, R. D. M, Schaap, P, & Devreotes, P. N. (1994) *Mol. and Cell. Biol.* **5**, 703–711.

[48] Milne, J. L & Devreotes, P. N. (1993) *Mol Biol Cell (BAU)* **4**, 283–292.

[49] Bominaar, A. A & Van Haastert, P. J. M. (1997). Unpublished data.

[50] Schaap, P & Van Driel, R. (1985) *Exp. Cell Res.* **158**, 388–398.

[51] Oyama, M & Blumberg, D. D. (1986) *PNAS* **83**, 4819–4823.

[52] Mann, S. K. O & Firtel, R. A. (1989) *PNAS* **86**, 1924–1928.

[53] Soede, R. D. M, Insall, R. H, Devreotes, P. N, & Schaap, P. (1994) *Development* **120**, 1997–2002.

[54] Lilly, P, Wu, L, Welker, D. L, & Devreotes, P. N. (1993) *Genes and Dev.* **7**, 986–995.

[55] Milne, J. L. S, Wu, L, Caterina, M. J, & Devreotes, P. N. (1995) *J. Biol. Chem.* **270**, 5926–5931.

[56] Okaichi, K, Cubitt, A. B, Pitt, G. S, & Firtel, R. A. (1992) *Mol. and Cell. Biol.* **3**, 735–747.

[57] Wu, L, Valkema, R, Van Haastert, P. J. M, & Devreotes, P. N. (1995) *J. Cell Biol.* **129**, 1667–1675.

[58] Dharmawardhane, S, Cubitt, A. B, Clark, A. M, & Firtel, R. A. (1994) *Development* **120**, 3549–3561.

[59] Theibert, A & Devreotes, P. N. (1986) *J. Biol. Chem.* **261**, 15121–15125.

[60] Schulkes, C. C. G. M, Schoen, C. D, Arents, J. C, R., & Van Driel, R. (1992) *Biochim. Biophys. Acta (A0W)* **1135**, 73–78.

[61] Lilly, P. J & Devreotes, P. N. (1994) *J. Biol. Chem.* **269**, 14123–14129.

[62] Lilly, P. J & Devreotes, P. N. (1995) *J. Cell Biol.* **129**, 1659–1665.

[63] Segall, J. E, Kuspa, A, Shaulsky, G, Ecke, M, Maeda, M, Gaskins, C, Firtel, R. A, & Loomis, W. F. (1995) *J. Cell Biol.* **128**, 405–413.

[64] Insall, R. H, Borleis, J, & Devreotes, P. N. (1996) *Curr. Biol.* **6**, 719–729.

[65] Kuwayama, H & Van Haastert, P. J. M. (1996) *J. Biol. Chem.* **271**, 23718–23724.

[66] Riedel, V, Malchow, D, Gerisch, G, & Nagele, B. (1972) *Biochem. Biophys. Res. Comm.* **46**, 279–287.

[67] Gerisch, G. (1976) *Cell Differ* **5**, 21–25.

[68] Faure, M, Franke, J, Hall, A. L, Podgorski, G. J, & Kessin, R. H. (1990) *Mol. and Cell. Biol.* **10**, 1921–1930.

[69] Hall, A. L, Franke, J, Faure, M, & Kessin, R. H. (1993) *Dev. Biol.* **157**, 73–84.

[70] Yeh, R. P, Chan, F. K, & Coukell, M. B. (1978) *Dev. Biol.* **66**, 361–374.

[71] Franke, J & Kessin, R. H. (1981) *J. Biol. Chem.* **256**, 7628–7637.

[72] Wu, L & Franke, J. (1990) *Gene* **91**, 51–56.

[73] Klein, C & Juliani, M. H. (1977) *Cell* **10**, 329–335.

[74] Kesbeke, F & Van Haastert, P. J. M. (1985) *Biochim Biophys Acta* **847**, 33–39.

[75] Wang, M, Van Haastert, P. J. M., Devreotes, P. N, & Schaap, P. (1988) *Dev. Biol*. **128**, 72–77.

[76] Van Haastert, P. J. M, Wang, M, Bominaar, A. A, Devreotes, P. N, & Schaap, P. (1992) *Mol. and Cell. Biol.* **3**, 603–612.

[77] Van Haastert, P. J. M & de Wit, R. J. (1984) *J. Biological Chemistry* **259**, 13321–13328.

[78] Caterina, M. J, Devreotes, P. N, Borleis, J, & Hereld, D. (1995) *J. Biol. Chem.* **270**, 8667–8672.

[79] Van Haastert, P. J. M. (1987) *J. Biol. Chem.* **262**, 7700–7704.

[80] Devreotes, P. N & Sherring, J. A. (1985) *J. Biol. Chem.* **260**, 6378–6384.

[81] Dinauer, M. C, Steck, T. L, & Devreotes, P. N. (1980) *J. Cell Biol.* **86**, 554–561.

[82] Van Haastert, P. J. M. (1987) *J. Cell Biol.* **105**, 2301–2306.

[83] Van Haastert, P. J. M. & Van der Heijden, P. (1983) *J. Cell Biol.* **96**, 347–353.

[84] van Haastert, P. J. M., de Wit, R. J, Janssens, P. M, Kesbeke, F, & DeGoede, J. (1986) *J. Biol. Chem.* **261**, 6904–6911.

[85] Van Haastert, P. J. M. (1987) *Biochem.* **26**, 7518–7523.

[86] Van Haastert, P. J. M. (1984) *Biochem. Biophys. Res. Comm.* **124**, 597–604.

[87] Ludrus, M. E. E, Spijkers, M. J, & Driel, R. V. (1990) *J. Cell Sci.* **95**, 623–629.

[88] Van Haastert, P. J. M. (1987) *J. Biol. Chem.* **262**, 7705–7710.

[89] Klein, P, Theibert, A, Fontana, D, & Devreotes, P. N. (1985) *J. Biol. Chem.* **260**, 1757–1764.

[90] Kim, J. Y, Soede, R, Schaap, P, Valkema, R, Borleis, J. A, Van Haastert, P. J. M, Devreotes, P, & Hereld, D. (1997) *J. Biol. Chem.* **272**, 2731–27318.

[91] Caterina, M. J, Hereld, D, & Devreotes, P. N. (1995) *J. Biol. Chem.* **270**, 4418–4423.

[92] Valkema, R & Van Haastert, P. J. M. (1994) *Molec. Biol. Cell* **5**, 575–585.

[93] Peters, D. J, Van Lookeren Campagne, M. M, Van Haastert, P. J. M., Spek, W., & Schaap, P. (1989) *J. Cell Sci.* **93**, 205–210.

[94] Bominaar, A. A, Kesbeke, F, & Van Haastert, P. J. M. (1994) *Biochem. J.* **297**, 181–187.

[95] Drayer, A. L, Meima, M. E, Derks, M. W. M, Tuik, R, & Van Haastert, P. J. M. (1995) *Biochem. Jour.* **311**, 505–510.

[96] Wurster, B, Schubiger, K, Wick, U, & Gerisch, G. (1977) *FEBS Letts* **76**, 141–144.

[97] Mato, J. M, Van Haastert, P. J. M, Krens, F. A, Rhijnsburger, E. H, Dobbe, F. C. P. M, & Konijn, T. M. (1977) *FEBS Letters* **79**, 331–336.

[98] Kesbeke, F, Snaar-Jagalska, B. E, & Van Haastert, P. J. M. (1988) *J. Cell Biol.* **107**, 521–528.

[99] Hadwiger, J. A, Lee, S, & Firtel, R. A. (1994) *PNAS* **91**, 10566–10570.

[100] Van Haastert, P. J. M. (1983) *Biochem. Biophys. Res. Comm* **115**, 130–136.

[101] Janssens, P. M. W, Jong, C. C. C. D, Vink, A. A, & Van Haastert, P. J. M. (1989) *J. Biol. Chem.* **264**, 4329–4335.

[102] Insall, R, Kuspa, A, Lilly, P. J, Shaulsky, G, Levin, L. R, Loomis, W. F, & Devreotes, P. (1994) *J. Cell Biol.* **126**, 1537–1545.

[103] Musacchio, A, Gibson, T, Rice, P, Thompson, J, & Saraste, M. (1997) *TIBS* **18**, 343–348.

[104] Inglese, J, Koch, W. J, Touhara, K, & Lefkowitz, R. J. (1995) *TIBS* **20**, 151–156.

[105] Pupillo, M, Insall, R, Pitt, G. S, & Devreotes, P. N. (1992) *Mol. Biol. Cell* **3**, 1229–1234.

[106] Snaar-Jagalska, E & Van Haastert, P. J. M. (1990) *Molec. Cell. Biochem.* **92**, 177–189.

[107] Snaar-Jagalska, B. E, Van Es, S, Kesbeke, F, & Van Haastert, P. J. M. (1991) *Eur. J. Biochem.* **195**, 715–721.

[108] Goldbeter, A. (1975) *Nature* **253**, 540–542.

[109] Goldbeter, A & Segel, L. A. (1977) *PNAS* **74**, 1543–1547.

[110] Goldbeter, A & Segel, L. A. (1980) *Differentiation* **17**, 127–135.

[111] Sperb, P. P. (1979) *Bull. Math. Biol.* **41**, 555–572.

[112] Barchilon, M & Segel, L. A. (1988) *J. Theor. Biol.* **133**, 437–446.

[113] Martiel, J. L & Goldbeter, A. (1987) *Biophys. Jour.* **52**, 807–828.

[114] Monk, P. B & Othmer, H. G. (1990) *Proc. Roy. Soc. (Lon)* **240**, 555–589.

[115] Tyson, J. J & Murray, J. D. (1989) *Development* **106**, 421–426.

[116] Bretschneider, T, Siegert, F, & Weijer, C. J. (1995) *PNAS* **92**, 4387–4391.

[117] Palsson, E & Cox, E. C. (1996) *PNAS* **93**, 1151–1155.

[118] Rapp, P. E, Monk, P. B, & Othmer, H. G. (1985) *Math. Biosci.* **77**, 35–78.

[119] Monk, P. B & Othmer, H. G. (1989) *Phil. Trans. R. Soc. London.* **323**, 185–224.

[120] Schaap, P, Brandt, R, & Es, S. V. (1995) *Dev. Biol.* **168**, 179–188.

[121] Siegert, F & Weijer, C. J. (1989) *J. Cell Sci.* **93**, 325–335.

[122] Berman, D. M, Wilkie, T. M, & Gliman, A. G. (1996) *Cell* **86**, 445–452.

[123] Tang, Y & Othmer, H. G. (1995) *Phil. Trans. Roy. Soc. (Lon.)* **B349**, 179–195.

[124] Chen, M, Insall, R, & Devreotes, P. (1996) *TIG* **12**, 52–57.

[125] Stern, P, Edwards, F. A, & Sakmann, B. (1992) *J. Physiol.* **449**, 247–278.

[126] Gerisch, G & Wick, U. (1975) *Biochem. Biophys. Res. Comm.* **65**, 364–370.

[127] Roos, W, Scheidegger, C, & Gerisch, G. (1977) *Nature* **266**, 259–260.

[128] Berg, H. C & Purcell, E. M. (1977) *Biophys. Jour.* **20**, 193–219.

[129] Eigen, M & Hammes, G. (1963) *Adv. Enztmology*, ed. Nord, F. F. (Interscience) Vol. 25, pp. 1–38.

[130] DeLisi, C & Marchetti, F. (1982) *Cell Biophys.* **4**, 211–229.

[131] Tranquillo, R & Lauffenburger, D. (1987) *J. Math. Biol.* **25**. chemotaxis.

[132] Tranquillo, R. T, Brosteanu, O, & Alt, W. (1994) *NATO ASI series. Series H, Cell biology* pp. 437–444.

[133] Tomchik, K. J & Devreotes, P. N. (1981) *Science* **212**, 443–446.

[134] Newell, P. C. (1983) in *Fungal Differentiation: A Contemporary Synthesis*, ed. Smith, J. E. (Marcel Dekker, New York), pp. 43–71.

[135] Foerster, P, Müller, C, & Hess, B. (1990) *Dev.* **109**, 11–16.

[136] Siegert, F & Weijer, C. (1989) *J. Cell Sci.* **93**, 325–335.

[137] Varnum, B & Soll, D. R. (1984) *J. Cell Biol.* **99**, 1151–1155.

[138] Varnum, B, Edwards, K. B, & Soll, D. R. (1985) *J. Cell Biol.* **101**, 1–5.

[139] Fisher, P, Merkl, R, & Gerisch, G. (1989) *J. Cell Biol.* **92**, 807–821.

[140] McDonald, S. A. (1986) *Dev. Biol.* **117**, 546–549.

[141] DeYoung, G, Monk, P. B, & Othmer, H. G. (1988) *J. Math. Biol.* **26**, 486–517.

[142] Alcantara, F & Monk, M. (1974) *J. Gen. Microbiol.* **85**, 321–334.

[143] Gingle, A. R. (1976) *J. Cell Sci.* **20**, 1–20.

[144] Glazer, P. M & Newell, P. C. (1981) *J. Gen. Microbiol.* **125**, 221–232.

[145] Cohen, M. H & Robertson, A. (1975) *Cellular organization and communication in Dictyostelium discoideum and other cellular slime molds* ed. Caianiello, E. R. (Leyden, Noordhoff), pp. 217–240.

[146] Nanjundiah, V & Malchow, D. (1976) *J. Cell Sci.* **22**, 49–58.

[147] Pate, E. F, Elwood, D, & Othmer, H. G. (1988) mPDE dramatically affects cAMP levels near aggregating *D. Dictyostelium* cells. Unpublished.

[148] Parnas, H & Segel, L. A. (1977) *J. Cell Sci.* **25**, 191–204.

[149] MacKay, S. (1978) *J. Cell. Sci.* **33**, 1–16.

[150] Vasieva, O. O, Vasiev, B. N, Karpov, V. A, & Zaikin, A. N. (1994) *J. Theor. Biol.* **171**, 361–367.

[151] Keller, E. F & Segel, L. A. (1971) *J. Theor. Biol.* **30**, 225–234.

[152] Nanjundiah, V. (1973) *J. Theor. Biol.* **42**, 63–105.

[153] Levine, H & Reynolds, W. (1991) *Phys. Rev. Letts.* pp. 2400–2403.

[154] Vasiev, B. N, Hogeweg, P, & Pantifilov, A. V. (1994) *Physical Review Letters* **73**, 3173–3176.

[155] Höfer, T, Sherratt, J. A, & Maini, P. K. (1995) *Proc. Roy. Soc. Lond. B* **259**, 249–257.

[156] Tyson, J. J, Alexander, K. A, Manoranjan, V. S, & Murray, J. D. (1989) *Physica. D, Nonlinear phenomena* **34**, 193–207.

[157] Cohen, M. H & Robertson, A. (1971) *J. Theor. Biol.* **31**, 101–118.

[158] Cohen, M. H & Robertson, A. (1971) *J. Theor. Biol.* **31**, 119–130.

[159] Dworkin, M & Keller, K. H. (1977) *J. Biol. Chem.* **252**, 864–865.

[160] Monk, P. B & Othmer, H. G. (1989) *Relay, Oscillations and Wave propagation in a Model of* Dictyostelium discoideum ed. Othmer, H. G. (A. Math. Soc., Providence, R. I.).

[161] Durston, A. J. (1974) *Dev. Biol.* **37**, 225–235.

[162] Gross, J. D, Peacey, M. J, & Trevan, D. J. (1976) *J. Cell Sci.* **22**, 645–656.

[163] Zykov, V. S & Morozova, O. L. (1980) *Biophysics* **24**, 739–744.

[164] Mikhailov, A. S & Krinsky, V. I. (1983) *Physica D* **9**, 346–371.

[165] Keener, J. P. (1986) *SIAM J. Appl. Math.* **46**, 1039–1056.

[166] Othmer, H. G & Monk, P. B. (1988) *Concentration waves in aggregation fields of a cellular slime mold* ed. Ricciardi, L. (Kluwer Academic Publishers, Dordrecht), pp. 381–398.

[167] Berg, H. C & Brown, D. A. (1972) *Nature* **239**, 500–504.

[168] Berg, H. C. (1975) *Sci. Am.* **233**, 36–44.

[169] Soll, D. R. (1995) *Int. Rev. Cytology*, eds. Jeon, K. W & Jarvik, J. (Acdemic Press) Vol. 163, pp. 43–104.

[170] Alt, W & Hoffman, G, eds. (1990) *Biological Motion* (Springer Verlag, Berlin).

[171] Wessels, D, Murray, J, & Soll, D. R. (1992) *Cell Motil. Cytoskel* **23**, 145–156.

[172] Swanson, J & Taylor, D. L. (1982) *Cell* **28**, 225–232.

[173] Vicker, M. G. (1994) *J. Cell Sci.* **107**, 659–667.

[174] Brenner, M & Thoms, S. D. (1984) *Dev. Biol.* **101**, 136–146.

[175] Dallon, J. C & Othmer, H. G. (1997) *Phil. Trans. Roy. Soc. London: Series B* **352**, 391–417.

[176] Van Duijn, B & Van Haastert, P. J. M. (1992) *J. Cell Sci.* **102**, 763–768.

[177] Futrelle, R, Traut, J, & McKee, W. G. (1982) *J. Cell. Biol.* **92**, 807–821.

[178] Varnum-Finney, B. J, Voss, E, & Soll, D. R. (1987) *Cell Motil. Cytoskel.* **8**, 18–26.

[179] Newell, P. C, Europe-Finner, G. N, Liu, G, Gammon, B, & Wood, C. A. (1990) in *Biology of the Chemotactic Response*, eds. Armitage, J. P & Lackie, J. M. (Cambridge University Press), pp. 241–272.

[180] Soll, D. R, Wessels, D, & Sylwester, A. (1993) *The Motile Behavior of Amoebae in the Aggregation Wave in* Dictyostelium discoideum eds. Othmer, H. G, Maini, P. K, & Murray, J. D. (Plenum, London).

[181] Newell, P. C & Liu, G. (1992) *BioEssays* **14**, 473–479.

[182] Patlak, C. S. (1953) *Bull. Math. Biophys.* **15**, 311–338.

[183] Alt, W. (1980) *J. Math. Biol.* **9**, 147–177.

[184] Keller, E. F & Segel, L. A. (1970) *J. Theor. Biol.* **26**, 399–415.

[185] Segel, L. (1977) *SIAM J. Appl. Math.* **32**, 653–665.

[186] Pate, E & Othmer, H. G. (1986) *J. Theor. Biol.* **118**, 301–319.

[187] Childress, S & Percus, J. K. (1981) *Math. Biosci.* **56**, 217–237.

[188] Schaaf, R. (1985) *Trans. AMS* **292**, 531–556.

[189] Lin, C.-S, Ni, W.-M, & Takagi, I. (1988) *J. Diff. Eqns.* **72**, 1–27.

[190] Jäger, W & Luckhaus, S. (1992) *Trans. Am. Math. Soc.* **329**, 819–824.

[191] Rascle, M & Ziti, C. (1995) *J. Math. Biol.* **33**, 388–414.

[192] Othmer, H. G & Stevens, A. (1997) *SIAM JAM* **57**, 1044–1081.

[193] Höfer, T, Sherratt, J. A, & Maini, P. K. (1995) *Proc. Roy. Soc. Lond B* **259**, 249–257.

[194] Othmer, H. G, Dunbar, S. R, & Alt, W. (1988) *J. Math. Biol.* **26**, 263–298.

[195] Koshland, D. E. (1980) *Bacterial Chemotaxis as a Model Behavioral System*. (Raven Press, New York, NY, USA).

[196] Berg, H. (1983) *Random Walks in Biology*. (Princeton University Press, Princeton, NJ, USA).

[197] Othmer, H. G. (1997) A model for chemokinesis and chemotaxis with internal state and adaptation. In preparation.

[198] Killich, T, Plath, P. J, Wei, X, Bultmann, H, Rensing, L, & Vicker, M. G. (1993) *J. Cell Sci.* **106**, 1005–1013.

[199] Shenderov, A & Sheetz, M. (1997) *Biophys. J.* **72**, 2382–2389.

[200] Goldstein, S. (1951) *Quarterly J. Mech. Appl. Math.* **VI**, 129–156.

[201] Kac, M. (1974) *Rocky Mtn J. Math.* **3**, 497–509.

[202] McKean, H. (1967) *J. Math. Physics* **75**, 1–10.

[203] Segel, L. A. (1978) *Mathematical models for cellular behavior* ed. Levin, S. A. (MAA, Washington), pp. 156–190.

[204] Mato, J. M, Losada, A, Nanjundiah, V, & Konijn, T. M. (1975) *PNAS* **72**, 4991–4993.

[205] Mato, J. M, Krens, F. A, Van Haastert, P. J. M, & Konijn, T. M. (1977) *PNAS* **74**, 2348–2351.

[206] Zigmond, S. H. (1978) *J. Cell Biol.* **77**, 269–287.

[207] Othmer, H. G & Pate, E. F. (1987) *A model for pattern formation in Dictyostelium discoideum* eds. Teramoto, E & Yamaguti, M. (Springer-Verlag, Berlin), pp. 224–233.

[208] Gerisch, G, Hulser, D, Malchow, D, & Wick, U. (1975) *Phil. Trans. Roy. Soc. Lond.* **272**, 181–192.

[209] Gilbert, S. H, Perry, K, & Fay, F. S. (1994) *J. Cell Biol.* **127**, 489–503.

[210] Brundage, R. A, Fogarty, K. E, & Fay, F. S. (1991) *Science* **254**, 703–706.

[211] Gerisch, G, Malchow, D, Huesgen, A, Nanjundiah, V, Roos, W, & Wick, U. (1975) *Cyclic AMP reception and cell recognition in* Dictyostelium discoideum eds. McMahon, D & Fox, C. F. (Benjamin, New Yokr, NY), pp. 76–88.

[212] Rossier, C, Eitle, E, Van Driel, R, & Gerisch, G. (1980) *Biochemical regualtion of cell development and aggregation in* Dictyostelium discoideum eds. Gooday, G. W, Lloyd, D, & Trinci, A. P. J. (Society for General Microbiology, Cambridge University Press, Cambridge, UK), pp. 405–427.

[213] Pate, E & Odell, G. (1981) *J. Theor. Biol.* **88**, 201–239.

[214] Savill, N & Hogeweg, P. (1997) *J. Theor. Biol.* **184**, 229–235.

[215] Kuwayama, H, Ishida, S, & Van Haastert, P. J. M. (1993) *J. Cell Biol.* **123**, 1453–1462.

[216] Dallon, J & Othmer, H. G. (1997) A continuum analysis of the chemotactic signal seen by *Dictyostelium discoideum*. J. Theor. Biol., To appear.

[217] Roos, W, Nanjundiah, V, Malchow, D, & Gerisch, G. (1975) *FEBS Letters* **53**, 139–142.

[218] Malchow, D, Fuchida, J, & Nanjundiah, V. (1975) *Biochem. Biophys. Acta* **385**, 421–428.

[219] Green, A & Newell, P. (1975) *Biochem. J.* **140**, 313–322.

[220] Konijn, T. M & Raper, K. B. (1961) *Dev. Biol.* **3**, 725–756.

[221] Nanjundiah, V & Malchow, D. (1976) *J. Cell Sci.* **22**, 49–58.

[222] Futrelle, R. (1982) *J. Cell. Biochem.* **18**, 197–212.

[223] Zigmond, S. H. (1989) *Curr. Opin Cell Biol (AOE)* **1**, 80–86.

[224] Tranquillo, R. T. (1990) in *Biology of the Chemotactic Response*, eds. Armitage, J. P & Lackie, J. M. (Cambridge University Press, New York), pp. 35–75.

[225] Schnitzer, M. J, Block, S. M, Berg, H. C, & Purcell, E. M. (1990) *Strategies for chemotaxis* eds. Armitage, J. P & Lackie, J. M. pp. 15–34.

[226] Wilkinson, P. C. (1996) *Methods* **10**, pp. 74–84.

[227] Lee, K, Cox, E. C, & Goldstein, R. E. (1996) Competing patterns of signalling activity in *Dictyostelium discoideum*. Preprint.

[228] Lauzeral, J, Halloy, J, & Goldbeter, A. (1997) *PNAS* **94**, pp. 9153–9158.

[229] Levine, H, Aronson, I, Tsimring, L, & Truong, T. V. (1996) *PNAS* **93**, pp. 6382-6386.

[230] Raper, K. B. (1984) *The Dictyostelids*. (Princeton University Press), pp. 126–127.

[231] Fisher, P. R. (1990) *Cell Biol.* **1**, 87–97.

[232] Othmer, H. G., Lilly, B. & Dallon, J. C. (1998) Pattern formation in a cellular slime mold. To appear.

[233] Höfer, T & Maini, P. (1997) *Phys. Rev. E* **56**, 1–7.

[234] Fukui, Y. (1993) *Int. Rev. Cytology* **144**, 85–128.

[235] Williams, J & Morrison, A. (1994) *Prog. Nucleic Acid Res. Mol. Biol.* **47**, 3–28.

[236] Abe, T, Early, A, Siegert, F, Weijer, C, & Williams, J. (1994) *Cell* **77**, pp. 687–699.

[237] Bottino, D. (1996) Ph.D. thesis (Tulane University, New Orleans).

[238] Rietdorf, J, Siegert, F, Dharmawardhane, S, Firtel, R. A, & Weijer, C. J. (1997) *Dev. Biol.* **181**, pp. 79–90.

[239] Siegert, F & Weijer, C. J. (1992) *PNAS* **89**, 6433–6437.

[240] Siegert, F & Weijer, C. J. (1995) *Curr. Biol*. **5**, 937–943.

[241] Steinbock, O, Siegert, F, Muller, S. C, & Weijer, C. J. (1993) *PNAS* **90**, 7332–7335.

[242] Pitt, G. S, Milona, N, Borleis, J, Lin, K. C, Reed, R. R, & Devreotes, P. N. (1992) *Cell* **69**, 305–315.

[243] Schaap, P & Spek, W. (1984) *Differentiation* **27**, 83–87.

[244] Kim, J.-Y, Van Haastert, P. J. M., & Devreotes, P. N. (1996) *Chem. Biol.* **3**, 239–243.

[245] Doolittle, K. W, Reddy, I, & McNally, J. G. (1994) Multiple motile behaviors in tip-forming mounds as observed by 3D microscopy. Absts. of the Intl. Dd Conf.

[246] Doolittle, K. W, Reddy, I, & McNally, J. G. (1995) *Dev. Biol*. **167**, pp. 118–126.

[247] Shelden, E & Knecht, D. A. (1995) *J. Cell Sci.* **108**, 1105–1115.

[248] Rietdorf, J, Siegert, F, & Weijer, C. J. (1996) *Dev. Biol.* **177**, 427–438.

[249] Dormann, D, Siegert, F, & Weijer, C. J. (1996) *Development* **122**, 761–769.

[250] Vasiev, B, Siegert, F, & Weijer, C. J. (1997) *J. Theor. Biol.* **184**, 441–450.

[251] Schaap, P, Tang, Y, & Othmer, H. G. (1996) *Differentiation* **60**, 1–16.